1936-38

Advanced School on Synchrotron and Free Electron Laser Sources and their Multidisciplinary Applications

7 - 25 April 2008

Photo emission electron microscopy.

E. Bauer
Arizona State University.
U.S.A.

Photo emission electron microscopy

Outline

Introduction

Electron optics:

Resolution

Transmission

Instruments:

PEEM

PEEM + LEEM

SPELEEM

Methodic

Applications:

Magnetic imaging

Photo Emission Electron Microscopy (PEEM)

2 types

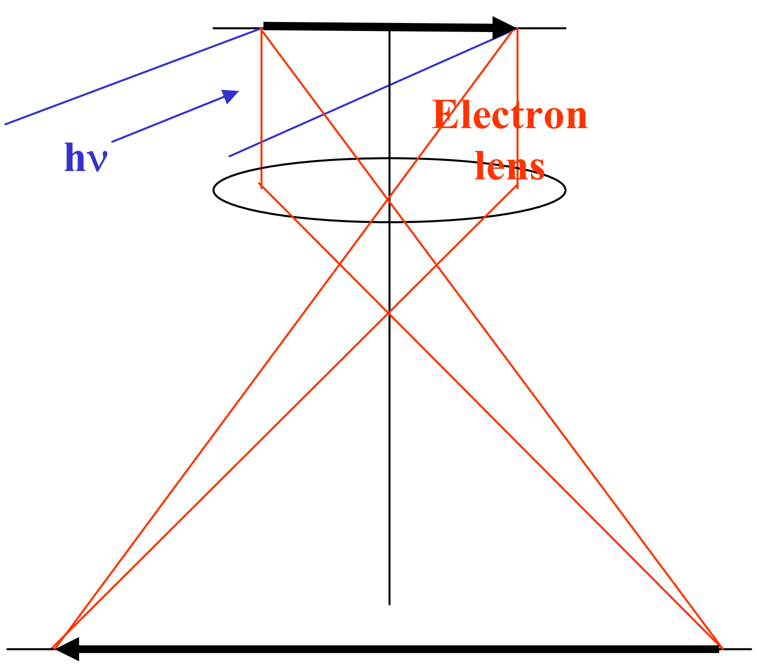

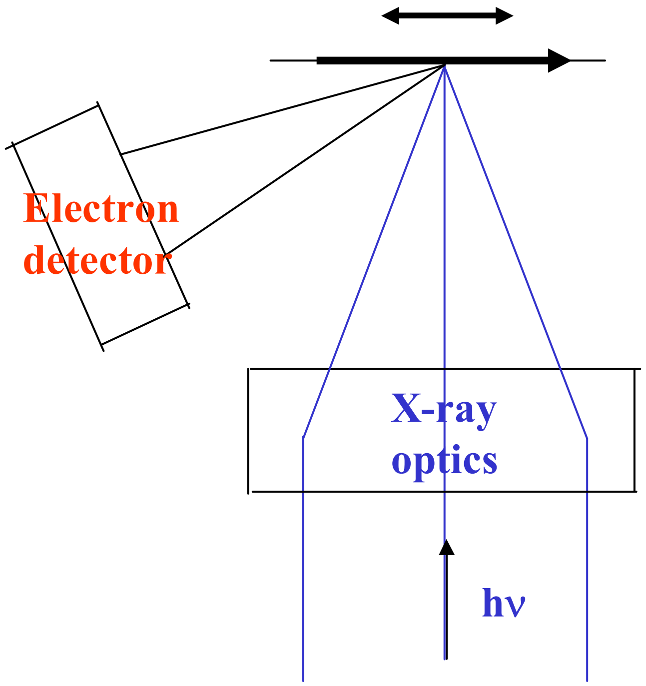

broad illumination

Full field

sample fixed

Bauer, Locatelli

PEEM

focused illumination

Scanning

sample scanned

Kiskinova

3 imaging modes

1	XPEEM	Photo electrons PE	with energy filter
2	XAEEM	Auger electrons AE	
3	XSEEM	Secondary electrons SE	

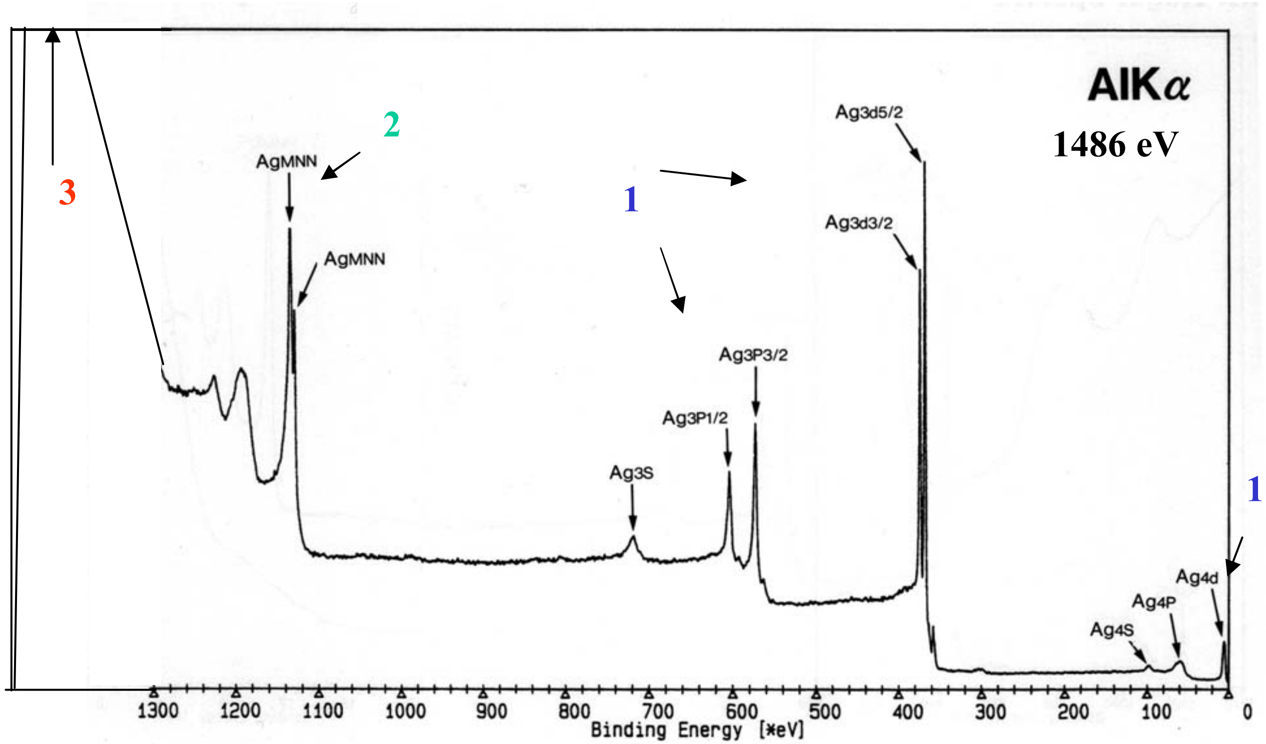

Angular distribution

Internal

Amorphous, polycrystalline, SE

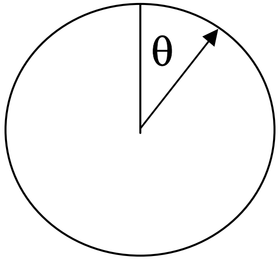

$I_i(\theta)$ = const.

single crystalline, PE, AE

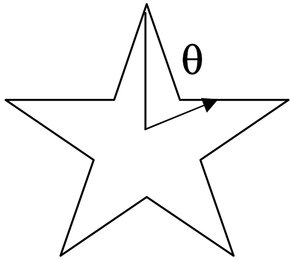

$I_i(\theta)$ due to diffraction

Internal (i) → External (e)

n ~

$\sqrt{E}$

$\sqrt{E+V_0}$

Refraction

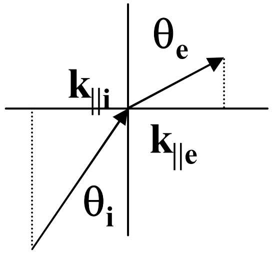

$k_{||}$ conservation **$k_{||e} = k_{||i}$**

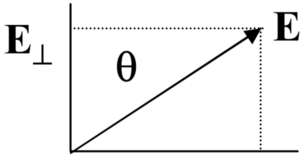

$E_\perp = E \cos\ \theta$

For escape necessary:

$E_\perp > \Phi$ (work function)
I (ionization energy)
U (HOMO)

External

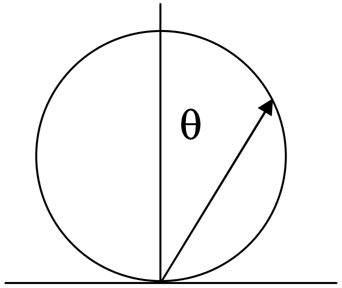

$I_e(\theta) = \cos\ \theta$

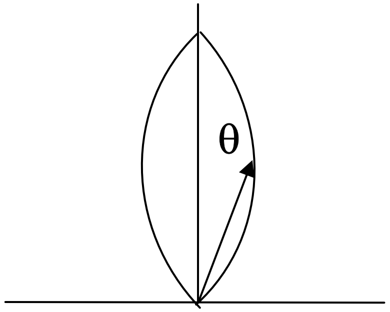

Electron optics

The cathode lens

In emission microscopy $\theta \equiv \alpha_0$ is large

Electron lenses can accept only small $\theta \equiv \alpha_0$ because of large chromatic and spherical aberrations

Solution of problem: accelerate electrons to high energy before lens

↓

Immersion objective lens = cathode lens

$$n \sin\theta = \text{const}$$

$$n \sim v \sim \sqrt{E}$$

$$\theta \rightarrow \alpha$$

$$\boxed{\sin \alpha / \sin \alpha_0 = \sqrt{E_0/E}}$$

Example for E = 20000 eV:

E_0	2 eV	200 eV
α for $\alpha_0 = 45^\circ$	0.4°	4.5°

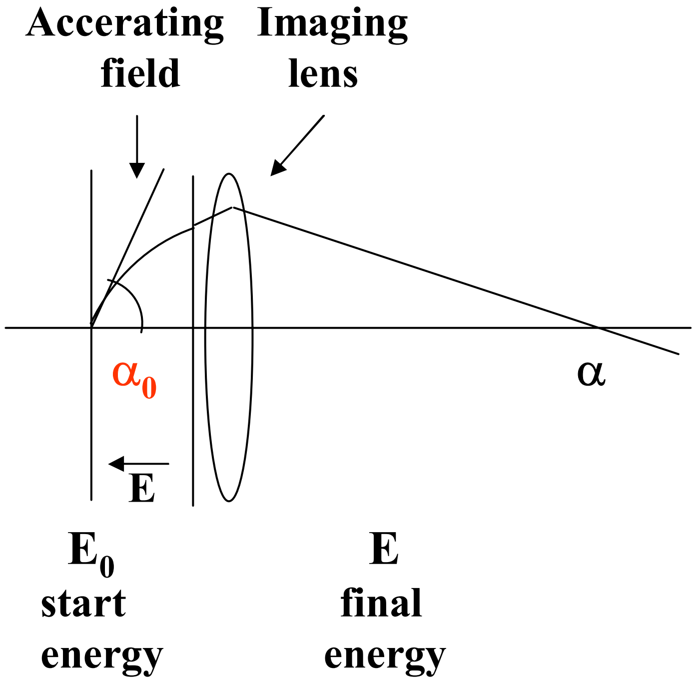

Aberrations

chromatic

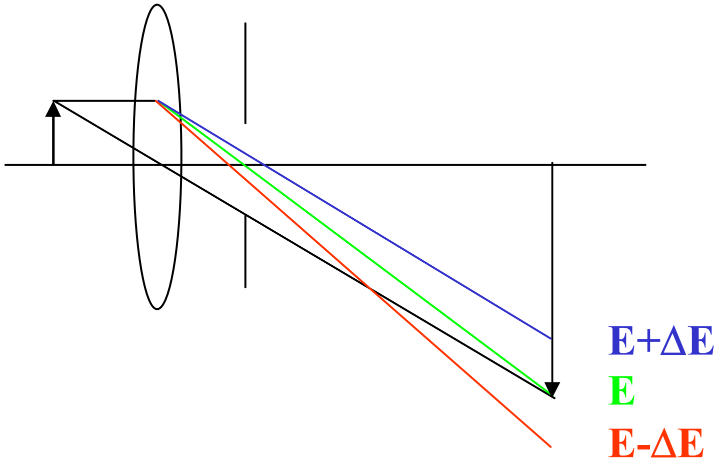

slower (faster) electrons
are more (less) deflected

spherical

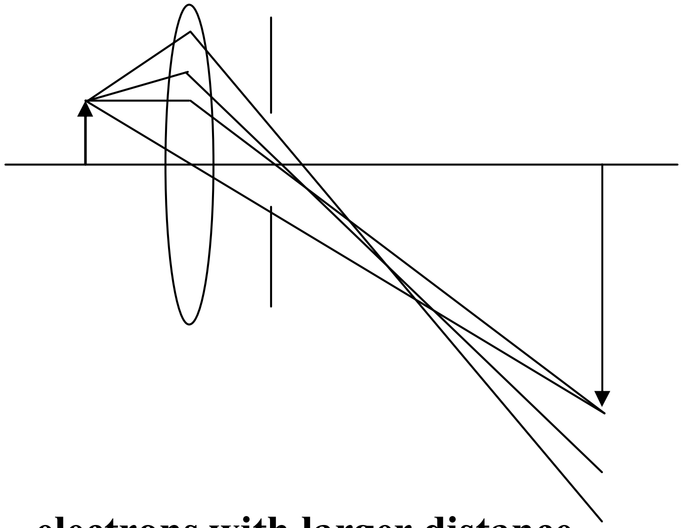

electrons with larger distance
from axis are more deflected
(stronger field!)

Cathode lens types

Electrostatic tetrode

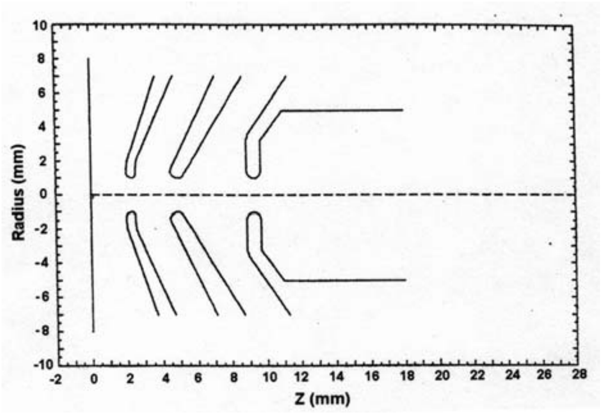

Lens comparison

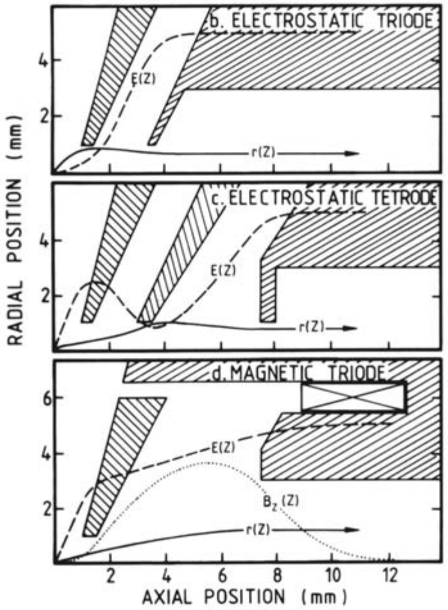

Magnetic diode

Estimation of aberrations:
Separate lens into acceleration and imaging regions

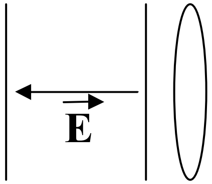

At low energies the aberrations of the accelerating region dominate

Aberrations of homogeneous acceleration field

$\rho_0 = E_0/E \quad \varepsilon = \Delta E_0/E \quad \rho = \rho_0 + \varepsilon$

Spherical aberration d_s

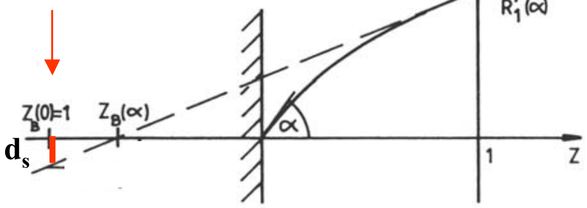

Chromatic aberration d_c

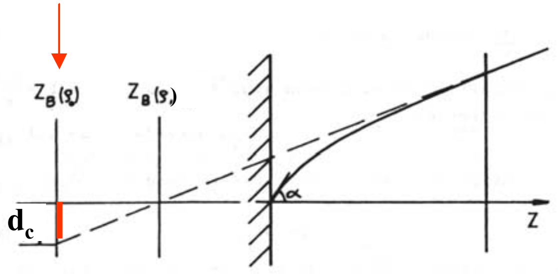

Analytical solution

Approximation: ρ_0 **and** $\varepsilon << 1/\cos\alpha^2 > 1$

Example: $E_0 = 100$ **eV,** $\Delta E_0 = 1$ **eV,** $E = 20000$ **eV**

$\varepsilon = \rho_0/100, \quad \rho_0 = 1/200$

$d_s \approx 2\,\rho \sin\alpha\,(1 - \cos\alpha)$

$\approx \rho\,\alpha^3$ **for small** α

$d_c \approx 2\,\rho \sin\alpha\,(\sqrt{}\,\rho_0/\rho - 1)$

$\approx \varepsilon \sin\alpha$ **for** $\varepsilon << \rho_0 \approx \rho$

$\approx \varepsilon\,\alpha$ **for small** α

α-dependent aberrations require α-limitation by angle-limiting aperture ("contrast aperture") with radius r_A

Diffraction by aperture: diffraction disc of confusion $d_B = 0.6\ \lambda / r_A$

Approximate resolution $d = \sqrt{d_S^2 + d_C^2 + d_B^2}$

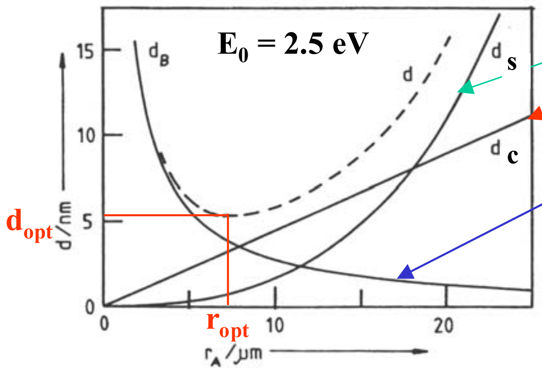

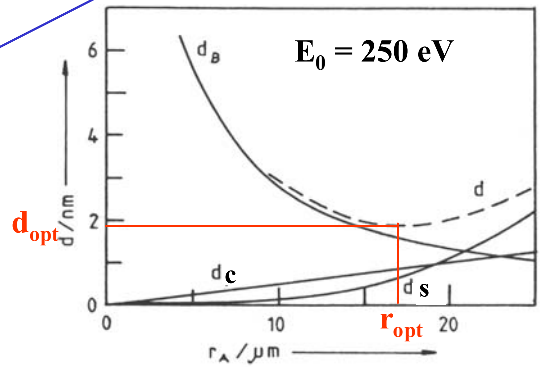

L = 3 mm   E = 25000 eV $\Delta E_0 =$ 0.25 eV

Optimum aperture radius

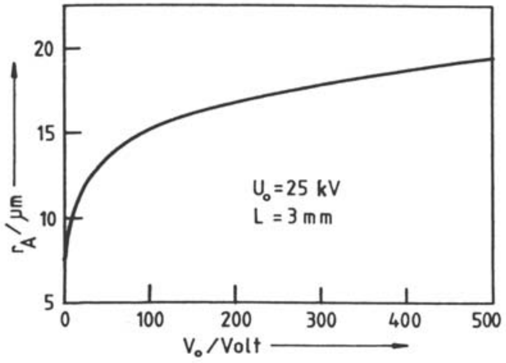

Optimum resolution

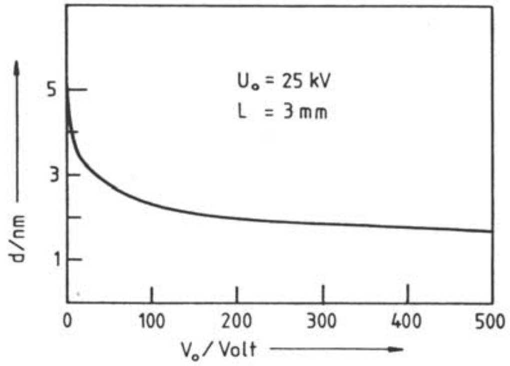

Note: small angle approximation $\sin \alpha \approx \alpha \sim r$

Complete lens

Combine acceleration and imaging regions

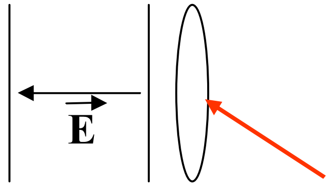

At low energies aberrations of accelerating region dominate

but

at high energies the spherical aberration of second part of lens becomes important

Resolution and optimum aperture of real lenses

Optimum aperture r and resolution-limiting contributions

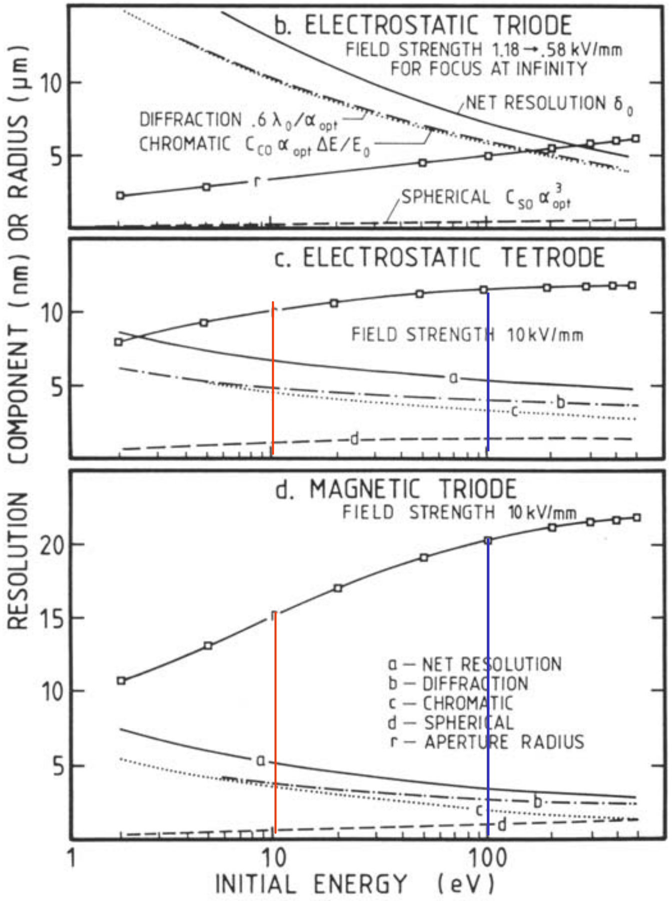

J. Chmelik et al, Optik 83 (1989)155

T. Müller, M.S. thesis, TU Clausthal 1995

Resolution with optimum aperture
E-dependence at fixed ΔE = 0.5 eV, U_0 = 20 keV

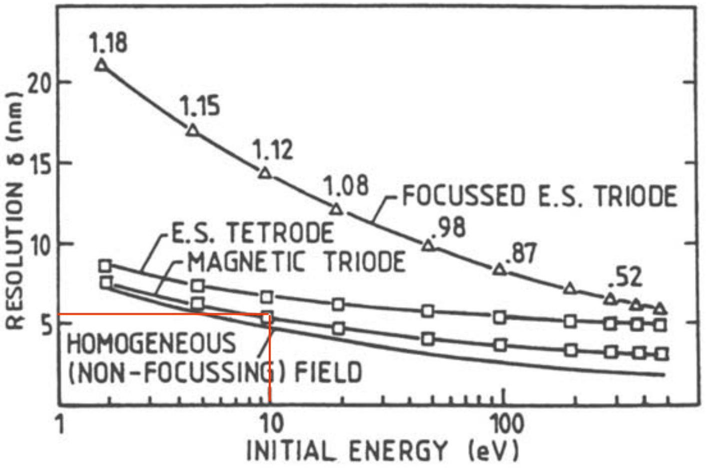

ΔE-dependence at fixed E = 10 eV, U_0 = 18 kV magnetic triode

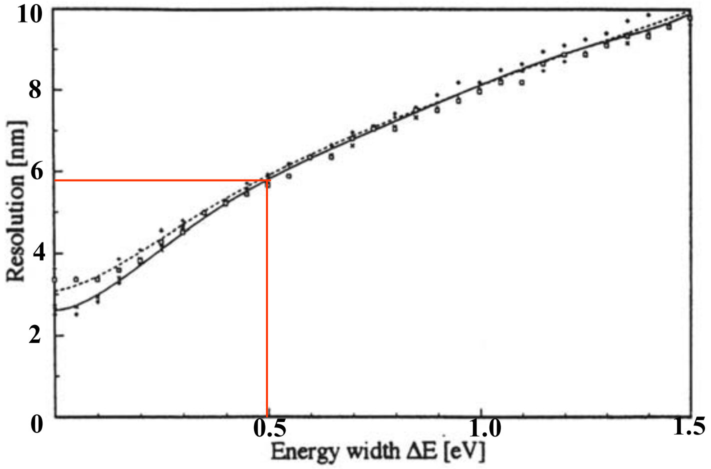

Transmission

limited by angle accepted by contrast aperture (r_A)

Axial distance (in back focal plane) of electron starting at angle α

$r \approx f \sin\alpha \sqrt{E_0/E}$ (f focal length)

↓

$$\sin\alpha \approx (r/f) \sqrt{E_0/ E}$$

Examples for f = 10 mm, E = 20000eV, r_A =10 μm

E_0	2 eV	200 eV
$\sin\alpha$	0.2	0.02
α	11.5°	1.15°

In emission microscopy (wide α range) optimum resolution condition reduces transmission T, therefore

optimize T^n/d^2 instead of $1/d^2$

For cos α distribution $T = \pi \sin^2\alpha$

$$T^n/d^2 = \pi \sin^{2n}/d^2$$

Transmission T_n, resolution r_n of homogeneous field

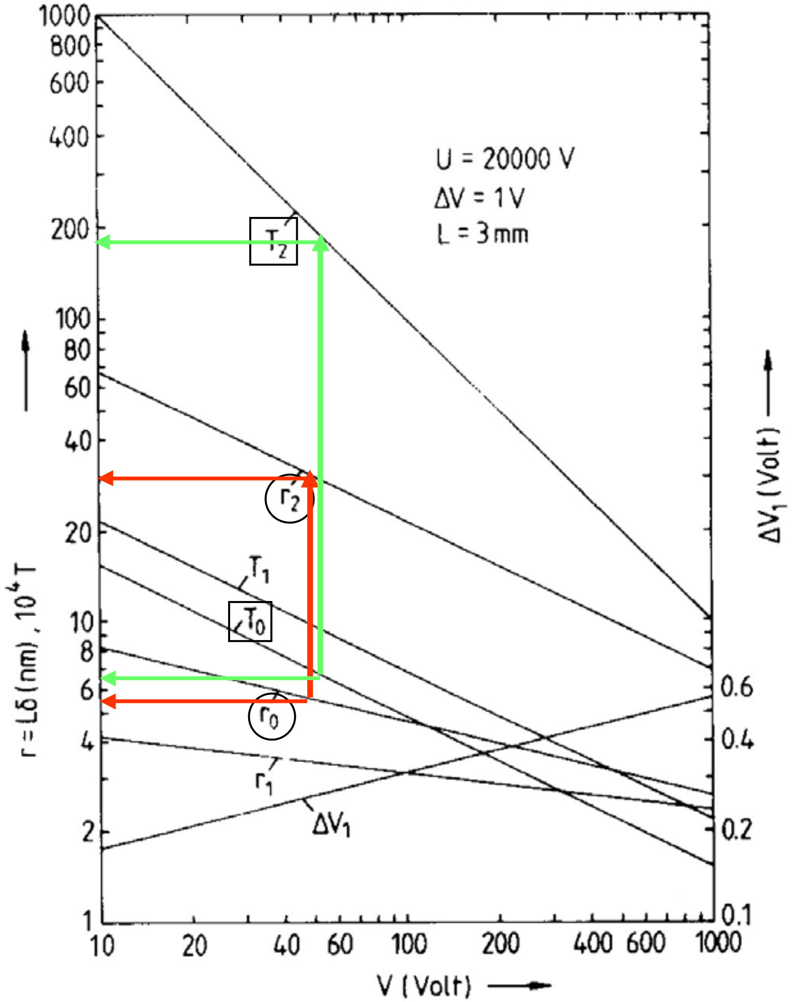

T_2

T and d equally weighted:

50 eV:
$\Delta T \cong 30$
$\Delta d \cong 5$

E. Bauer, Ultramicroscopy 36 (1991) 52

Influence of angle-limiting aperture on the energy distribution of secondary electrons

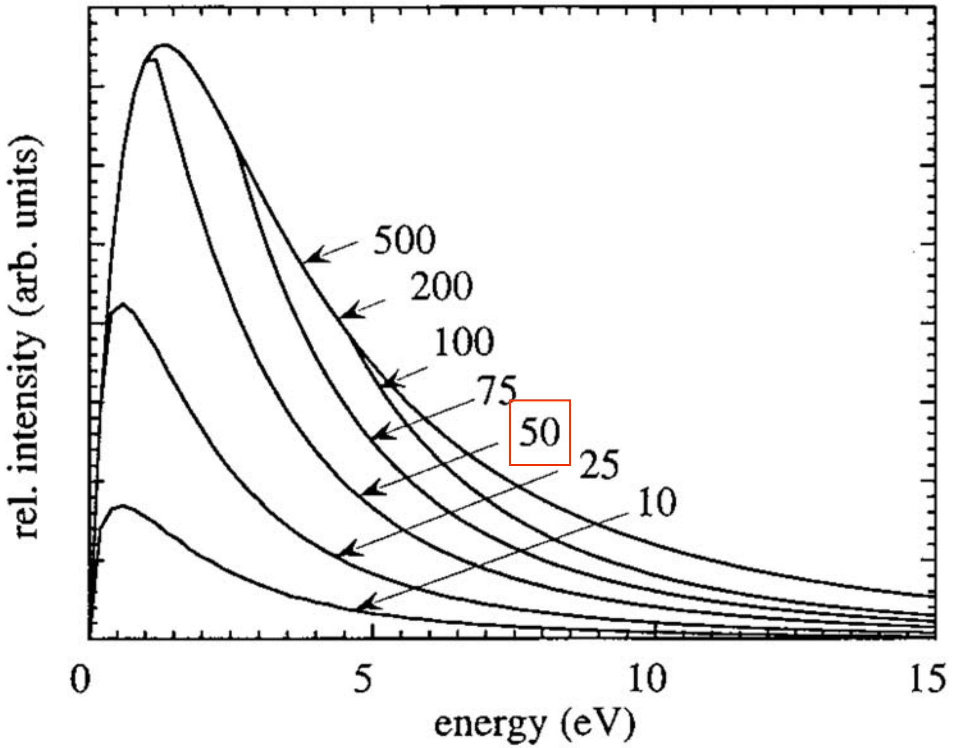

Work function Φ = 4 eV, accelerating voltage V = 20 kV
Parameter: aperture diameter in μm, ALS PEEM

S. Anders et al, Rev. Sci. Instrum. 70 (1999) 3973

Aberration correction in electron optics

Round **convex** lenses

electrostatic mirror

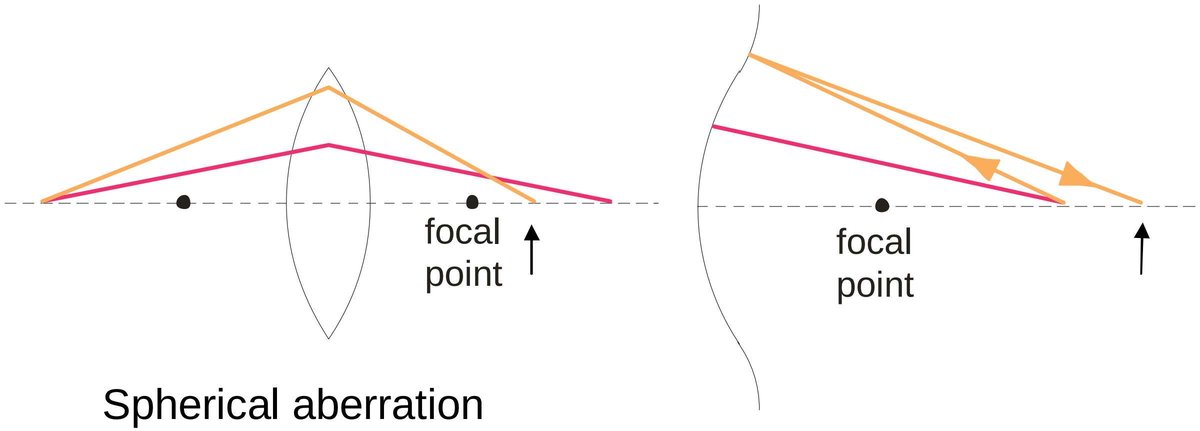

Spherical aberration

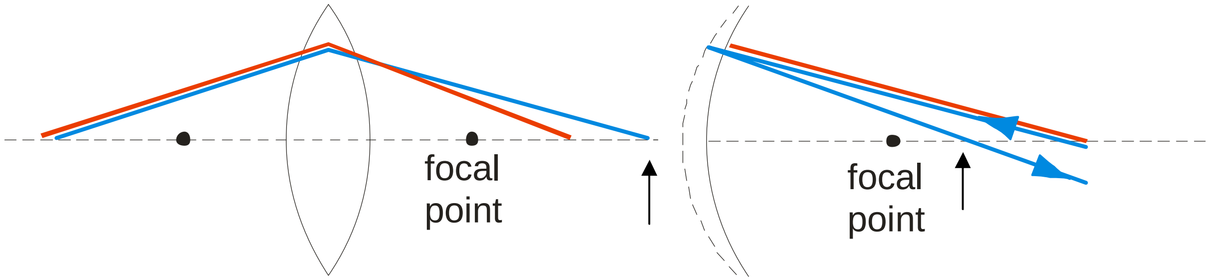

Chromatic aberration

Equipotential surfaces
in a diode mirror

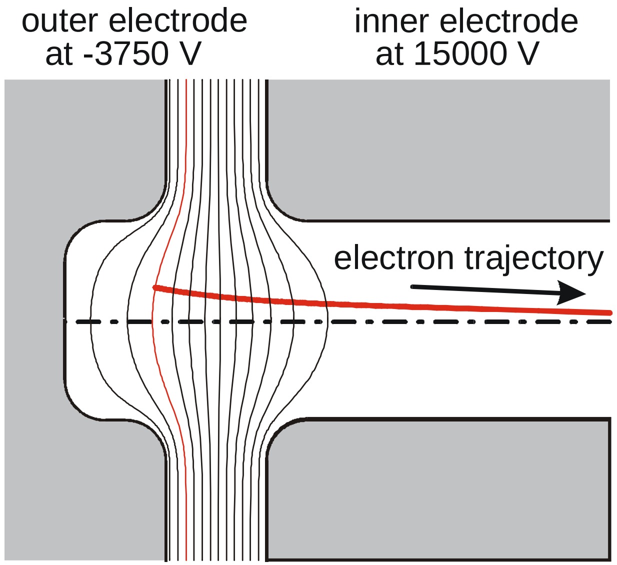

Resolution and transmission improvement with aberration correction

Example: SMART

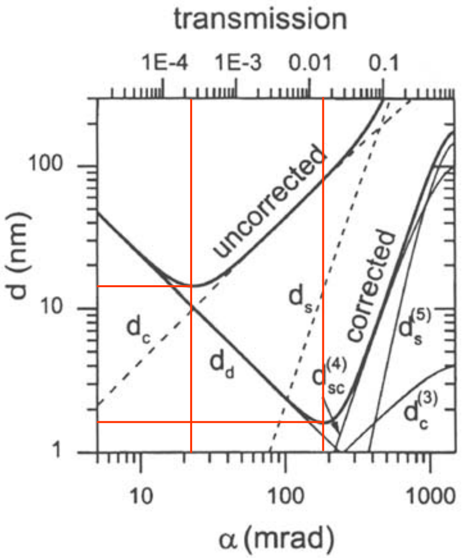

E_0 = 10 eV, ΔE = 2 eV, F = 5 kV/mm

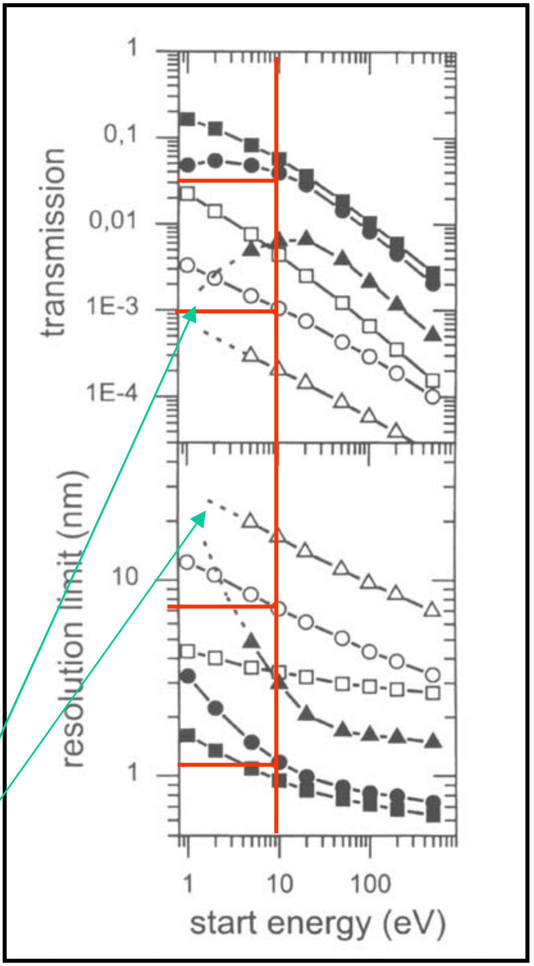

ΔE (eV)		
0.1	□	■
1.0	○	●
5.0	△	▲
	without	with

correction

Energy filter needed for secondary electrons

Calculations: D. Preikszas
From Th. Schmidt et al,
Surf. Rev. Lett. 9 (2002) 223

Instruments

Basic PEEM schematic

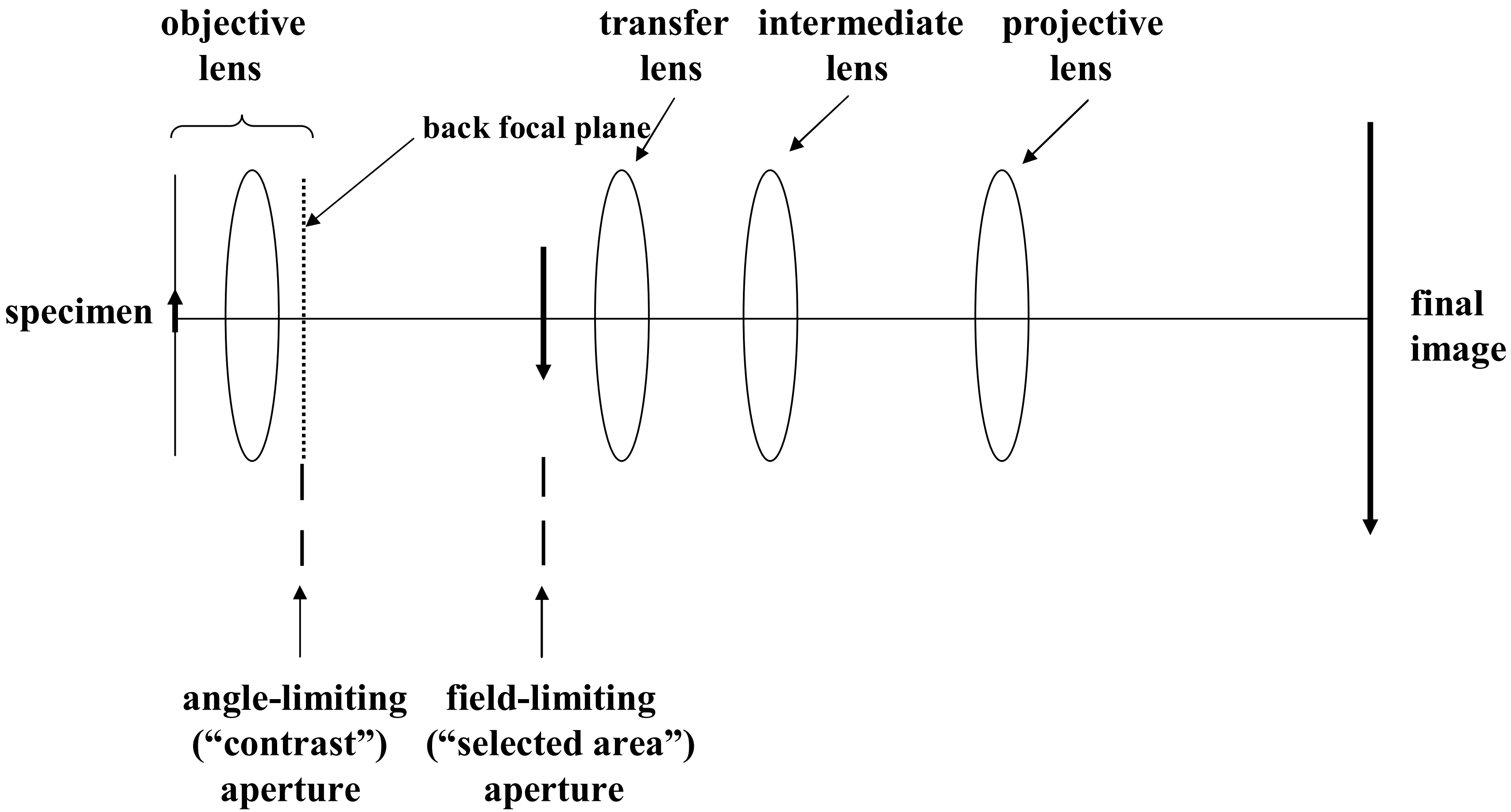

Electrostatic PEEM examples

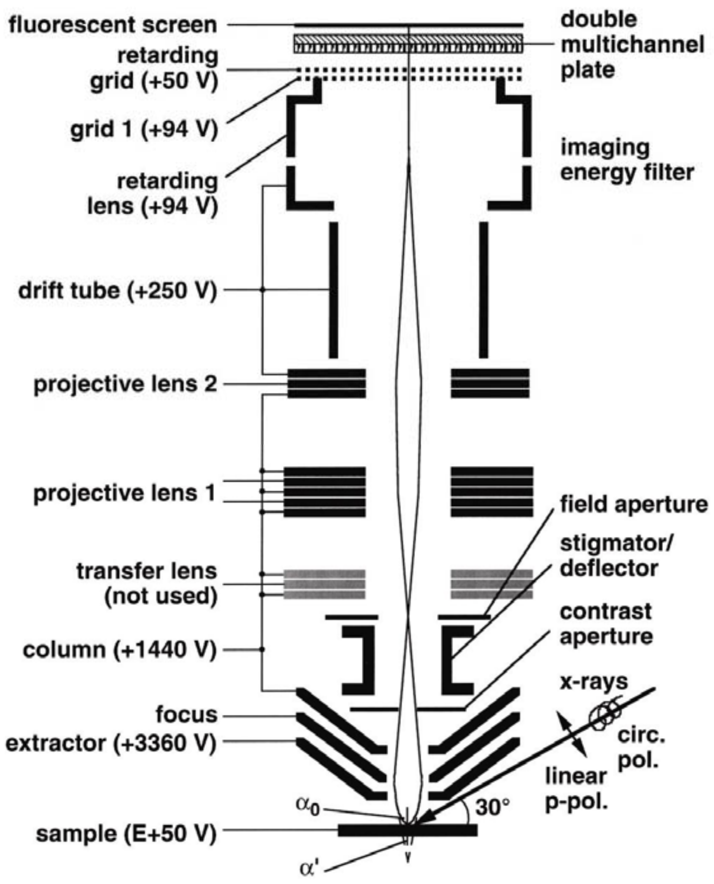

Focus PEEM
with high pass filter

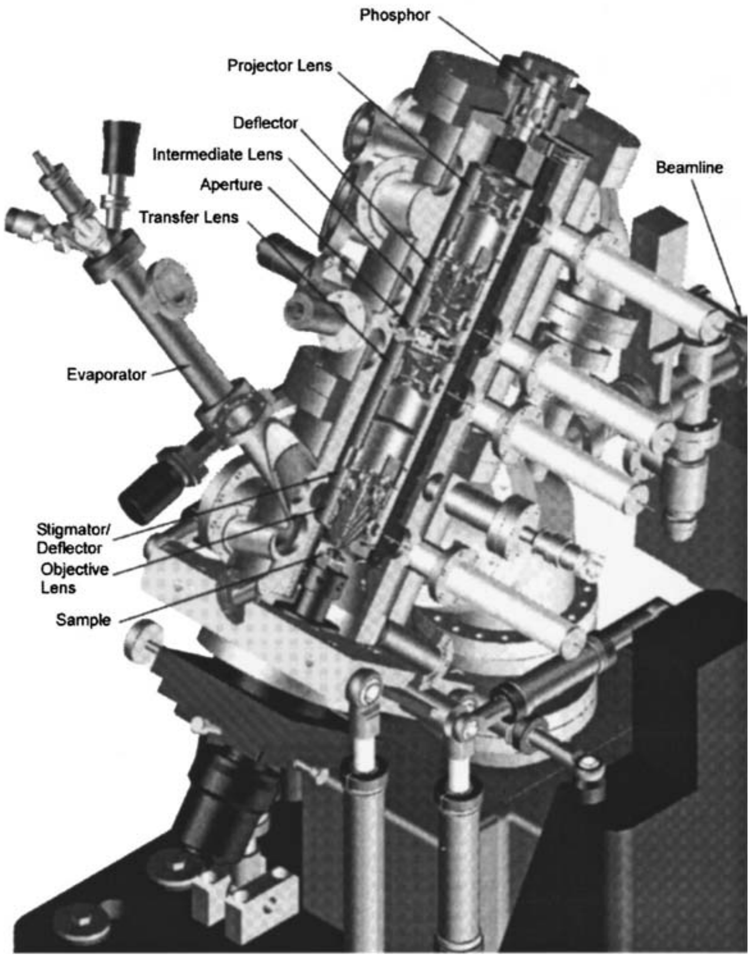

ALS PEEM II

Magnetic PEEM (ELMITEC)

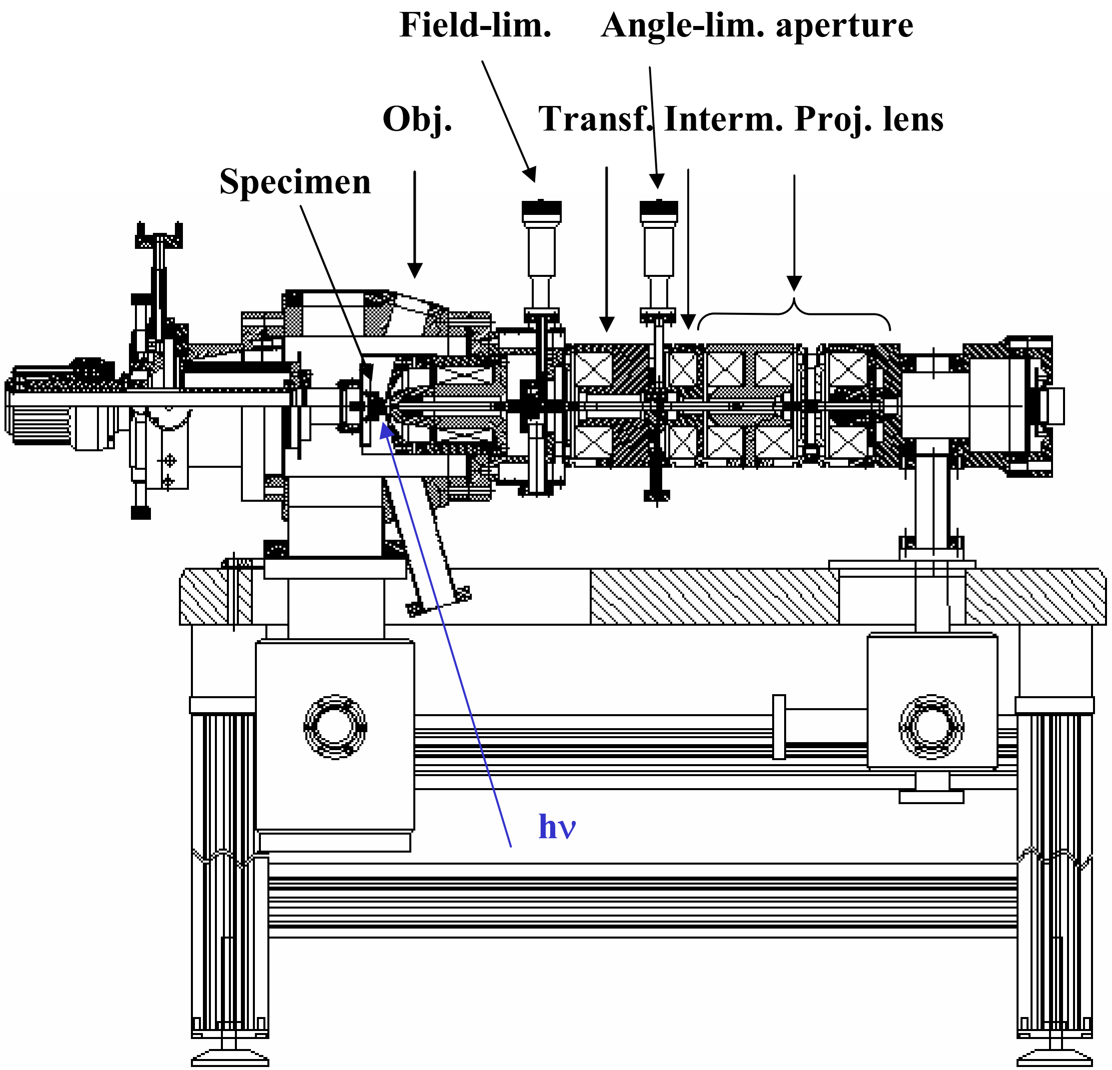

Spectroscopic PEEM with band pass filter

ELMITEC

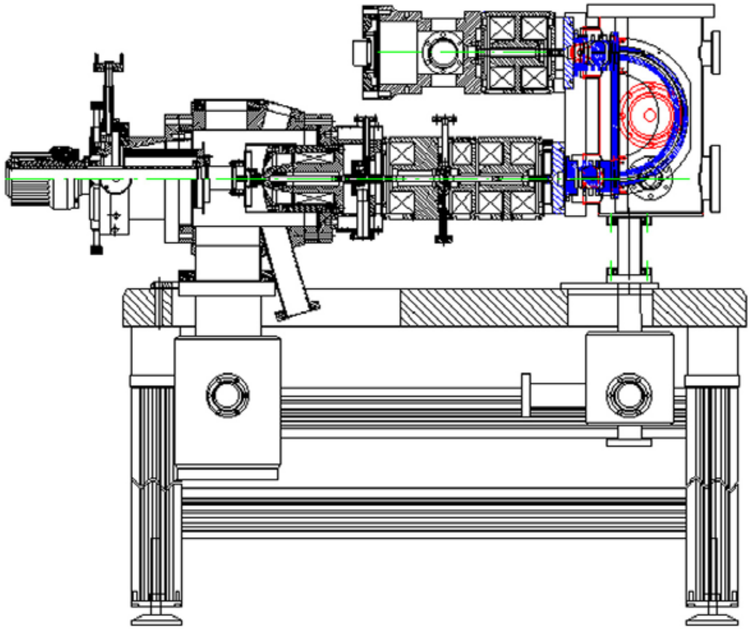

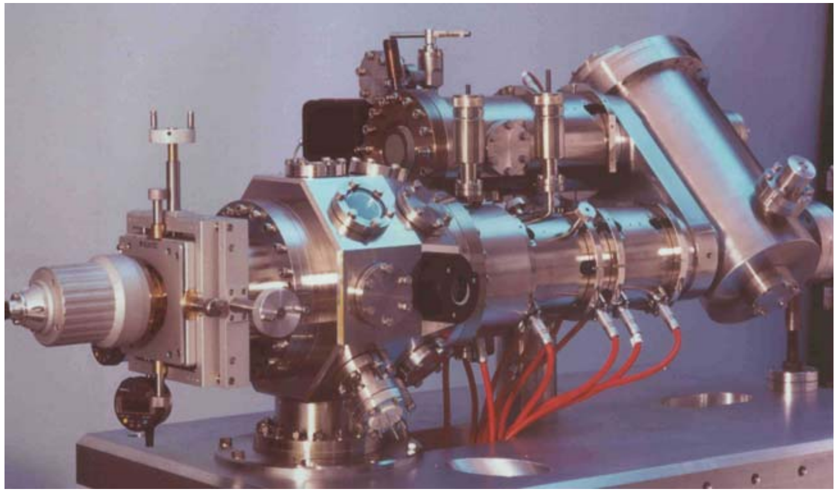

Contrast mechanisms

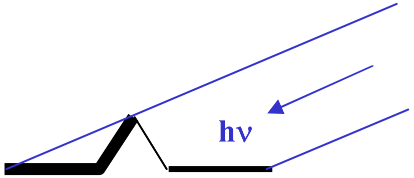

1 **Topographic contrast due to oblique illumination and field distortion**

2 **Work function contrast at low E_0 (escape probability!)**

3 **Chemical contrast due to inner shell ionization**

4 **Magnetic contrast via XMCD and XMLD**

No structural contrast, therefore combination with
Low Energy Electron Microscopy
(LEEM)

The usefulness of LEEM

Properties not visible with PEEM, but with LEEM

atomic steps

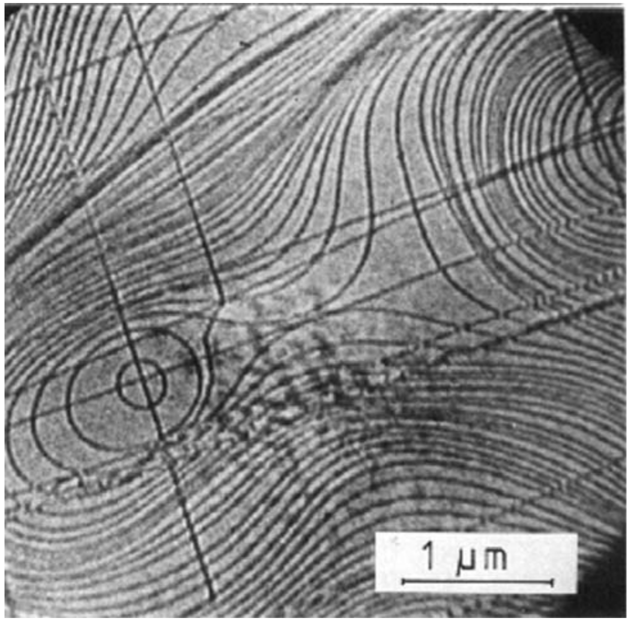

Mo(110)

Interference contrast

domain orientations

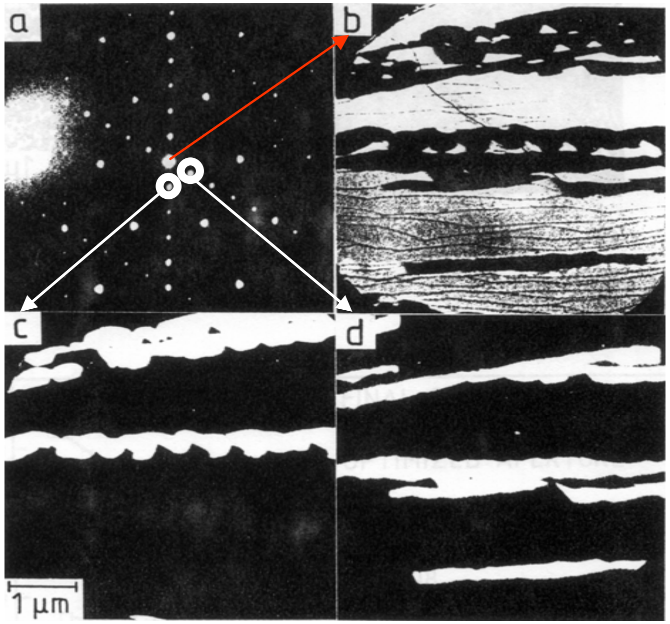

Au(√3×√3)-R30° + Au(5 ×2) on Si(111)
b c,d

Diffraction contrast

LEEM also much brighter and better resolution ⇒ use for focusing in XPEEM

LEED much easier to interpret than PED ⇒ use for structure analysis

Basic LEEM schematic

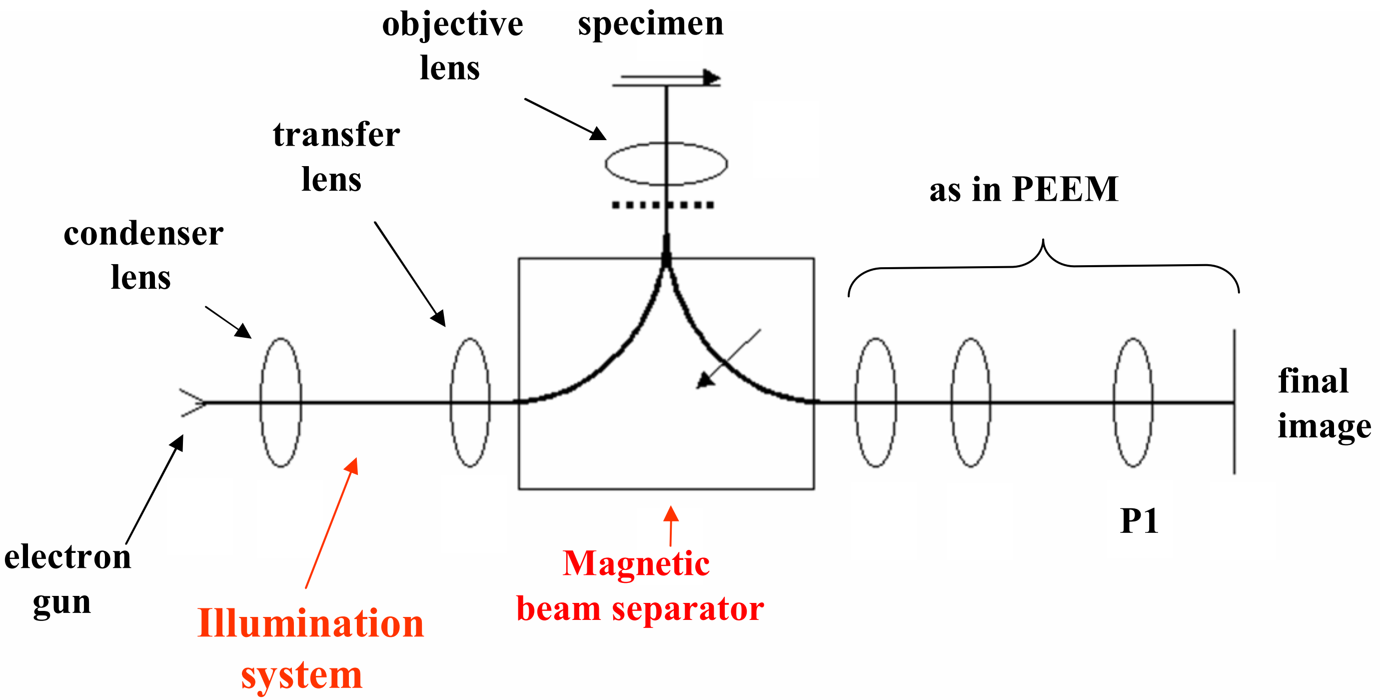

objective lens

specimen

transfer lens

condenser lens

as in PEEM

final image

P1

electron gun

Illumination system

Magnetic beam separator

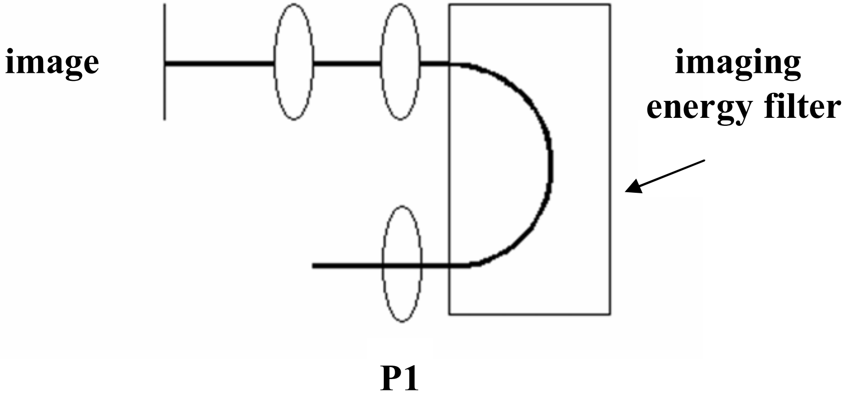

image

imaging energy filter

P1

Spectroscopic Photo Emission and Low Energy Electron Microscope

SPELEEM

ELMITEC

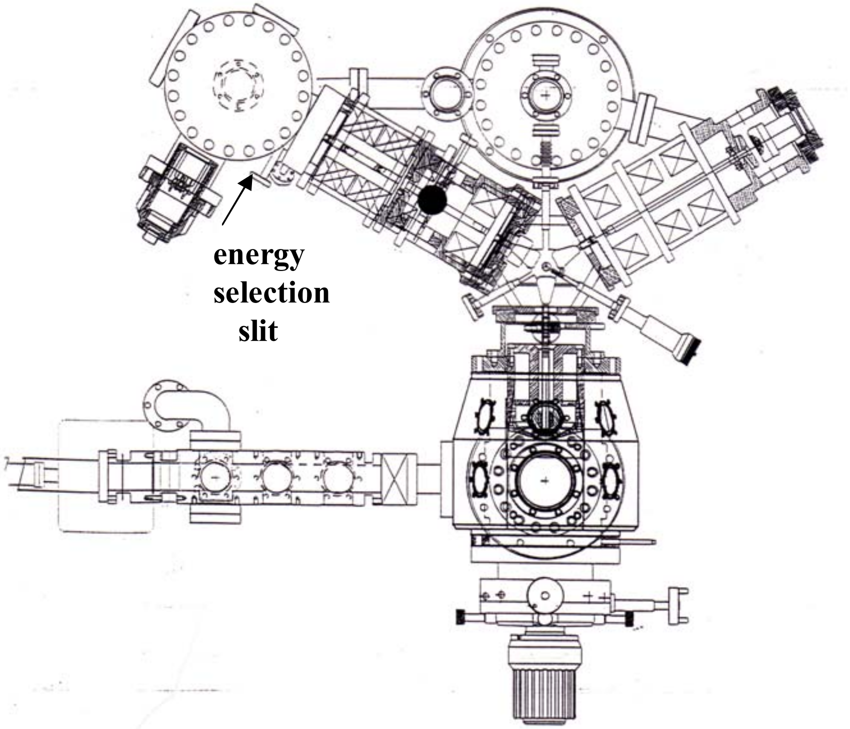

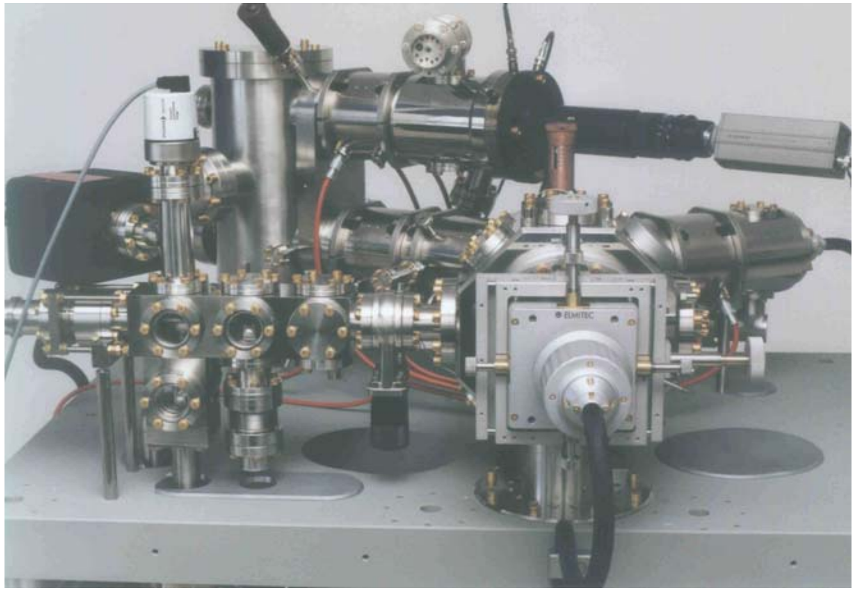

SPELEEM side view

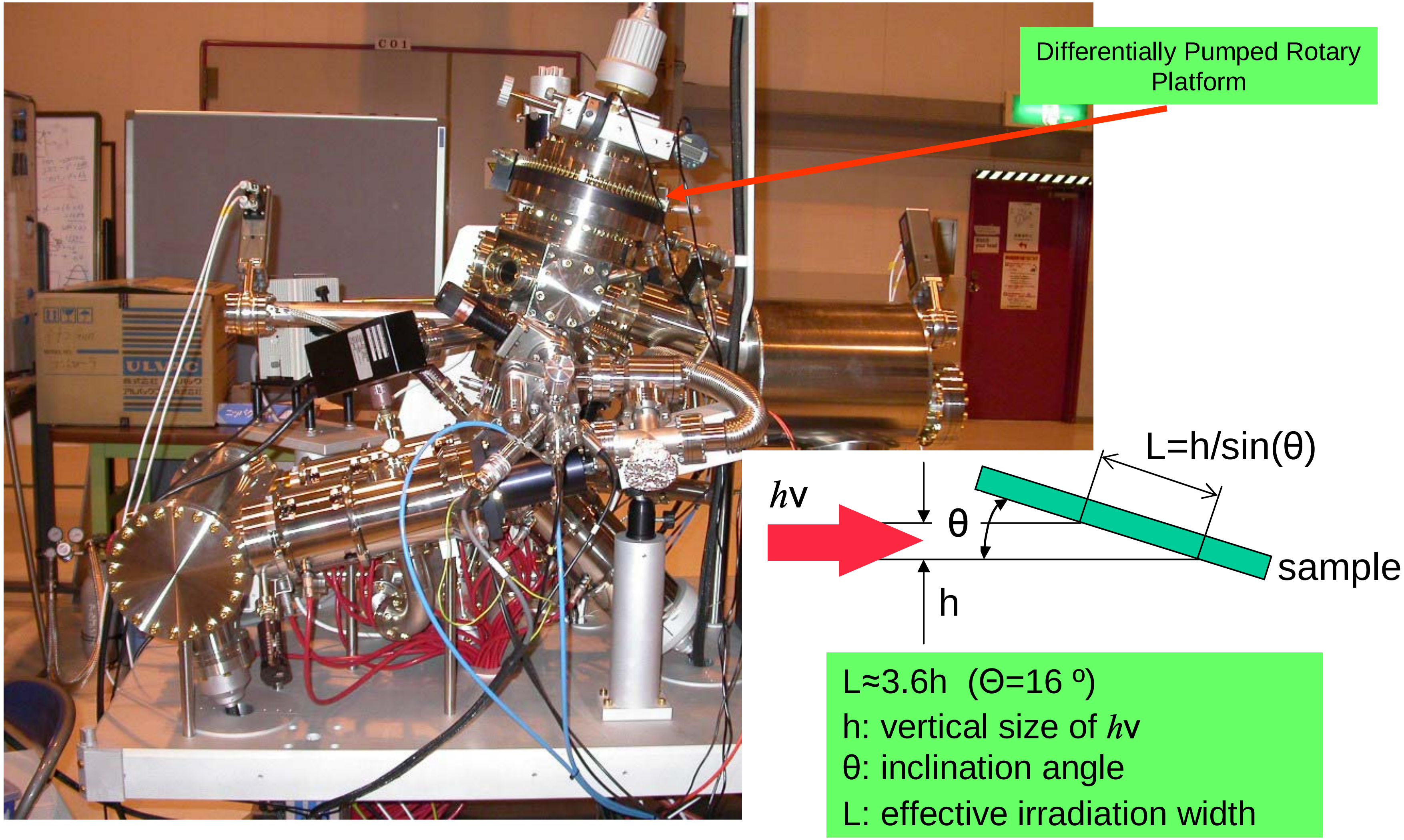

L≈3.6h (Θ=16 º)

h: vertical size of *h*ν

θ: inclination angle

L: effective irradiation width

SPring8

Future Soleil XPEEM

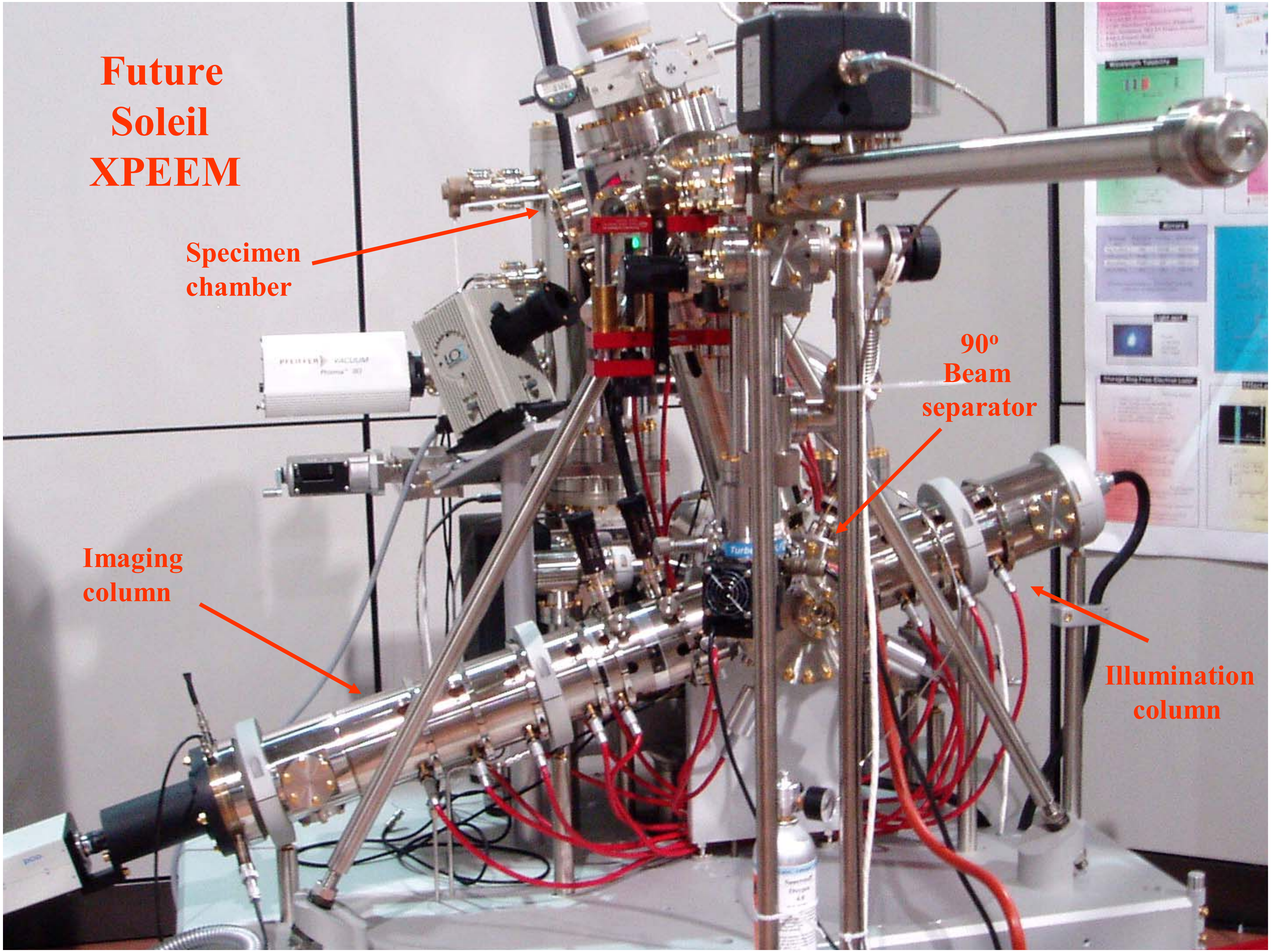

Specimen chamber

90^{o} Beam separator

Imaging column

Illumination column

LEEM with energy filter

JEOL

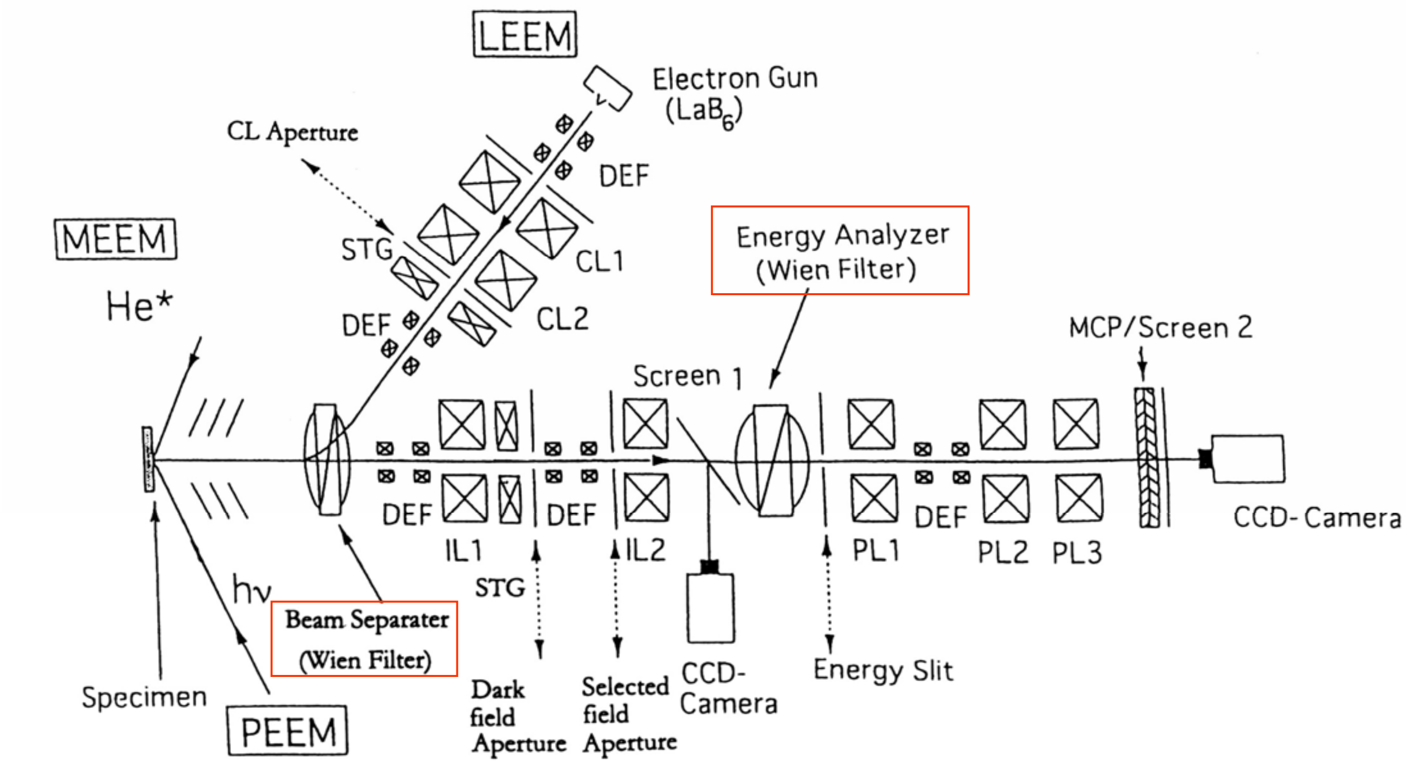

Y. Sakai et al, Surf. Rev. Lett. 5 (1998) 1199

Aberration-corrected SPELEEM

SMART (BESSY II)

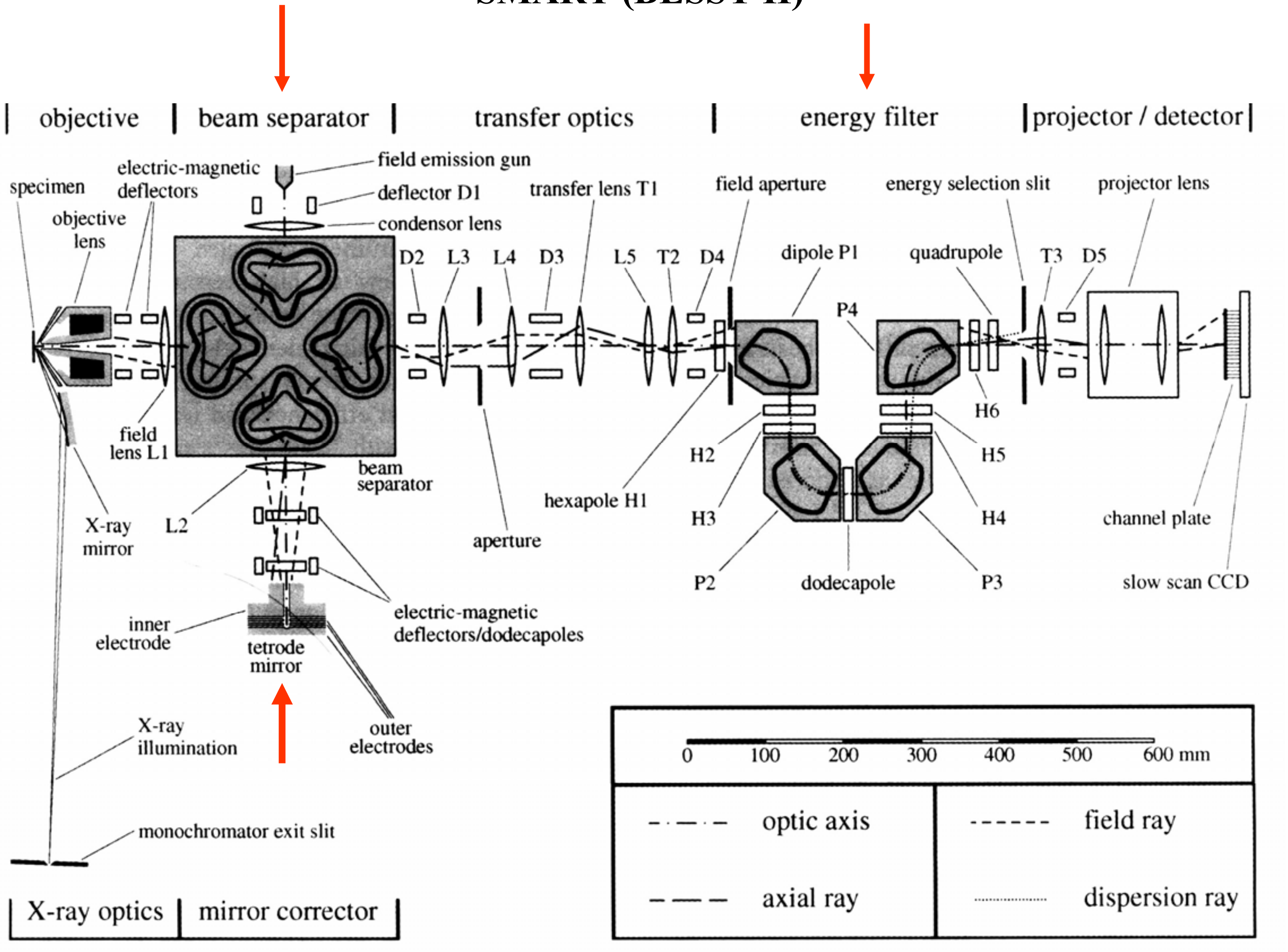

H. Rose, D. Preikszas, Nucl. Instr. & Meth. A363, 201 (1995)

SMART side view

Aberration corrected PEEM/LEEM with energy filtering

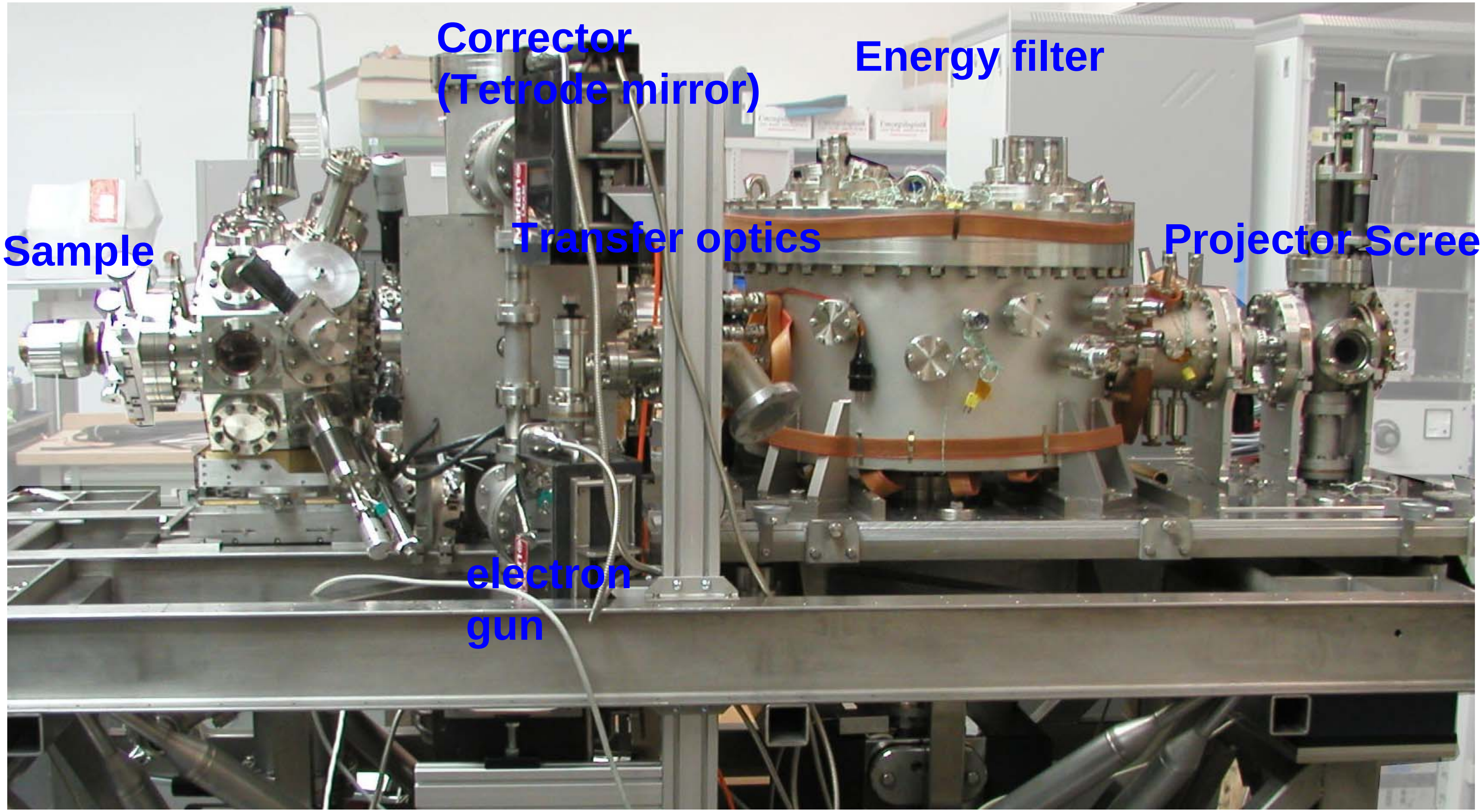

Th. Schmidt April 2004

SMART top view

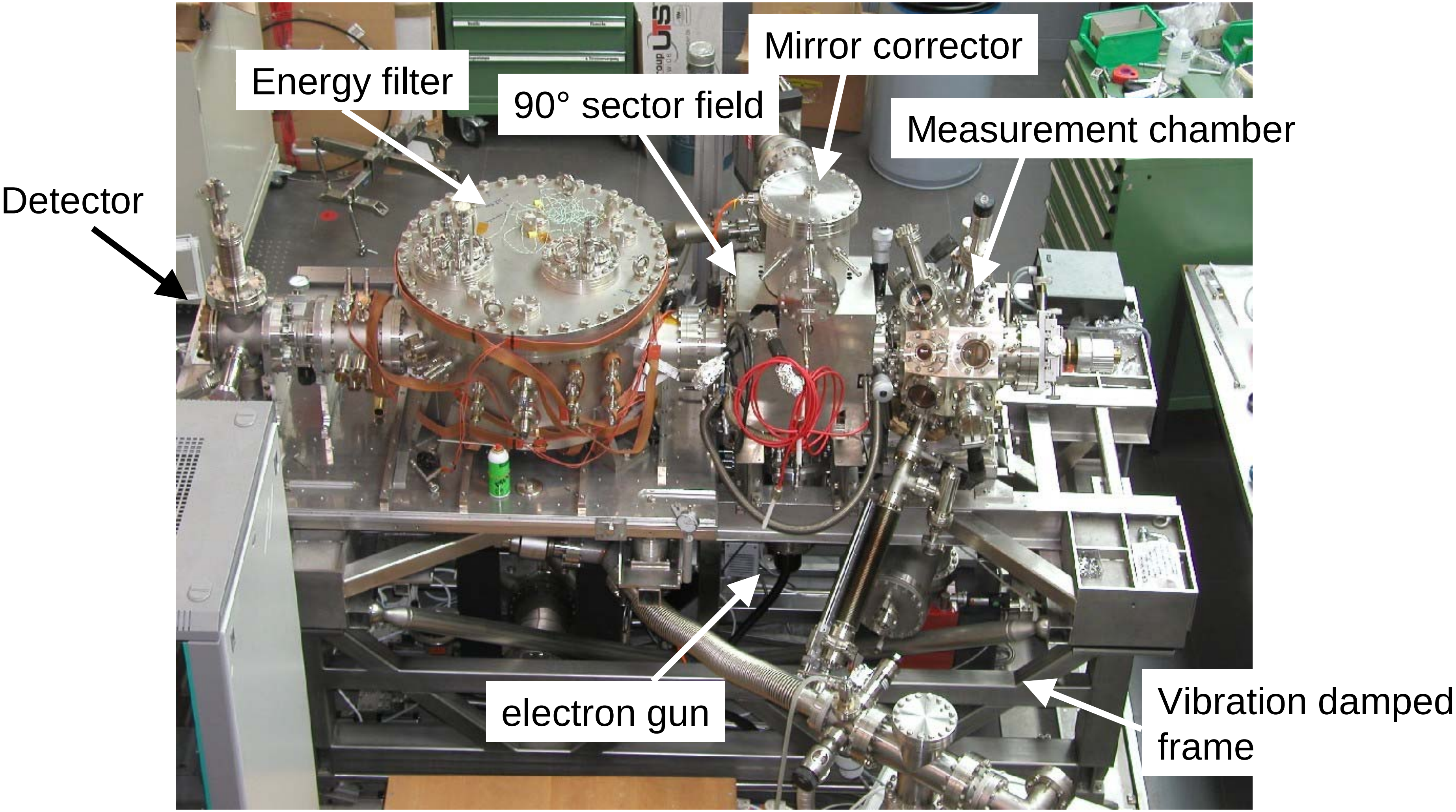

Th. Schmidt April 2004

Methodic

Operation modes of a SPELEEM

LEEM

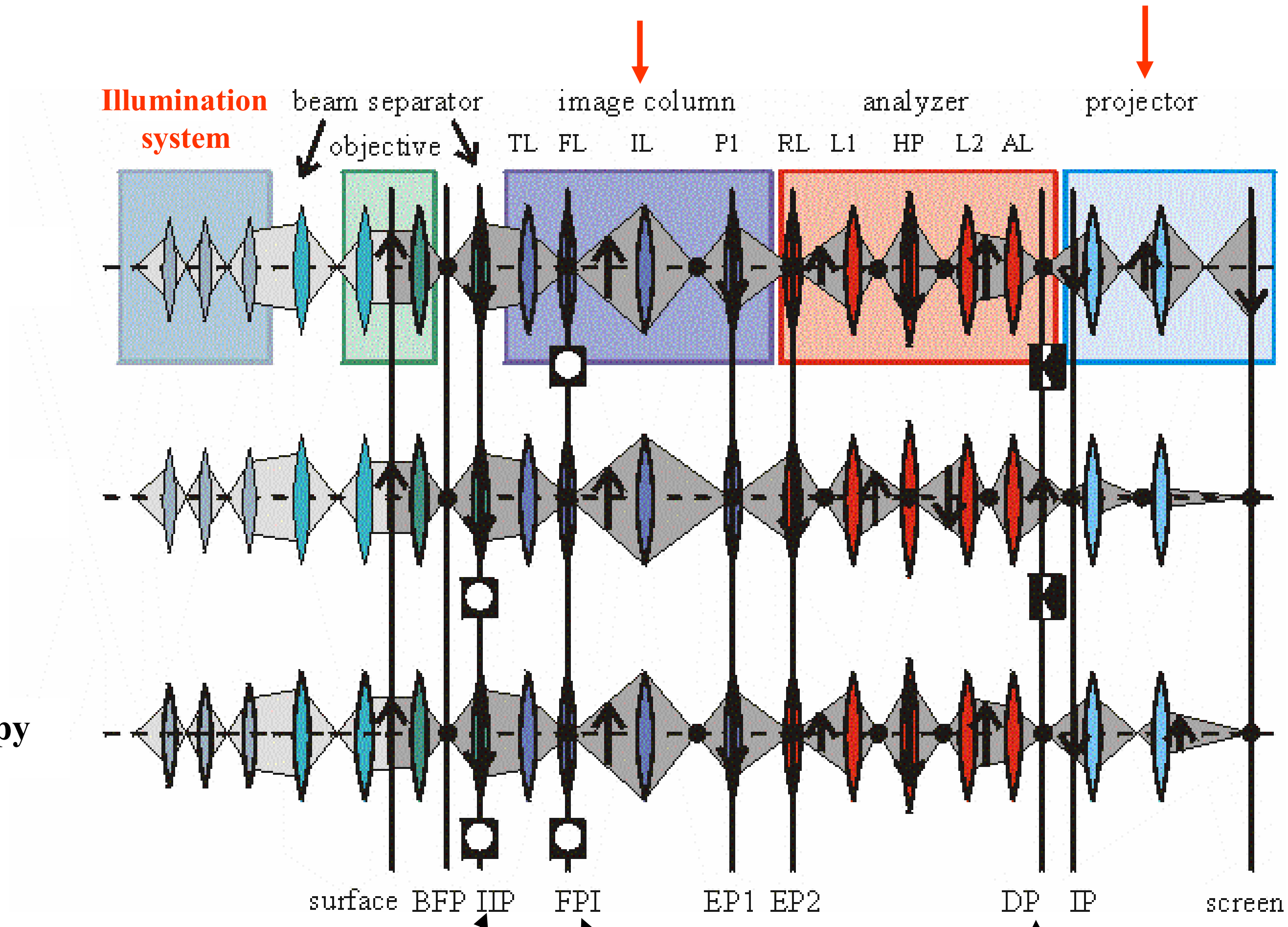

imaging — **LEEM**

diffraction — **LEED**

spectroscopy — **AES**
ELS

field
angle
limiting aperture

energy selection
slit

Th. Schmidt et al, Surf. Rev. Lett. 5 (1998) 1287

Operation modes of a SPELEEM with photons

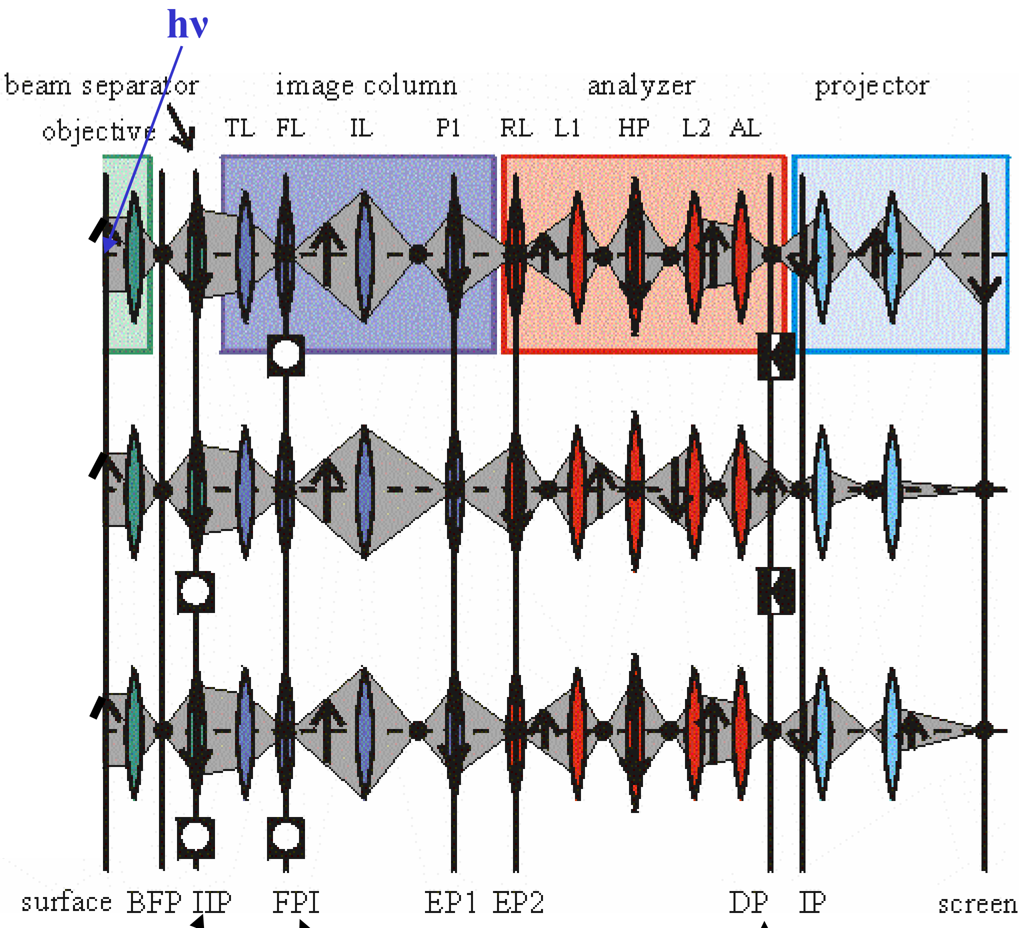

imaging — XPEEM

diffraction — XPD (PED)

spectroscopy — XPS (PES)
AES

field
angle
limiting aperture

energy selection
slit

Th. Schmidt et al, Surf. Rev. Lett. 5 (1998) 1287

PEEM practice

Ultrahigh vacuum (low 10^{-10} torr range)
but experiments up to 10^{-5} torr range possible

Surface cleaning: heating, sputtering or chemical reactions, e.g with oxygen for carbon removal

Choice of optimum photon energy:

Secondary electron imaging: $h\nu \approx E_i$ in:
XANES, NEXAFS, XMCD, XMLD

Photo electron imaging: $E_i + 50\ \text{eV} < h\nu < E_i + 200\ \text{eV}$

to minimize
secondary electron
background

to maximize
transmission
and
photo electron yield

Photo ionization cross sections

Photon energy selection

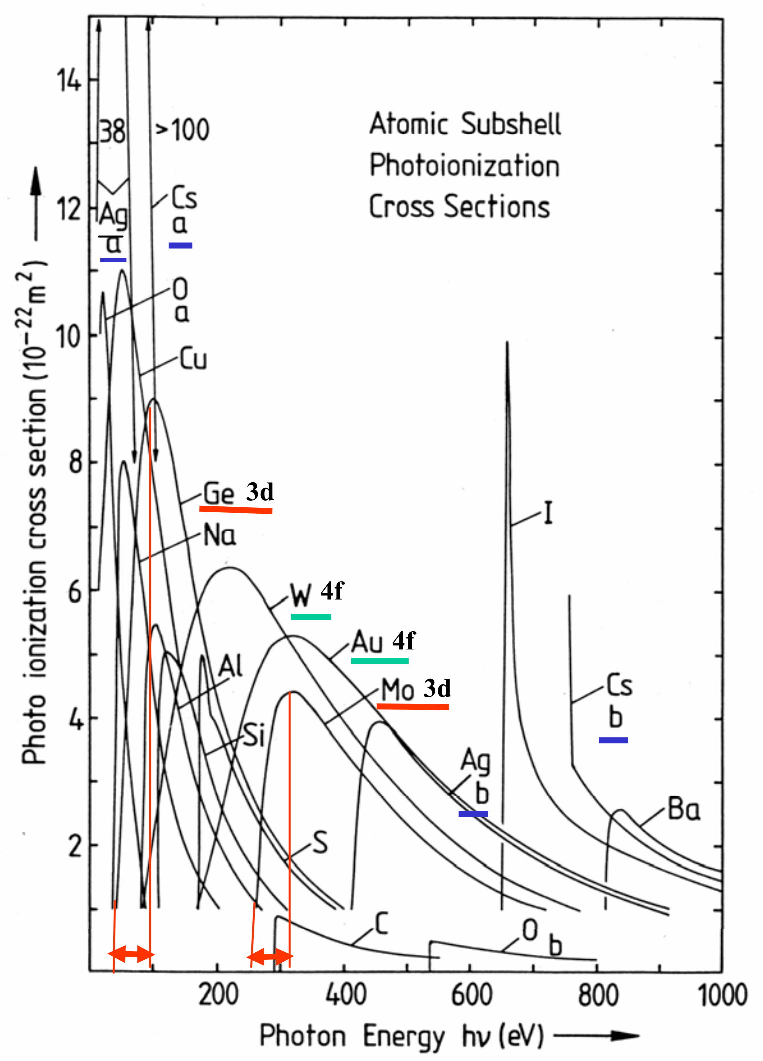

Binding energies (eV)

Ge 3d	29.8, 29.2
Mo 3d	231.1, 227.9
W 4f	33.6, 31.4
Au 4f	87.6, 84.0
Ag	
a 4d	≈ 5
b 3d	374.0, 368.3
Cs	
a 4d	79.8, 77.5
b 3d	740.5, 726.6

J.J. Yeh and I. Lindau,
Atomic Data 1985

Operation modes of a SPELEEM

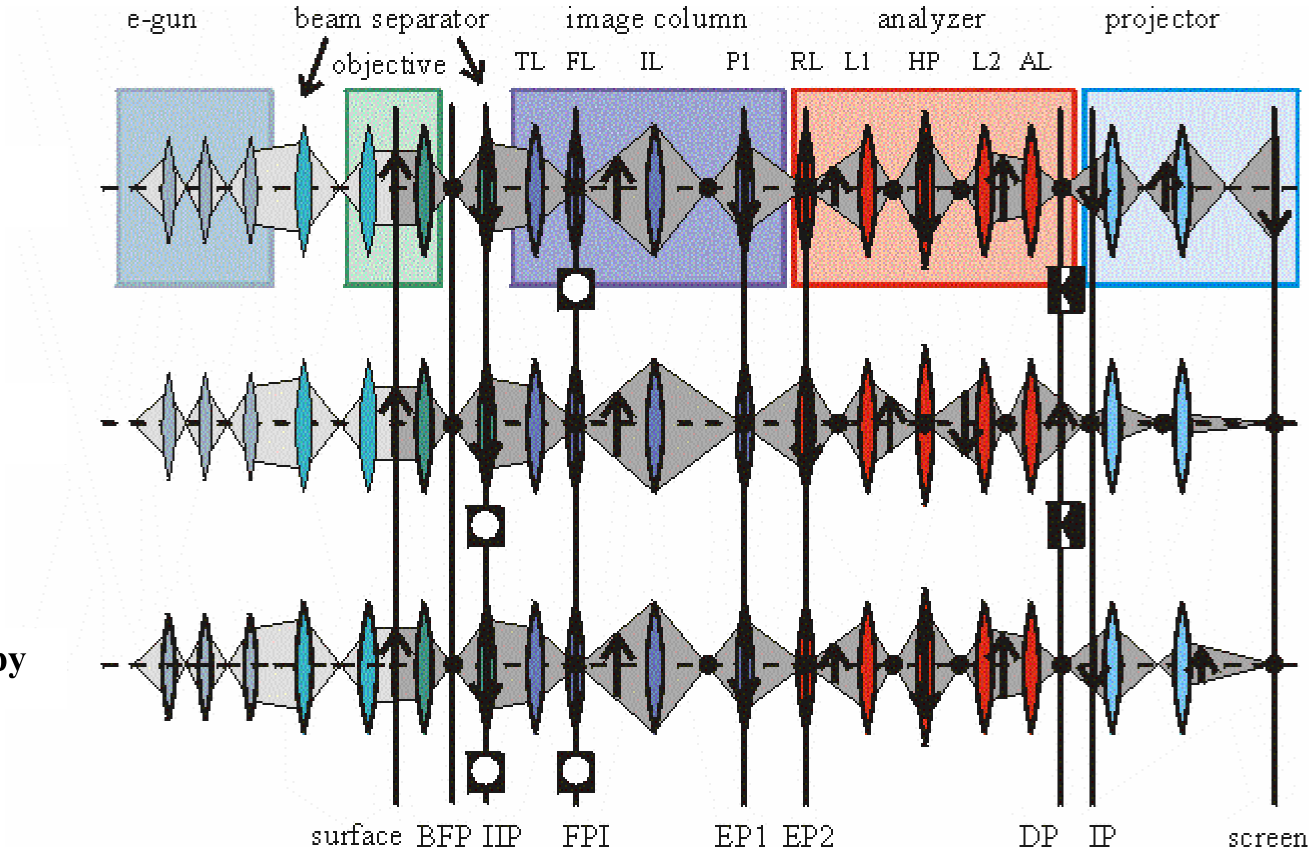

imaging

mode 1

XPEEM

LEEM

diffraction

XPD (PED)

LEED

spectroscopy

XPS (PES)

AES

ELS

field

angle

limiting aperture

energy selection slit

Image plane

Th. Schmidt et al, Surf. Rev. Lett. 5 (1998) 1287

Chemical imaging (mode 1)

secondary electrons
spatial resolution
$\sigma_{Ag4d} \approx 5\, \sigma_{W5d}$
$h\nu = 65\ \mathrm{eV} >> E_i < 10\ \mathrm{eV}$
$\Delta E_F \leq 1\ \mathrm{eV}$

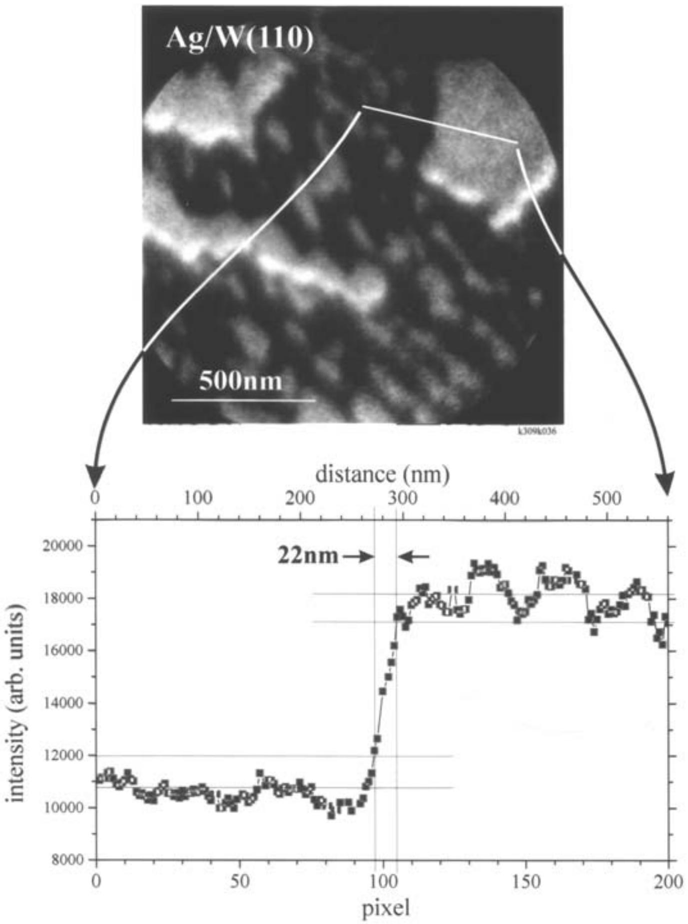

photo electrons
energy resolution
$h\nu = 65$ eV, images in 0.2 eV steps
10-60 sec/image 0.25 μm^2 areas
$\Delta E_F \leq 0.5\ \mathrm{eV}$, $\Delta E_{chem} \approx 0.15\ \mathrm{eV}$

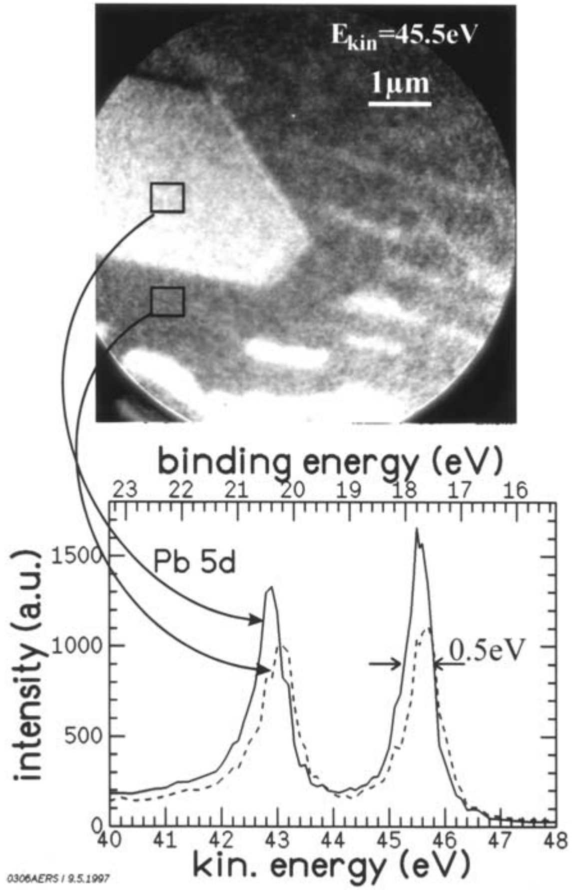

Pb/W(110)

Th. Schmidt et al, Surf. Rev. Lett. 5 (1998) 1287

Operation modes of a SPELEEM

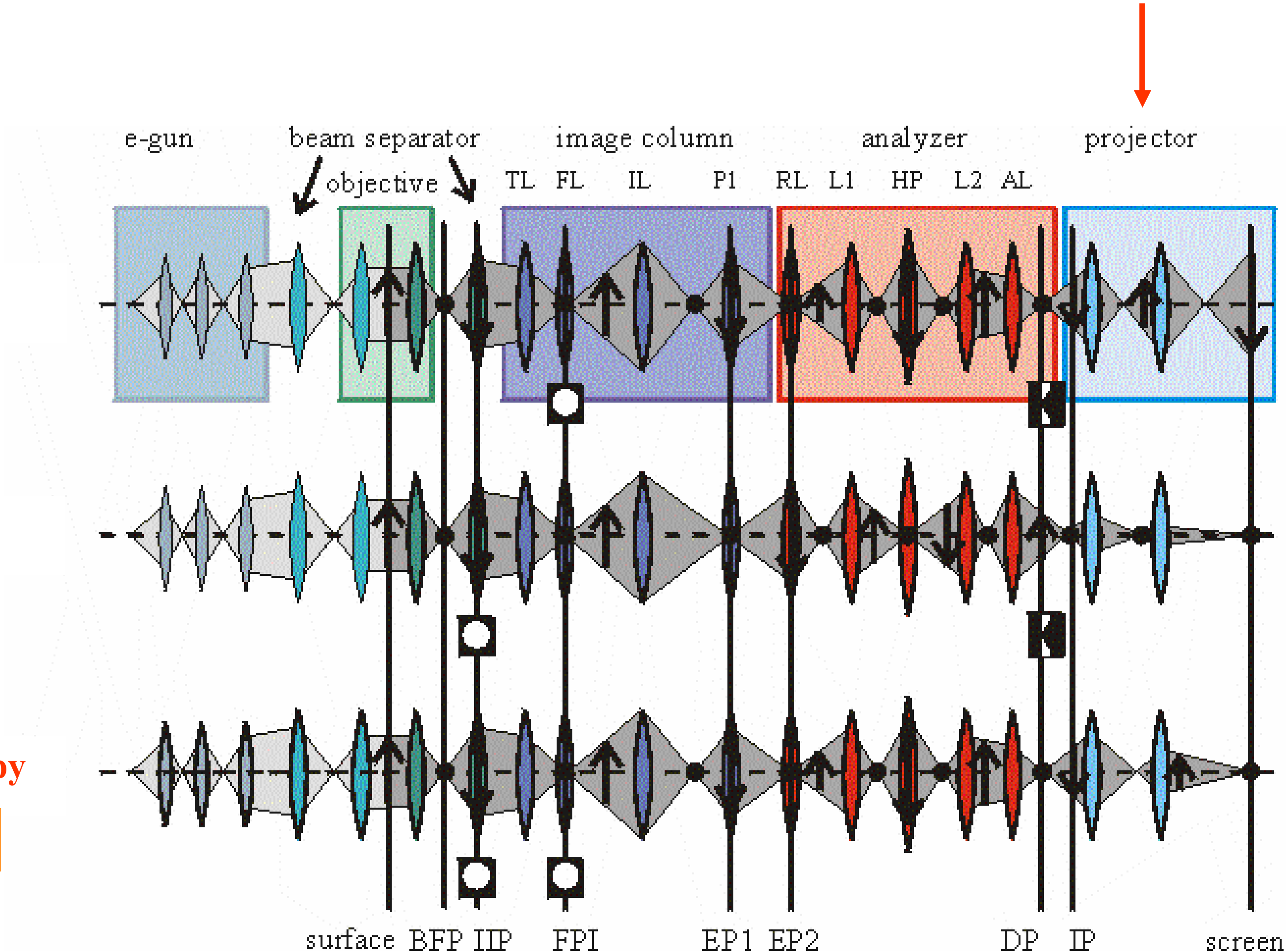

imaging

XPEEM
LEEM

diffraction

XPD (PED)
LEED

spectroscopy

mode 3

XPS (PES)
AES
ELS

field **angle**
limiting aperture

energy selection
slit

Dispersive plane

Th. Schmidt et al, Surf. Rev. Lett. 5 (1998) 1287

Fast local spectroscopy

by imaging the dispersive plane (mode 3)

$\alpha = 8^o$ (contrast aperture), 0.8μm^2 area (selected field aperture)
20 eV full dispersion, 60 sec
$h\nu = 48$ eV

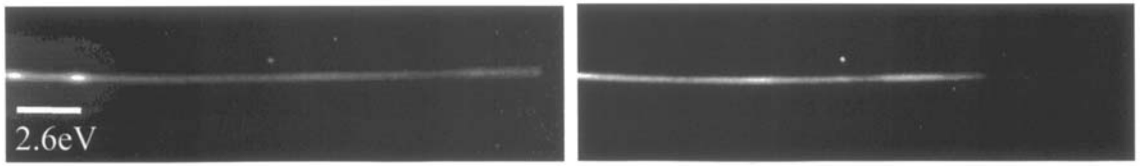

Dispersive plane

8 monolayers
Pb on Si(111)-
$\sqrt{3}\times\sqrt{3}$-Ag

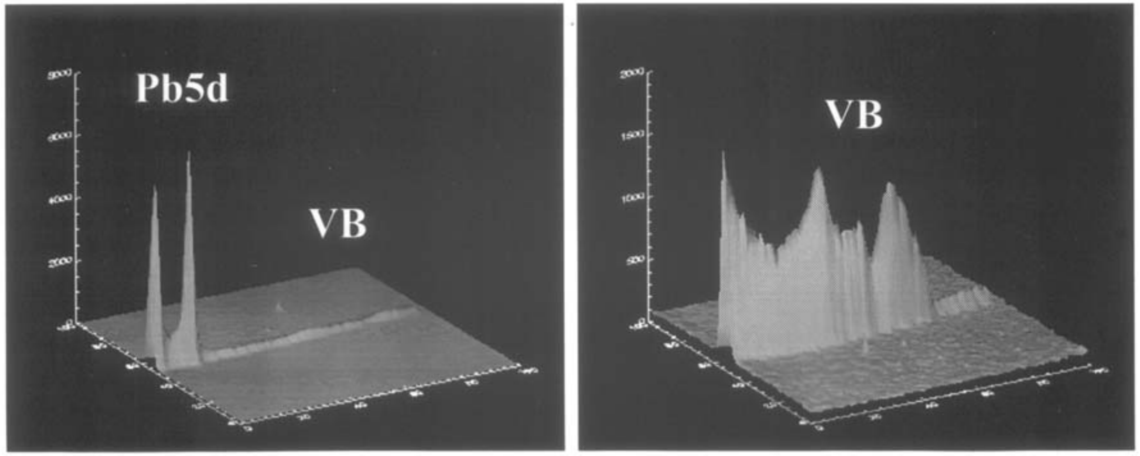

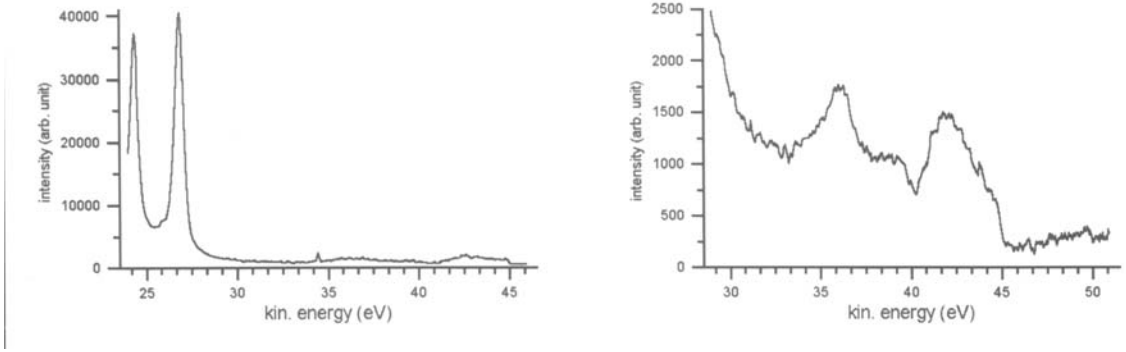

Th. Schmidt et al, Surf. Rev. Lett. 5 (1998) 1287

Surface sensitivity of photo electrons

versus secondary electrons

valence band region

hν = 48 eV

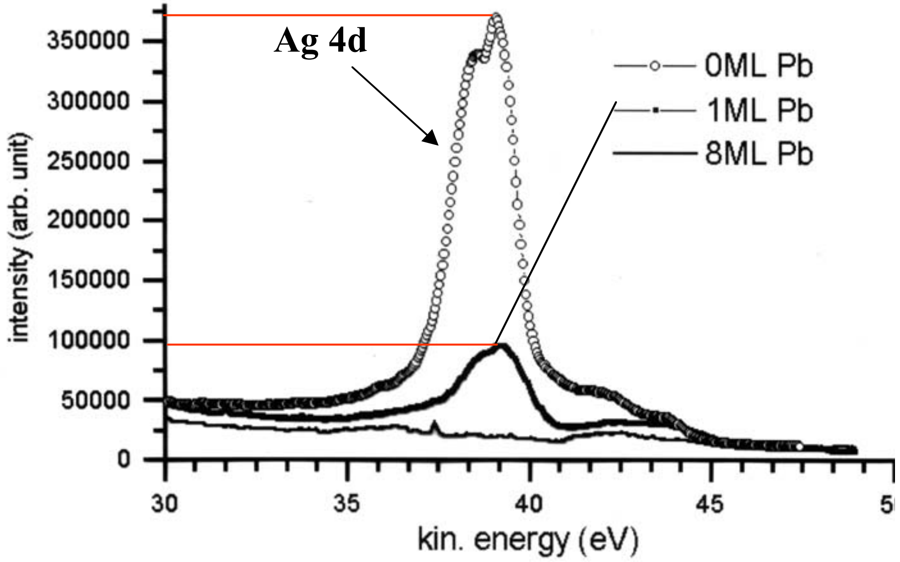

Pb on Si(111) – Ag (√3×√3) – R30°
(1 monolayer Ag)

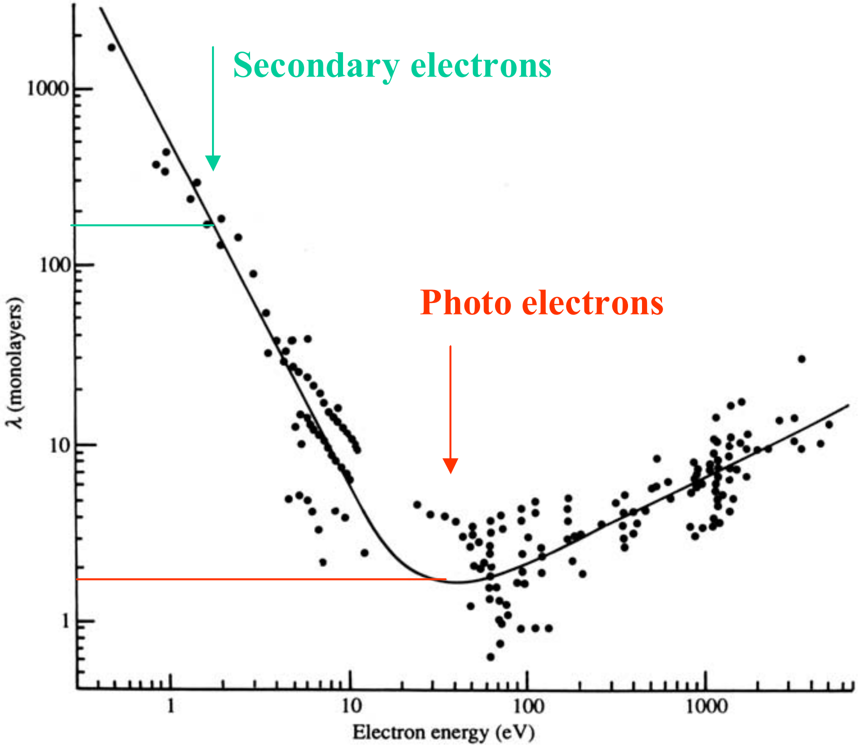

Inelastic mean free path
("universal curve")
determines sampling depth

Th. Schmidt et al, 1998

Operation modes of a SPELEEM

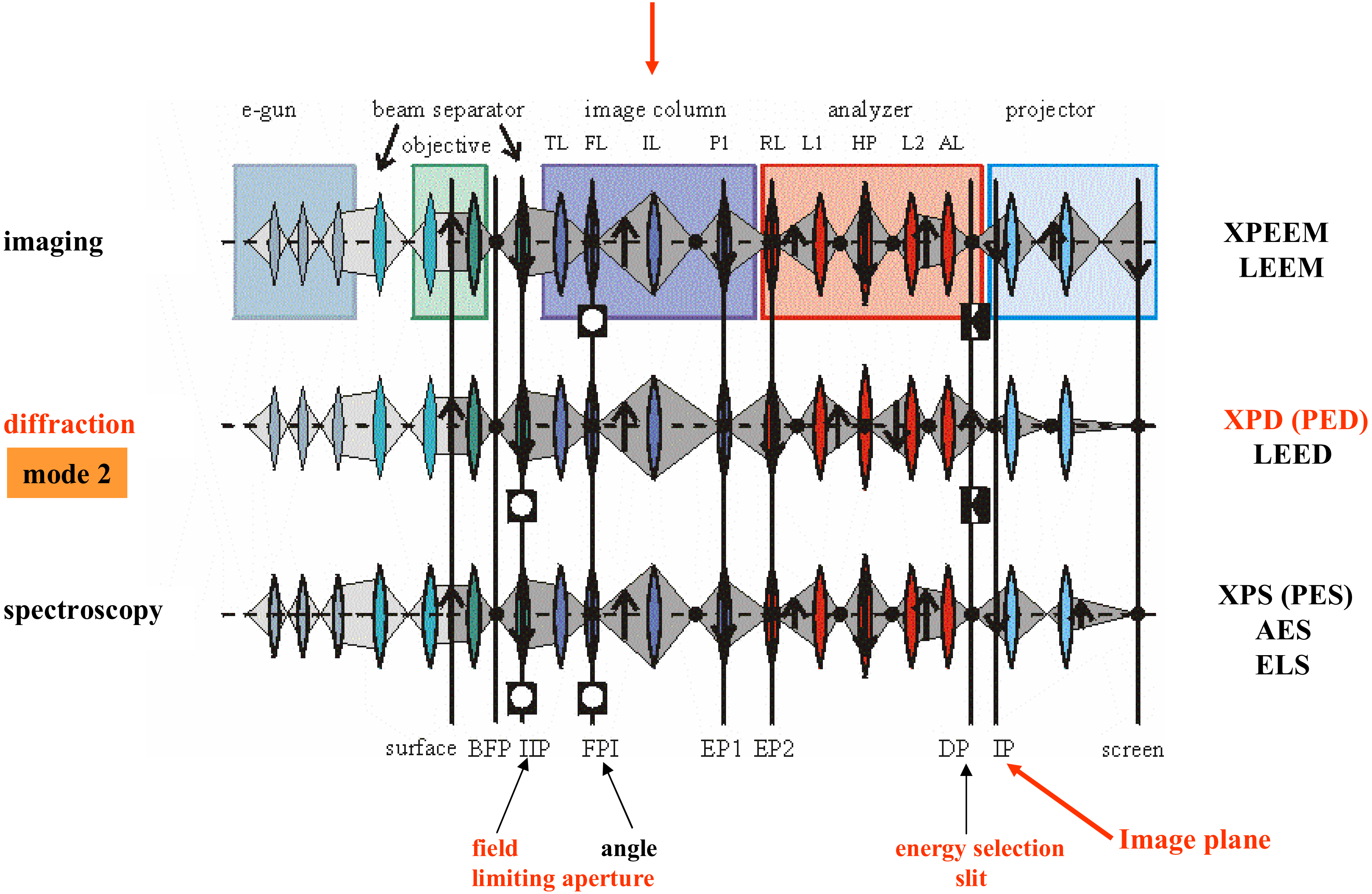

Th. Schmidt et al, Surf. Rev. Lett. 5 (1998) 1287

Local photo electron diffraction (mode 2)

Pb 5d photo electrons

from 0.8µm² area (selected field aperture)

E_{kin}	23.0 eV	28.0 eV	33.0 eV	38.0 eV

$5d_{3/2}$

$5d_{5/2}$

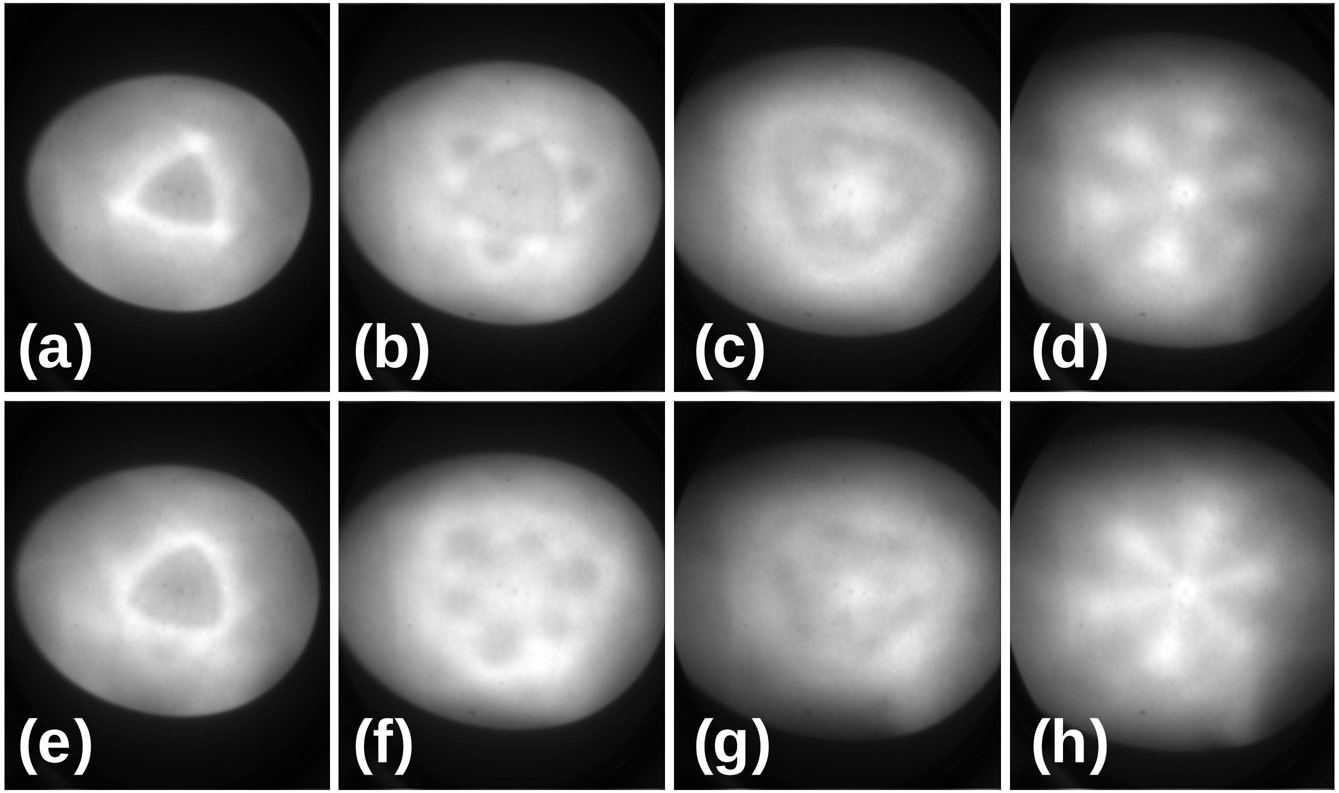

E_{kin}	25.6 eV	30.6 eV	35.6 eV	40.6 eV
hν	43.5 eV	48.5 eV	53.5 eV	58.5 eV

Th. Schmidt et al, Surf. Rev. Lett. 5 (1998) 1287

Simultaneously acquired PED and LEED pattern

Pb 5d 38 eV

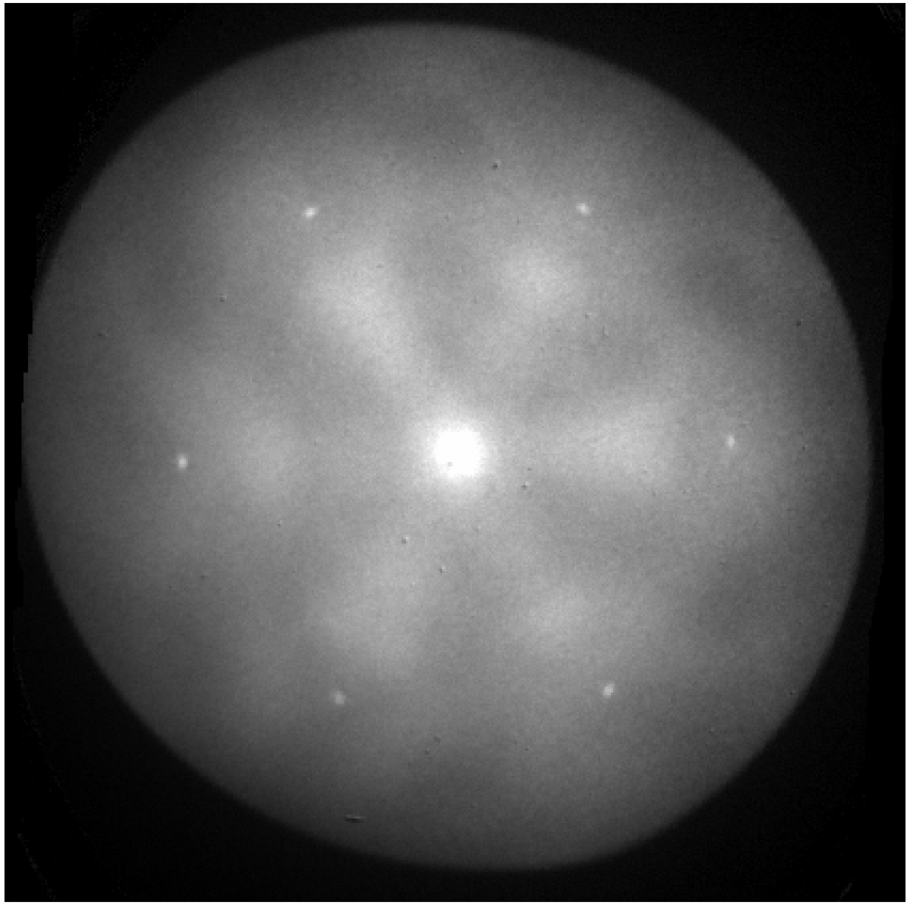

Local band structure analysis (mode 2)

Conduction band of Pb(111)

5 Pb monolayers on Si(111) – Au √3×√3 – R30°

hν = 73 eV, 0.8 μm² area (selected field aperture)

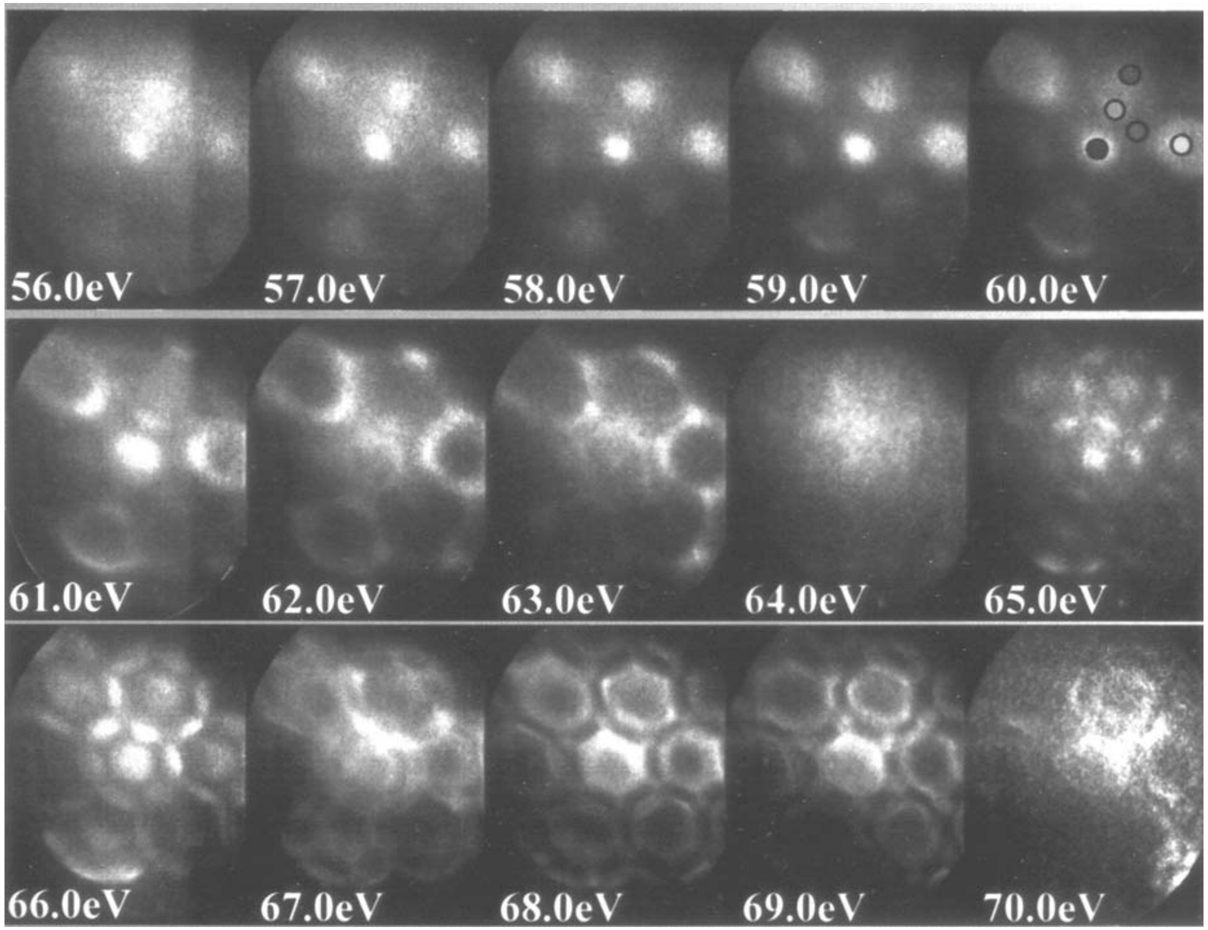

Parameter: E_{kin}

Th. Schmidt, 1997

Magnetic imaging

XMCD, XMLD

Methods

SPLEEM

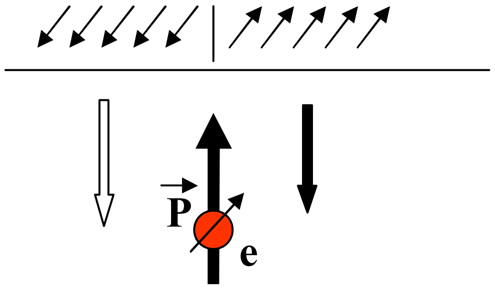

$E_i = E_r = 0 – 20$ eV

$I = I_{0r} + c\,\vec{P} \bullet \vec{M}$

XMCDPEEM

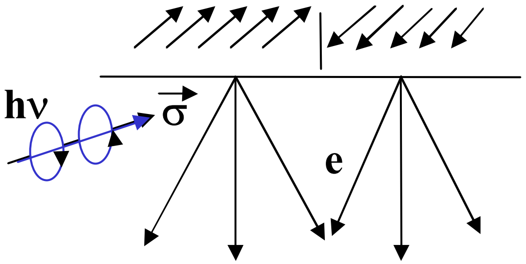

$E_e = 0 – 20$ eV (SE)

$I = I_{0e} + c\,\vec{\sigma} \bullet \vec{M}$

2 images with opposite $\vec{P}$ or $\vec{\sigma}$: I_+, I_-

$I_+ – I_-$ = magnetic image

$I_+ + I_-$

$2\,I_{0r}$

structural image

$|\vec{P}|$ typical 20%

$(I_+ – I_-) / (I_+ + I_-)$

asymmetry image

$2\,I_{0e}$

chemical
topographic
image

$|\vec{\sigma}|$ typical 80%

Basic mechanisms

SPLEEM

Spin-dependent scattering cross-section due to exchange interaction

↓

Spin-dependent reflectivity

6 ML Fe on W(110)

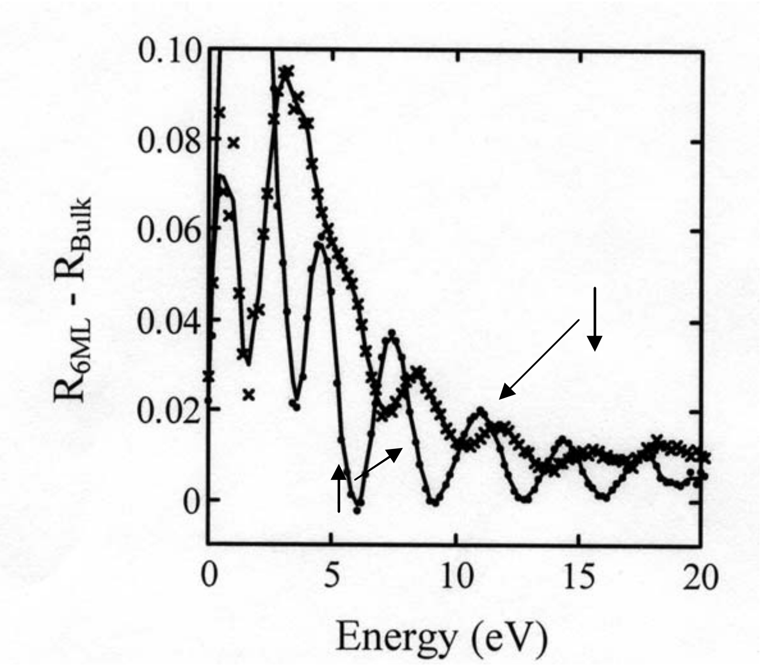

XMCDPEEM

Helicity-dependent transition probability from 2p to unoccupied 3d (↑↓) states

↓

Spin-dependent secondary electron emission

Secondary electron yield around Co $2p_{3/2}$ edge

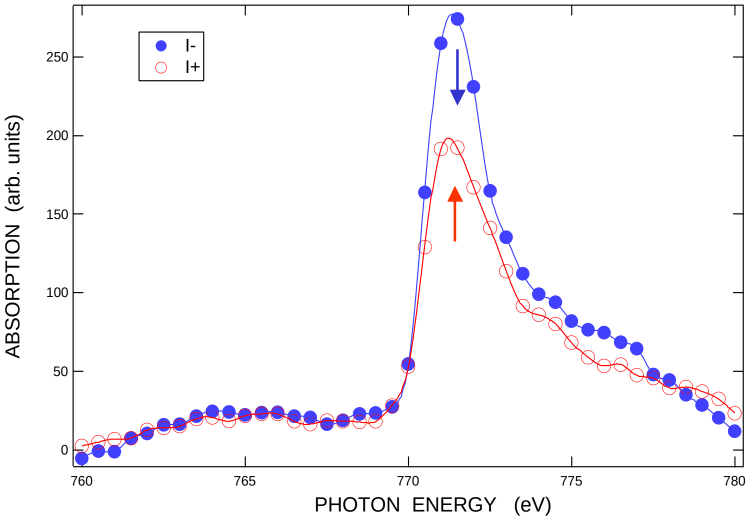

Closure domains in permalloy squares

Ion beam milled from permalloy film

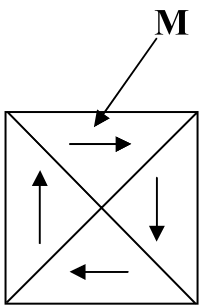

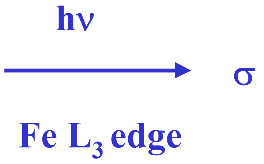

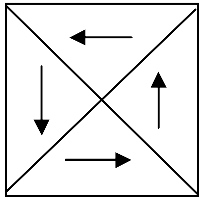

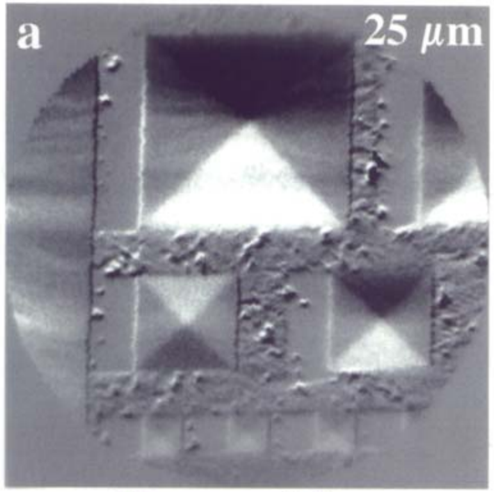

10 μm and 5 μm

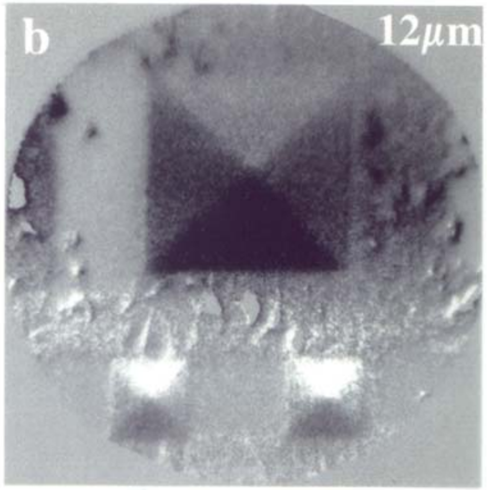

5μm and 2 μm

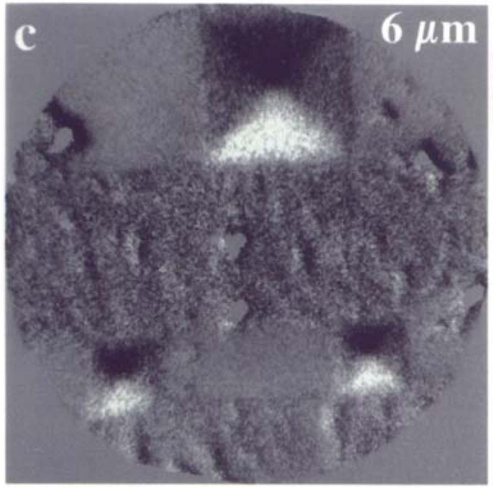

2 μm and 1μm

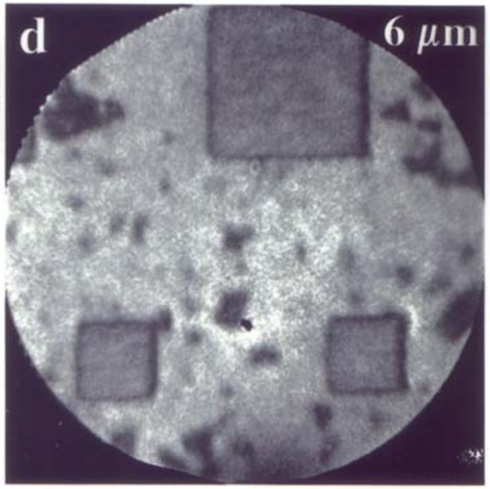

2 μm and 1μm (LEEM)

A. Locatelli et al, Surf. Rev. Lett. 9 (2002) 171

XMCDPEEM images of 20 nm thick Co elements

600×600

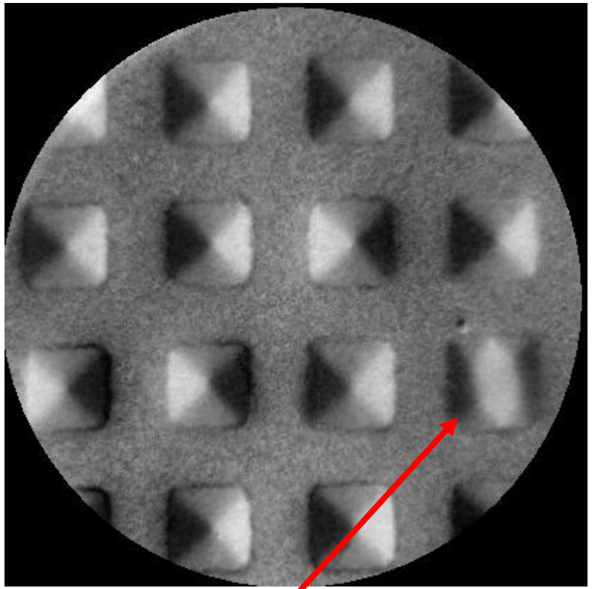

1200×600

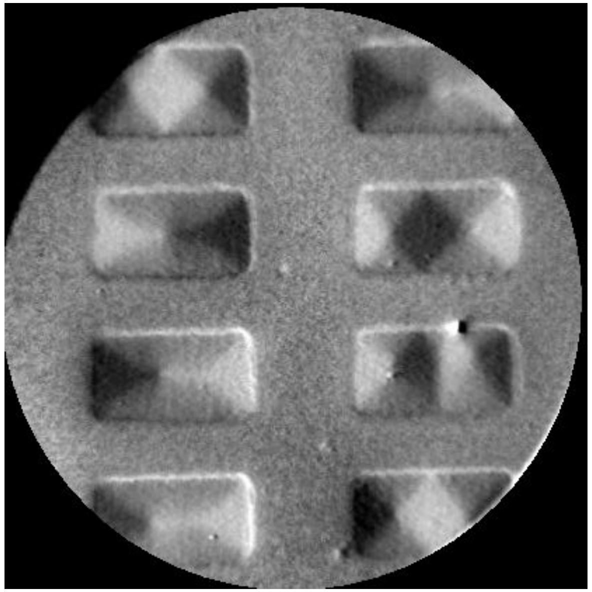

1200×400

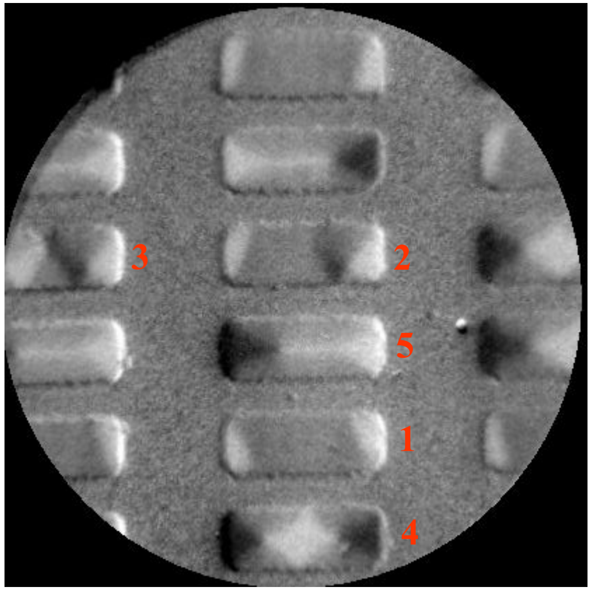

1200×600

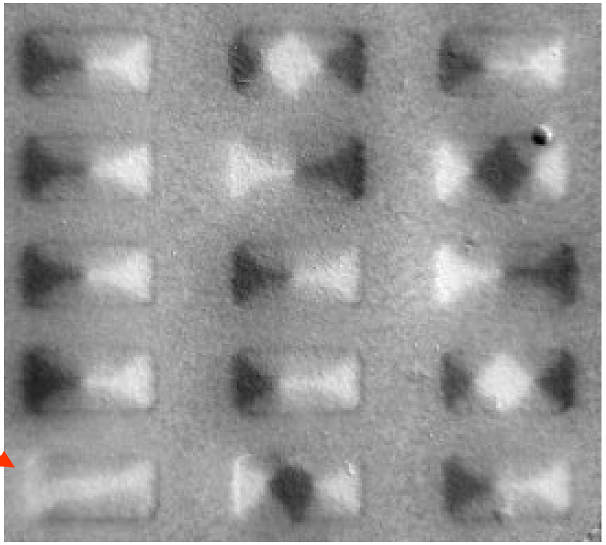

Virgin state

Micromagnetic simulations of rectangular Co elements

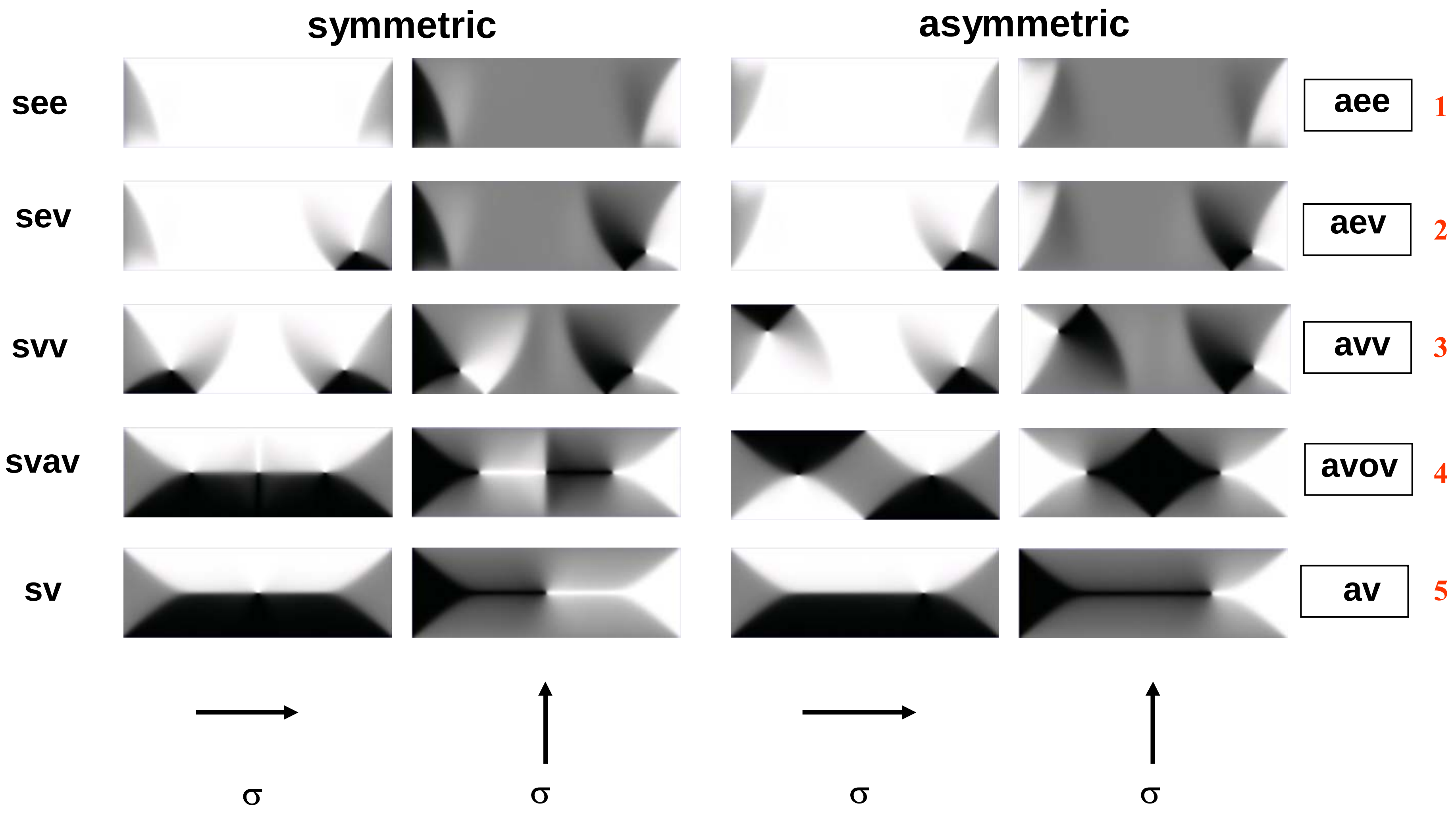

R. Hertel

Domain structures of complete and open ferromagnetic rings in the remanant state

Vortex walls

Transverse walls

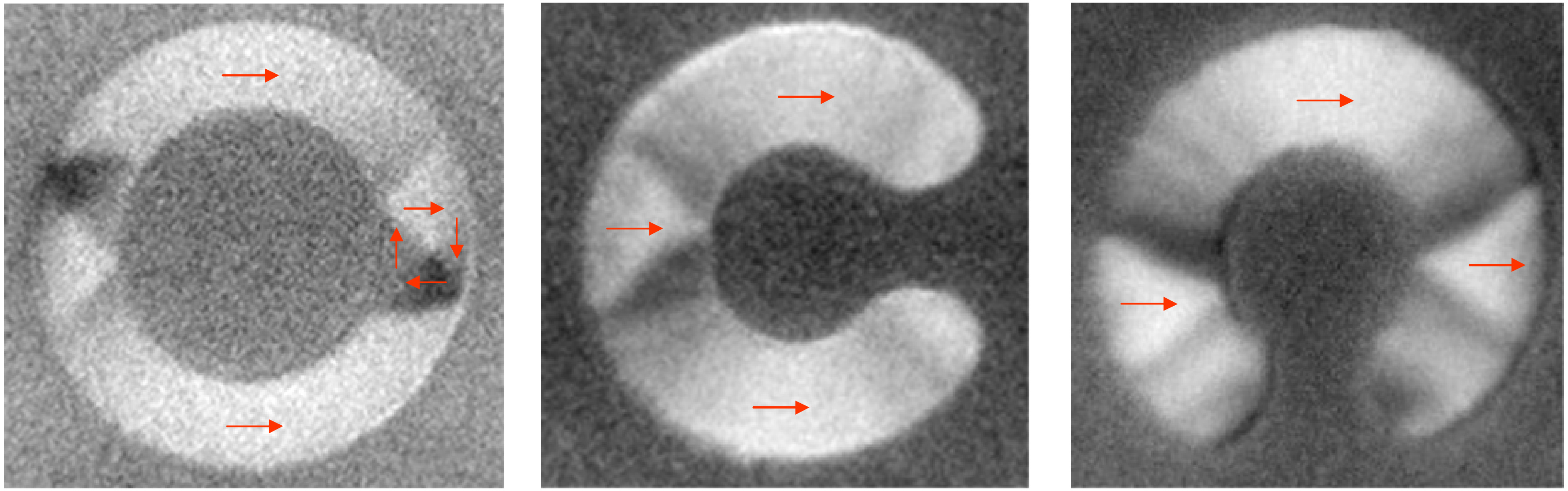

Permalloy
thickness 30 nm
O.D. 2400 nm
width 350 nm

$\vec{B}$

Cobalt
thickness 20 nm
O.D. 1600 nm
width 400 nm

Onion States

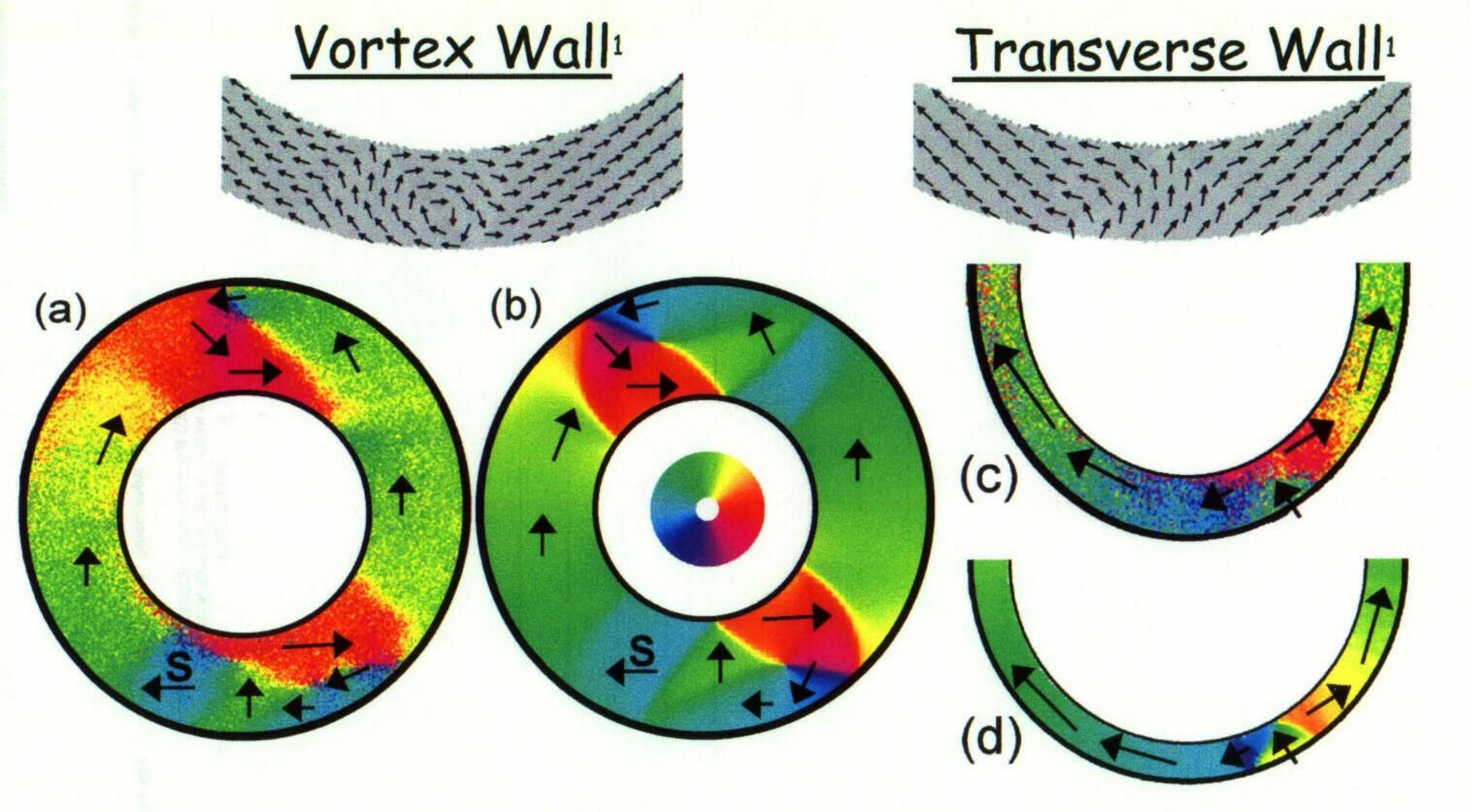

Kläui, priv.commun.

MnAs

Bulk properties

Magnetization

ferromagnetic | paramagnetic

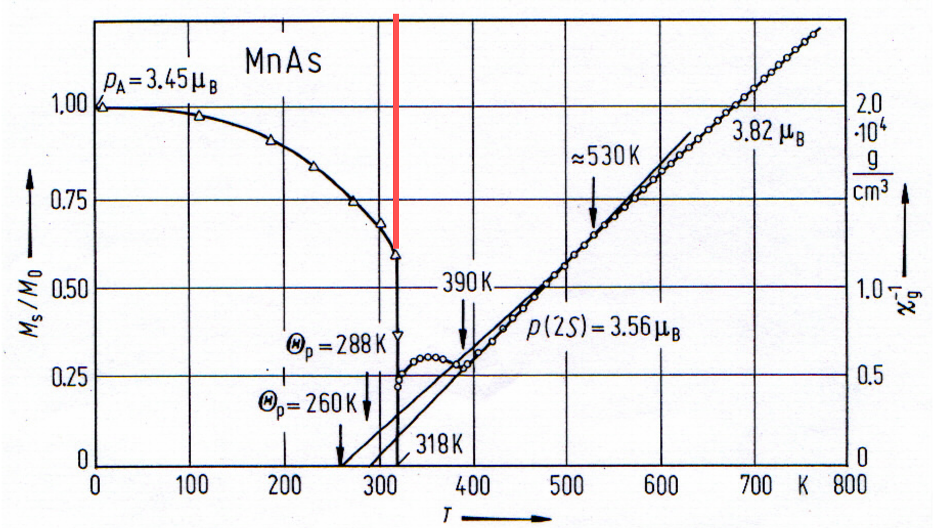

Sudden loss of magnetization
at structural transition

Thermal expansion

a, c

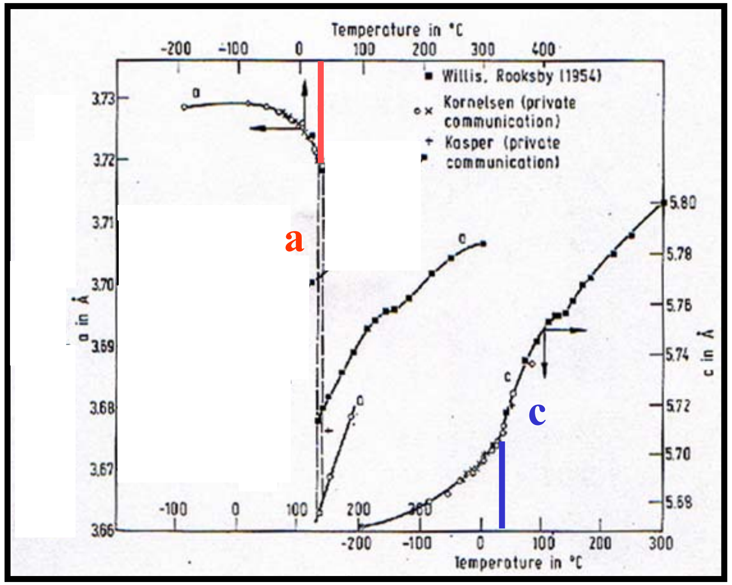

Large a contraction, little c expansion
at phase transition

MnAs

α T< ≈ 40 ^{o}C NiAs (hexagonal) ferromagnetic
β MnP (orthorhombic) paramagnetic
γ T > 125 ^{o}C NiAs (hexagonal) paramagnetic

MnAs for spin injection into GaAs at room temperature?

Problem: strain-induced phase coexistence between ferromagnetic and paramagnetic phase around room temperature

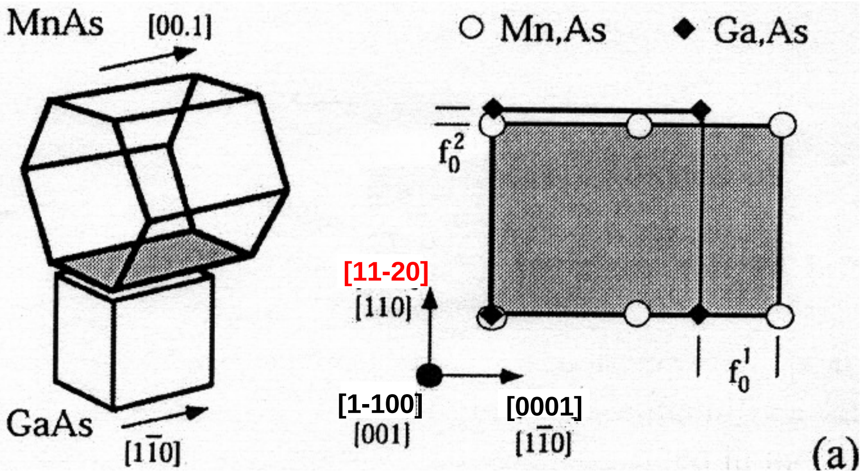

α MnAs / GaAs(100) $f_0^2 = 7.7\%$

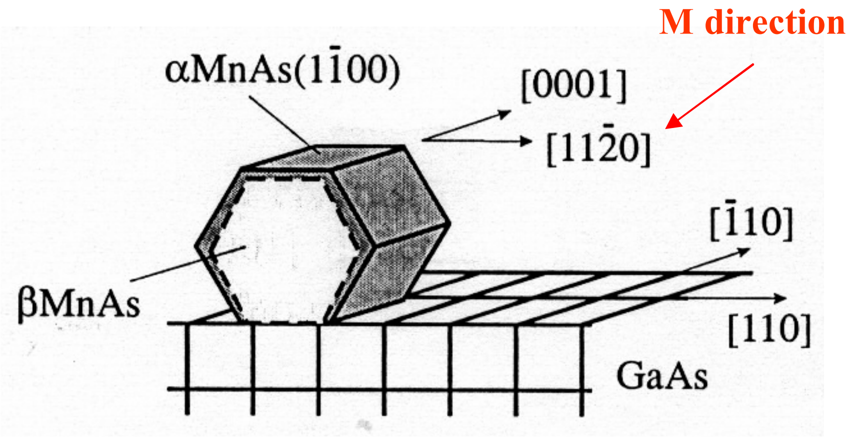

from L. Daeweritz et al ≥ 1999

Fully magnetized MnAs layer on GaAs (100)

partially covered with As
magnetic contrast formation

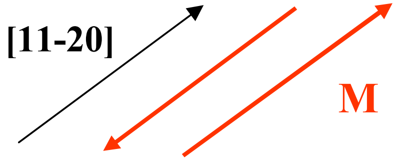

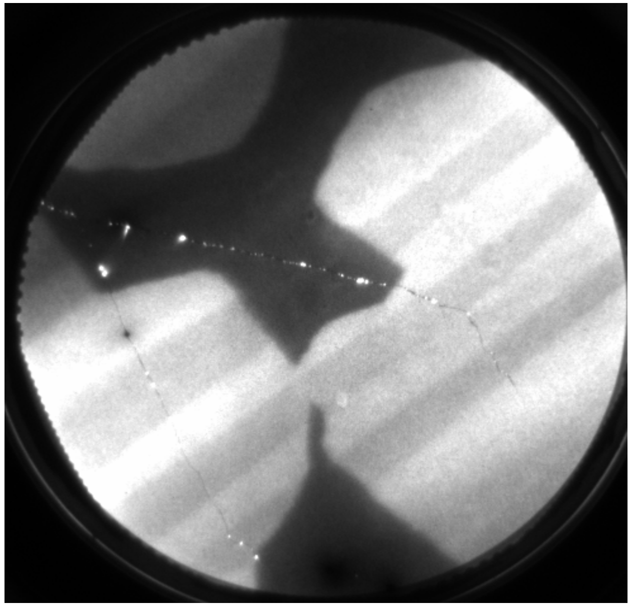

helicity 1

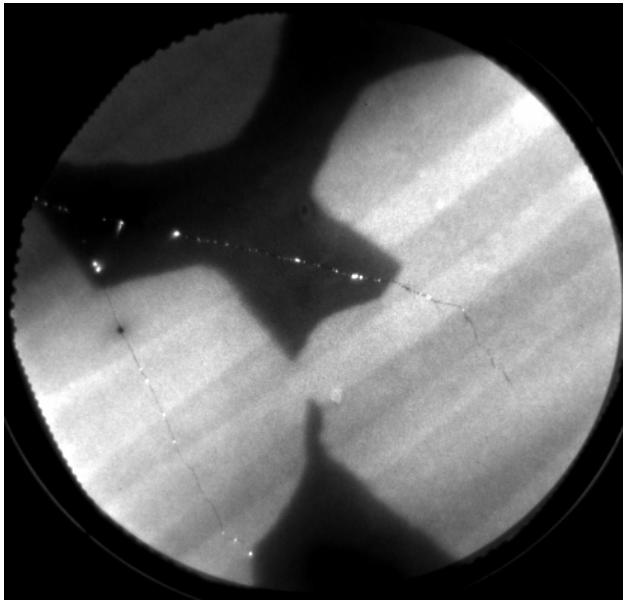

helicity 2

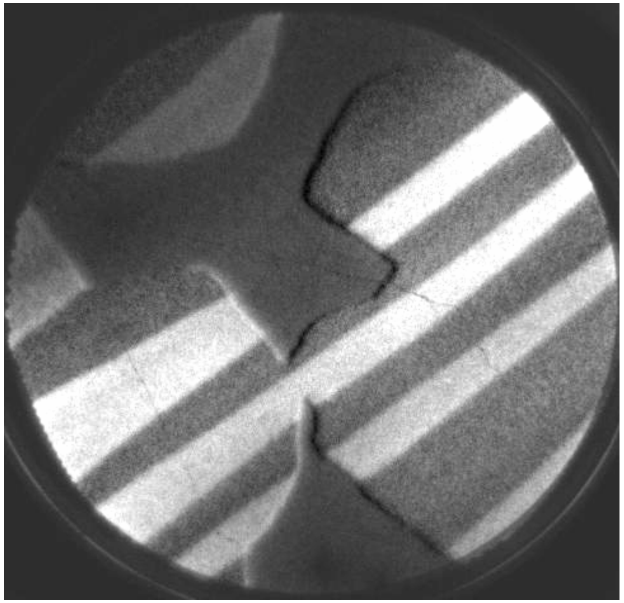

helicity 1 – helicity 2

1 μm

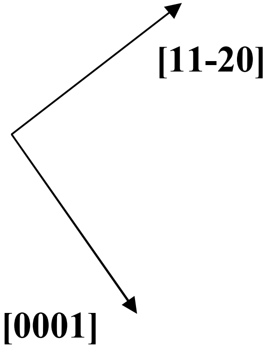

MnAs / GaAs(100) 40 nm

XMCDPEEM Mn $2p_{3/2}$ (639.5 eV)

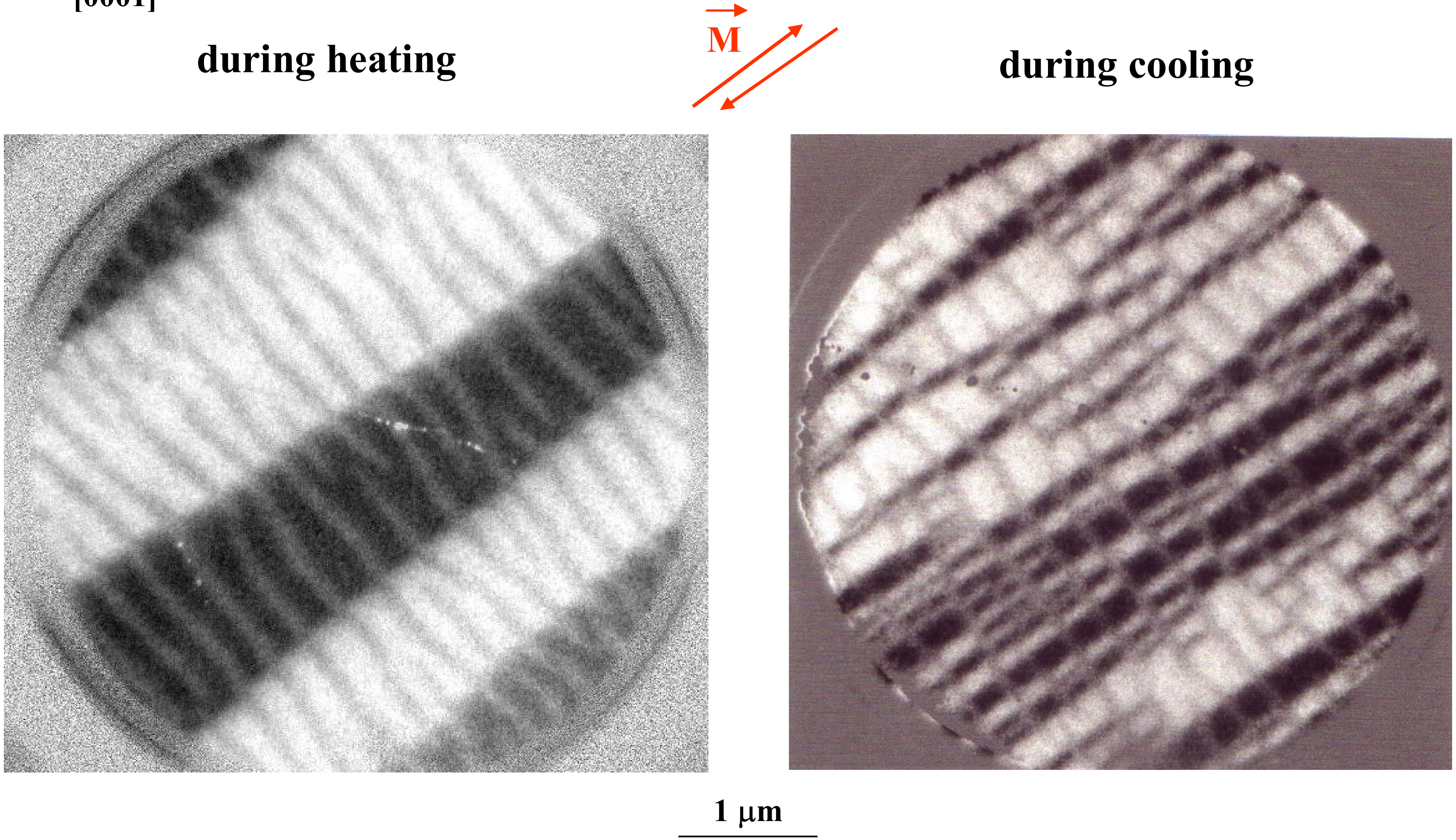

during heating

during cooling

MnAs on GaAs(100)

Thickness dependence of magnetic domain structure

Room temperature

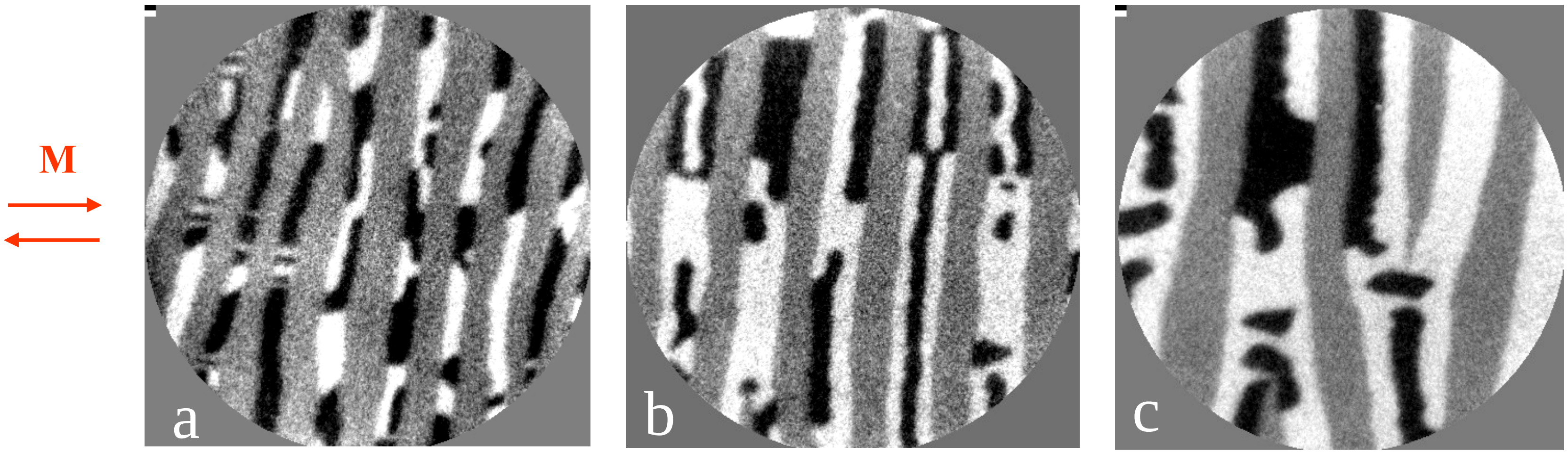

120 nm **180 nm** **300 nm**

Field of view 5 µm diameter

MnAs on GaAs(100)

Thickness 180 nm
heating

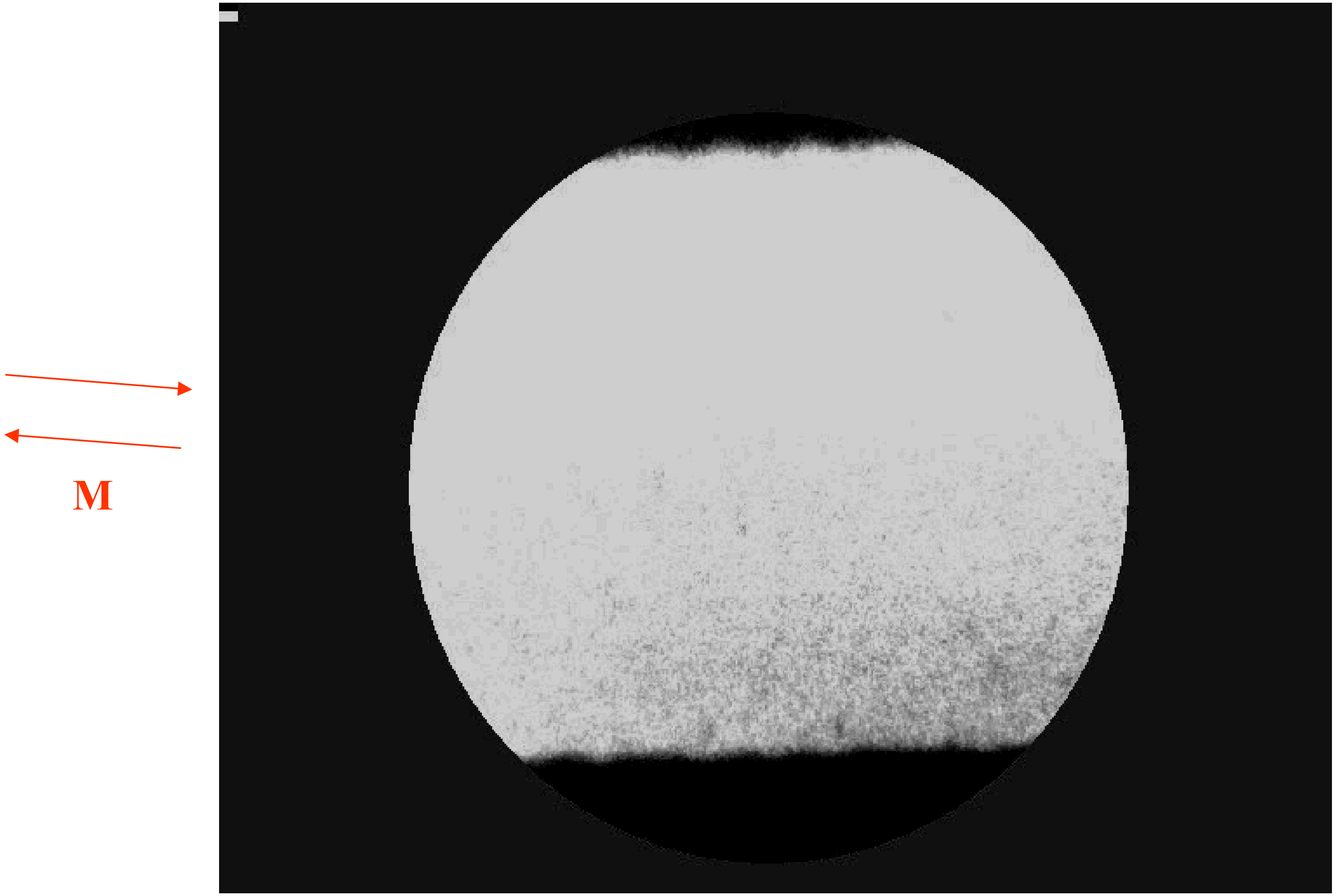

Field of view 5 μm diameter

MnAs on GaAs(100)

Room temperature

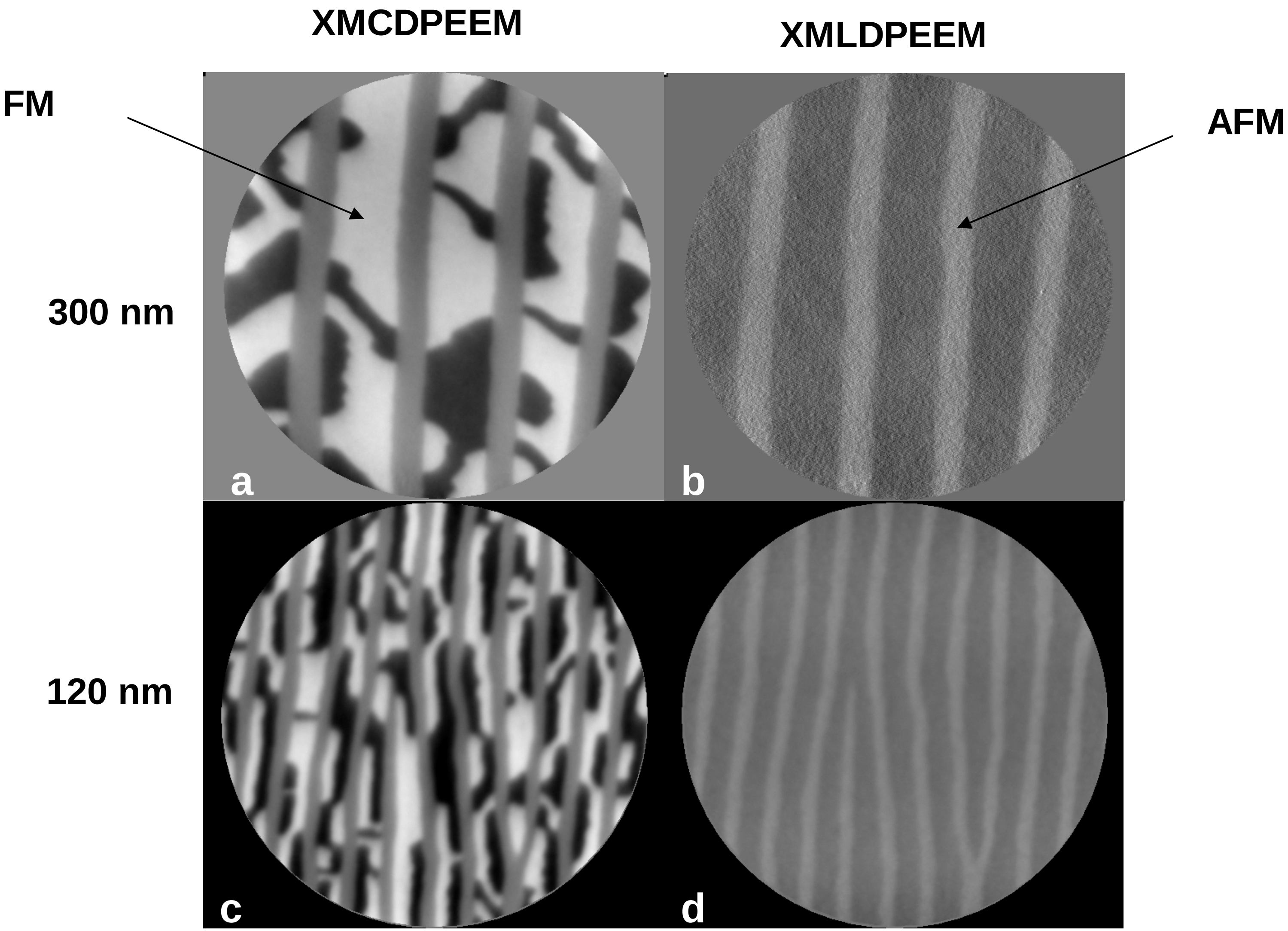

Conclusion

Full field XPEEM is one of the most important applications of the high brilliance of third generation synchrotron light, in particular when combined with a band pass energy filter and with LEEM because it allows a complete characterization of surfaces and thin films, presently on the 10 nm lateral resolution scale, with aberration correction in the future on the 1 nm scale (hopefully).

The main benefit of aberration correction, however, will be the strong increase of the transmission of the system which will reduce image acquisition time considerably. This will allow dynamical studies, which are presently limited to LEEM, also with XPEEM.

General references

E. Bauer and W. Telieps: *Emission and low energy reflection electron microscopy*, in: Surface and Interface Characterization by Electron Optical Methods, eds. A. Howie and U. Valdre, NATO ASI Series B: Physics, Vol. 191 (Plenum Press, New York 1988) p. 195-233

E. Bauer: *The possibilities for analytical methods in photoemission and low energy electron microscopy*, Ultramicroscopy 36 (1991) 52-62.

E. Bauer, T. Franz, C. Koziol, G. Lilienkamp and T. Schmidt: *Recent Advances in LEEM/PEEM for Structural and Chemical Analysis, in: Chemical, Structural and Electronic Analysis of Heterogeneous Surfaces on Nanometer Scale*, ed. R. Rosei (Kluwer Acad. Publ., Dordrecht 1997) p. 73- 84

E. Bauer, C. Koziol, G. Lilienkamp and T. Schmidt: *Spectromicroscopy in a Low Energy Electron Microscope*, J. Electron Spectrosc. Rel. Phenomena 84 (1997) 201 –209

E. Bauer: *Photoelectron Microscopy*, J. Phys.: Condens. Matter 13 (2001) 11391-11405

E. Bauer: *Photoelectron spectromicroscopy: present and future*, J. Electron Spectrosc.Relat. Phenom. 114 – 116 (2001) 976 –987.

E. Bauer and T. Schmidt: *Multi-Method High Resolution Surface Analysis with Slow Electrons, in: High Resolution Imaging and Spectroscopy of Materials*, ed. by F. Ernst and M. Ruehle (Springer, Berlin Heidelberg 2003) 363-390

Th. Schmidt, U. Groh, R. Fink, E. Umbach, O. Schaff, W. Engel, B. Richter, H. Kuhlenbeck, R. Schloegl, H.-J. Freund, A. M Bradshaw, D. Preikszas, P. Hartel, R. Spehr, H. Rose, G. Lilienkamp, E. Bauer and G. Benner: *XPEEM with energy-filtering: Advantages and first results from the SMART project*, Surf. Rev. Lett. 9 (2002) 223-232

Real lenses

Acceleration and imaging fields combined
Electrostatic triode

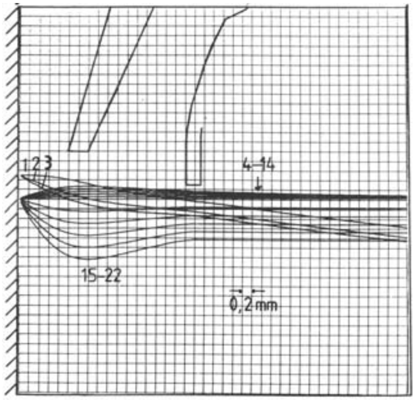

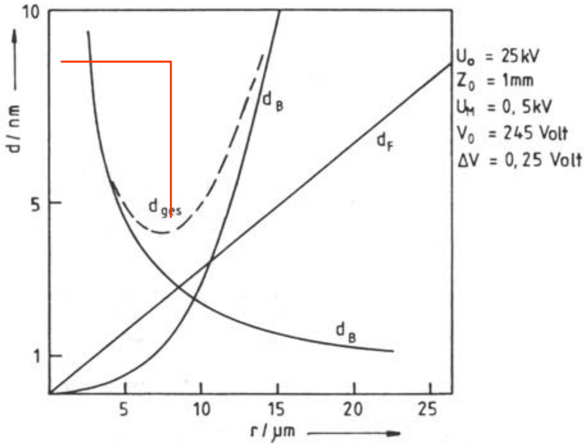

Optimum aperture

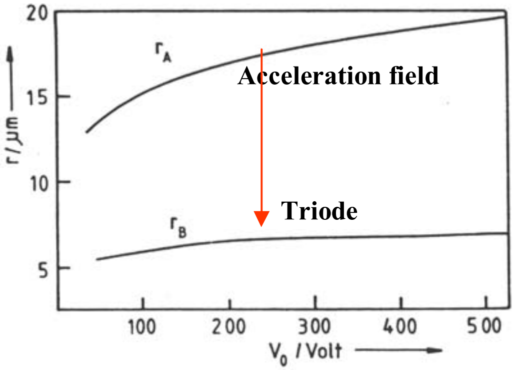

Resolution

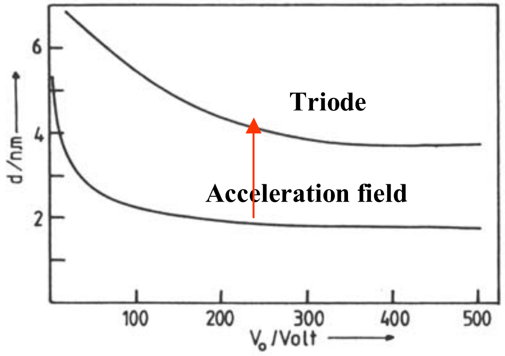

1,3: z_F, f, z_I
1,2 (ΔE): c_c
15-22 ($\times 50$): c_s $\alpha_{max} = 9^o$
4-14 to scale $\alpha_{max} = 80^o$

D.R. Cruise, J. Appl. Phys. 35 (1964) 3080

Resolution improvement by aberration correction

with electron mirror

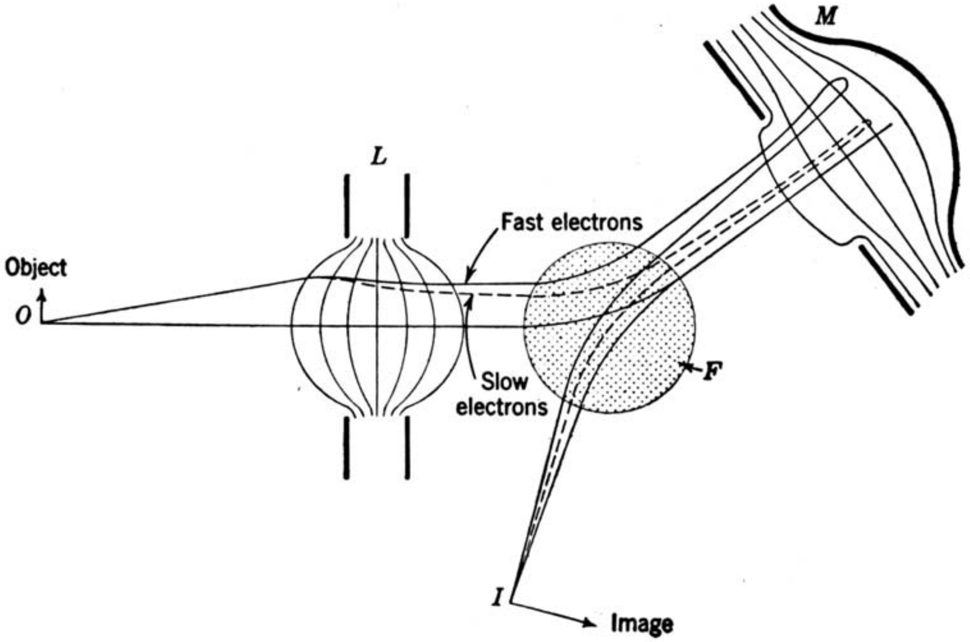

V.K. Zworykin et al, Electron Optics and the Electron Microscope, John Wiley, New York 1945

Recknagel 1935

Fe on Pb on W(100)

Surfactant action

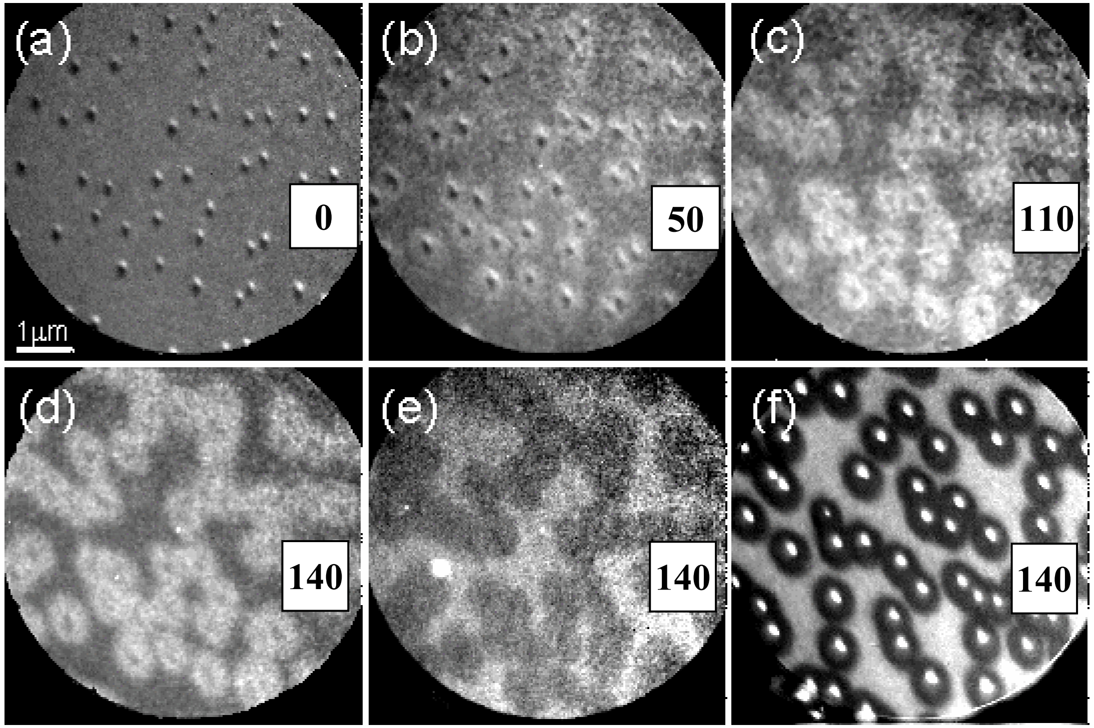

(a) – (d) Pb 5d images (hν = 70.5 eV, E_{kin} = 49 eV, (e) Fe 3d image, (f) LEEM image
270 K

Th. Schmidt et al, 1999

InAs nanocrystals on Se-passivated GaAs(100)

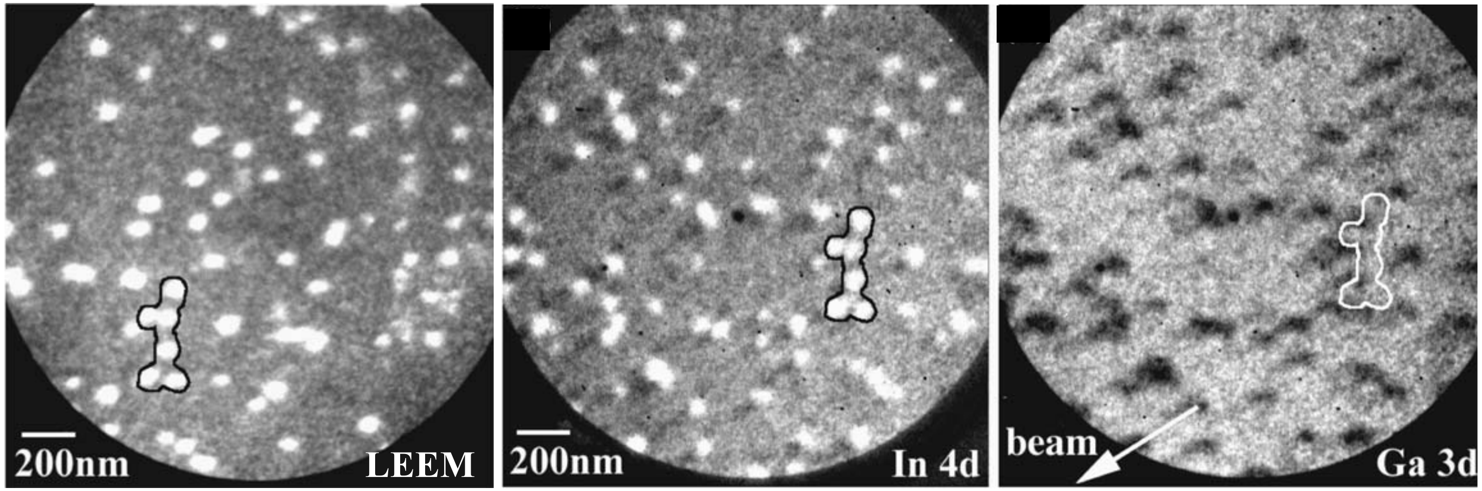

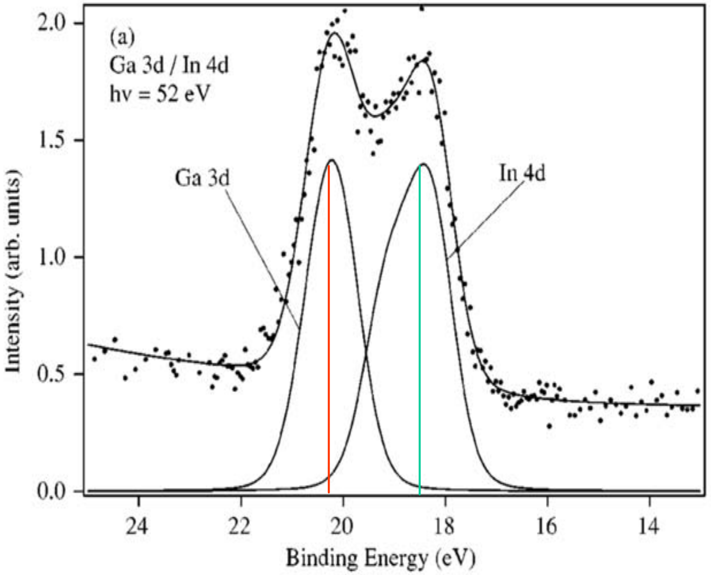

Overall spectra

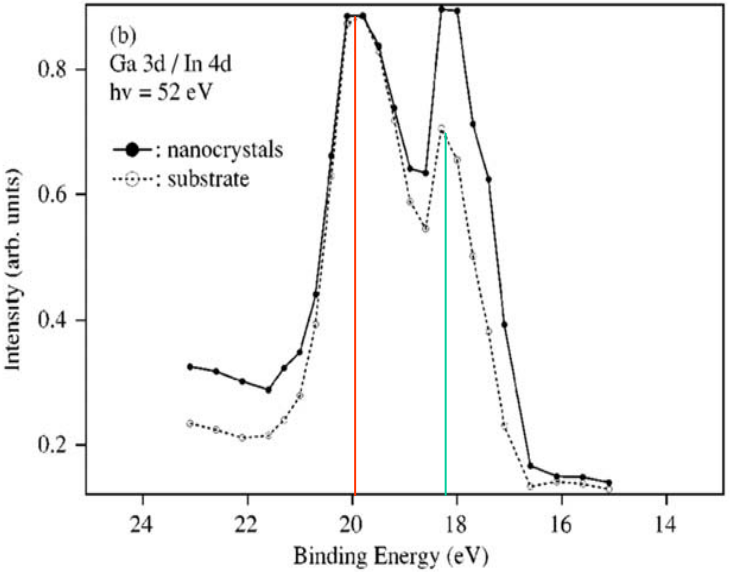

Local spectra

Ga on nanocrystals, In on substrate
intermixing SK growth

S. Heun et al , Phys. Rev B 63 (2001) 125335

Classical emission microscopy

Polycrystalline tantalum

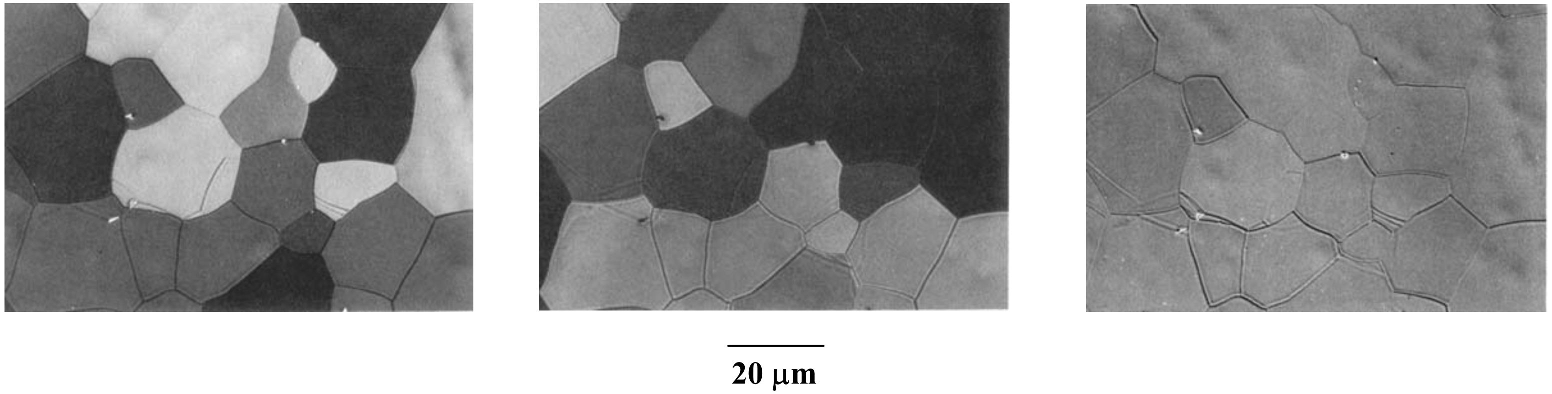

thermionic emission

threshold photo emission

secondary emission

Photo emission from polycrystalline beryllium bronce

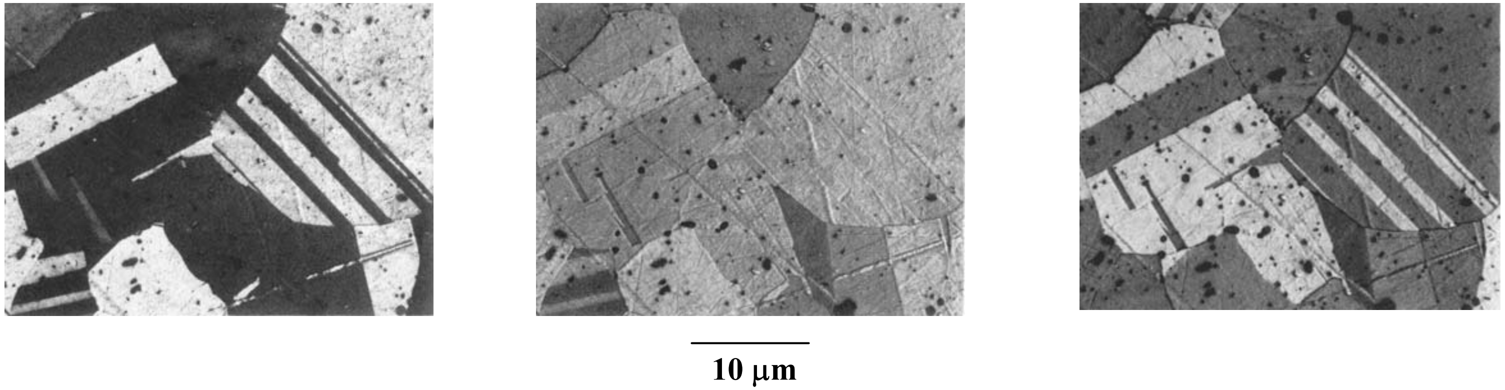

low

medium

high

energy region of the UV spectrum of a Hg high pressure lamp

W. Engel, Ph.D. thesis, TU Berlin 1968

Magnetic imaging in XPEEM

Ferromagnetism
Imaging modes

Sample: 10 Fe monolayers on W (100)

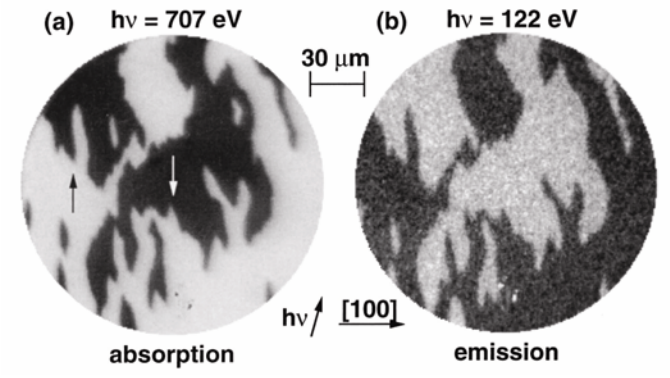

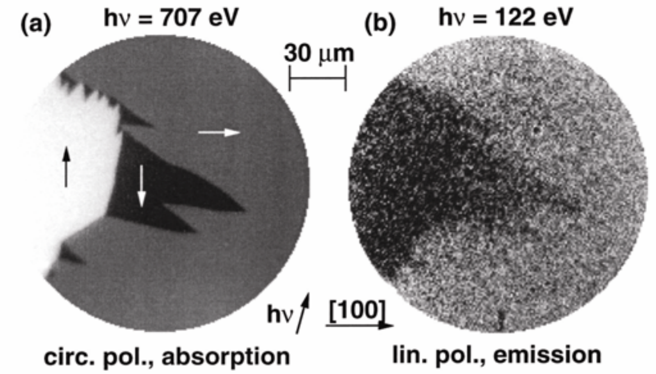

	XMCD		XMCD	XMLD
sensitive to	$M_{\parallel}$		$M_{\parallel}$	$M_{\perp}$
	secondary electrons from 2p ionization without filter	photo electrons from valence band with high pass filter E > 117 eV	secondary electrons from 2p ionization without filter	photo electrons from 3p level with high pass filter
	3 min/helicity	11 min/helicity		
gray scale:	25% asymmetry	4.7% asymmetry	25% asymmetry	25% asymmetry

asymmetry: XMCD: $(I_{\sigma-}-I_{\sigma+})/(I_{\sigma-}+I_{\sigma+})$ XMLD: $(I_l - I_h)/(I_l + I_h)$

W. Kuch et al, J. Vac. Sci. Technol. B 20 (2002) 2543

Magnetic imaging with XPEEM

Antiferromagnetism and ferromagnetism

NiO (100)

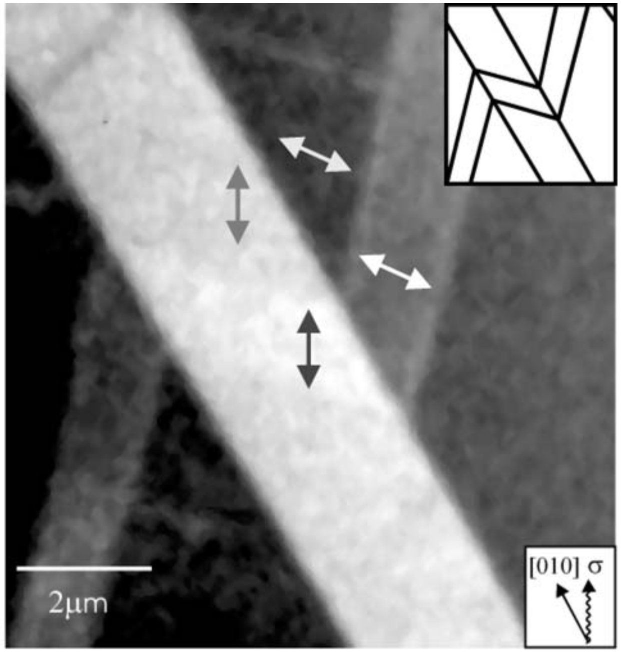

Contrast from intensity ratio of Ni L_2 doublet obtained with circular polarization ($E_\perp/E_{||}$) σ
Arrows: in-plane projections of AF axes obtained with linear polarization ($E_{||}$) π

AF maximum contrast when E ⊥ AF axis

8 Co monolayers on NiO (100)

AF domains Ni L_2 images

F domains Co L_3 images

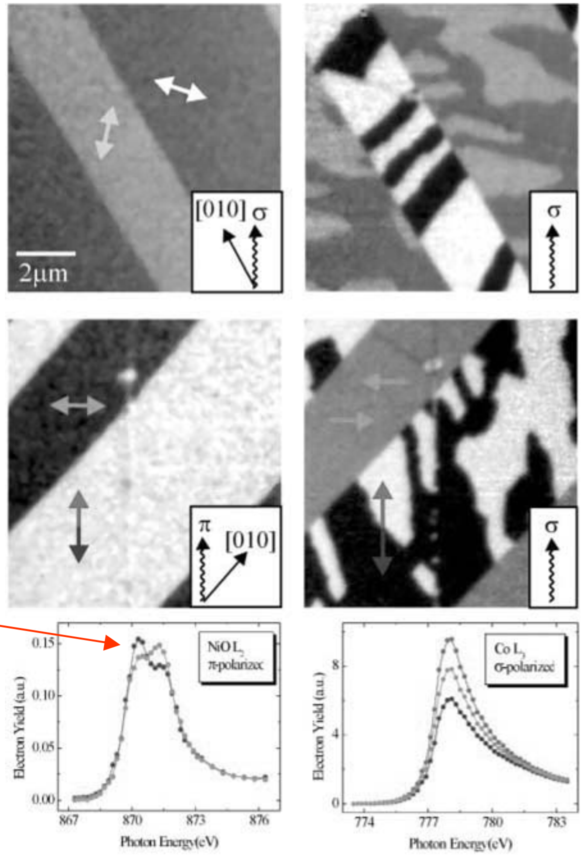

Exchange coupling

H. Ohldag et al, Phys. Rev. Lett. 86 (2001) 2878

Aberrations of homogeneous acceleration field

$\rho_0 = E_0/E \qquad \varepsilon = \Delta E_0/E \qquad \rho = \rho_0 + \varepsilon$

Spherical aberration $D_ö$

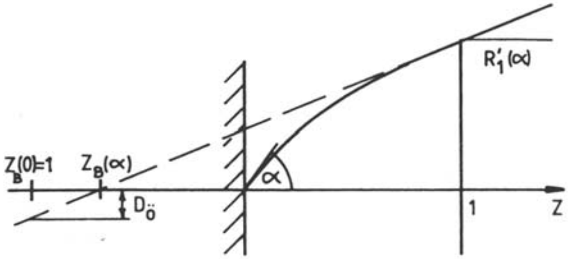

Chromatic aberration D_F

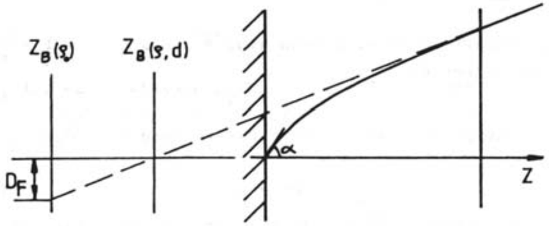

Approximation: ρ_0 and $\varepsilon << 1/\cos \alpha^2 > 1$
Example: $E_0 = 100$ eV, $\Delta E_0 = 1$ eV, $E = 20000$ eV
$\varepsilon = \rho_0 /100, \ \rho_0 = 1/200$

$D_ö \approx 2 \rho \sin \alpha \,(1 - \cos \alpha)$

$\approx 2 \rho \ (\alpha - 1/6\alpha^3)(1/2\alpha^2 - 1/24\, \alpha^4)$

45° 10.7%
60° 17.0%

$\approx \rho\, \alpha^3$ for small α

45° 20.5%
60° 36.2%

$D_F \approx 2 \rho \sin \alpha \,(\sqrt{\ } \rho_0 / \rho - 1)$

$\approx \varepsilon \sin \alpha$ for $\varepsilon << \rho_0$
$\approx \ \varepsilon\, (\alpha - 1/6\, \alpha^3)$

Error
45° 0.3%
60° 1.2%

$\approx \ \varepsilon\, \alpha$ for small α

45° 11.1%
60° 17.3%

XMCDPEEM

Aspect ratio dependence of the virgin domain structure of 1 μm wide Co bits

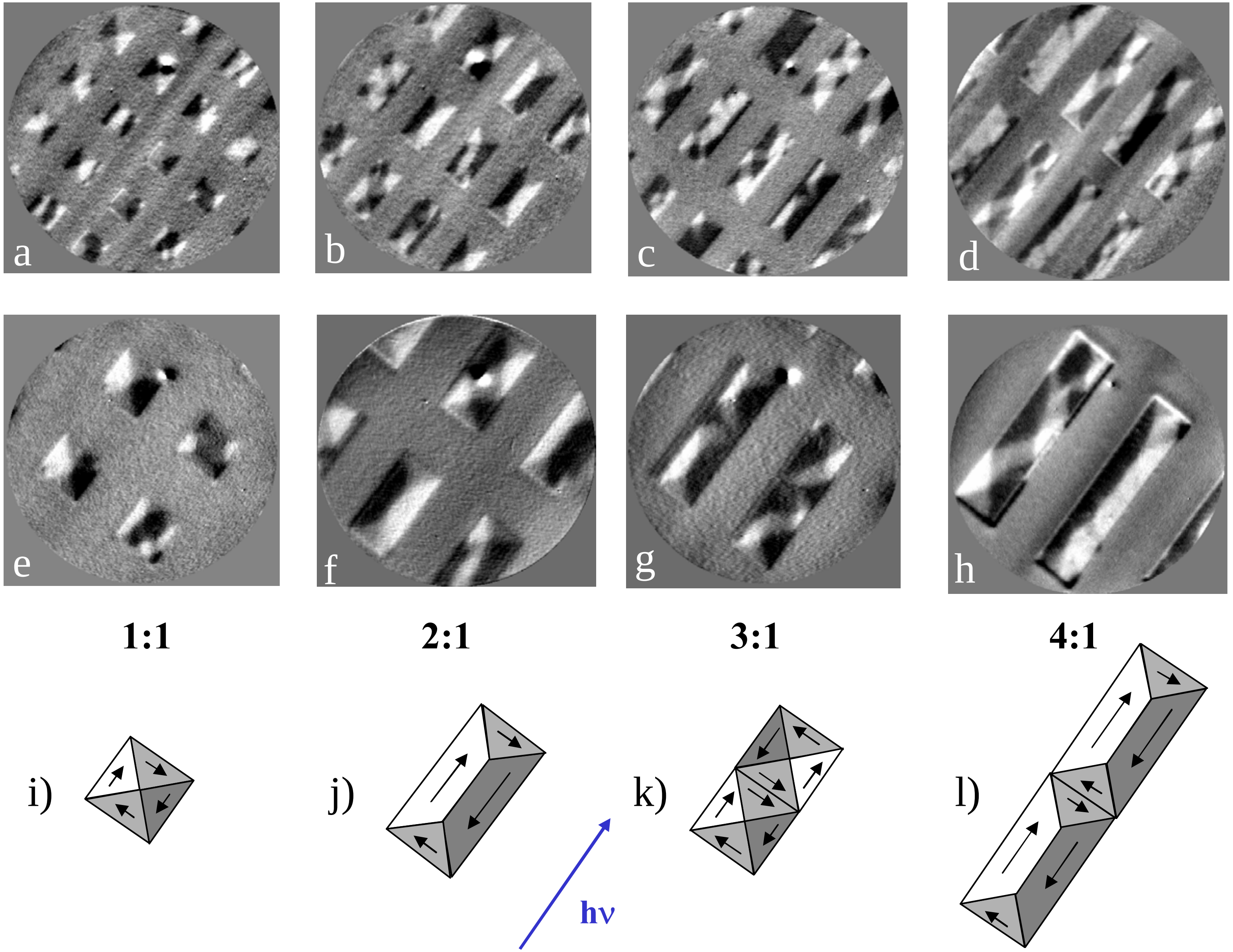

XMCDPEEM

Size dependence of the domain structure of 15 nm thick Co bits
Aspect ratio 3:1, virgin state

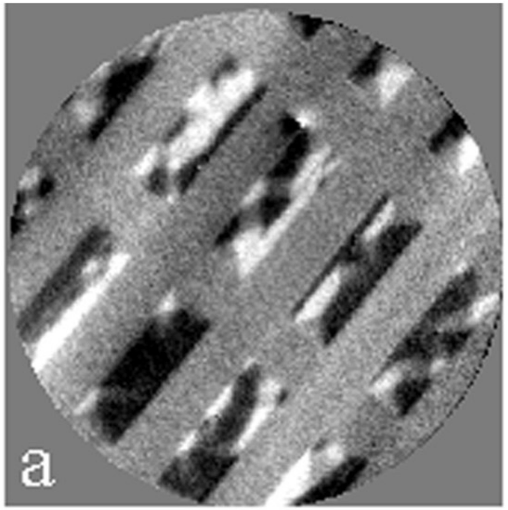

1000 nm

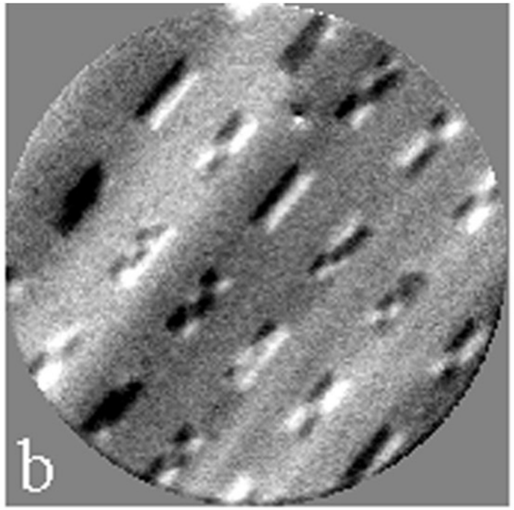

500 nm
width

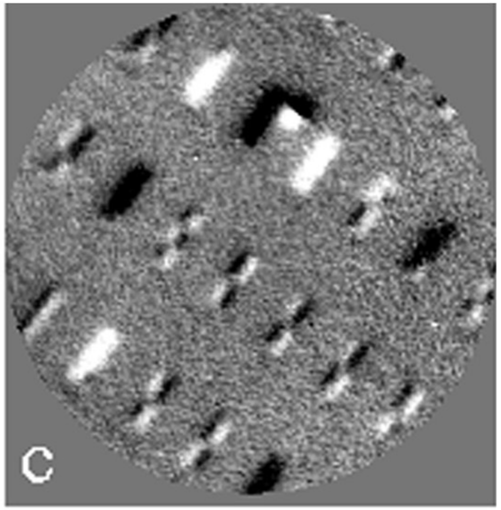

250 nm

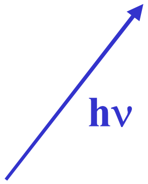

Micromagnetic simulations of permalloy bits with aspect ratio 2:1

R. Hertel, Z. Metallk. 93 (2002) 957

Landau **diamond** **S** **C**

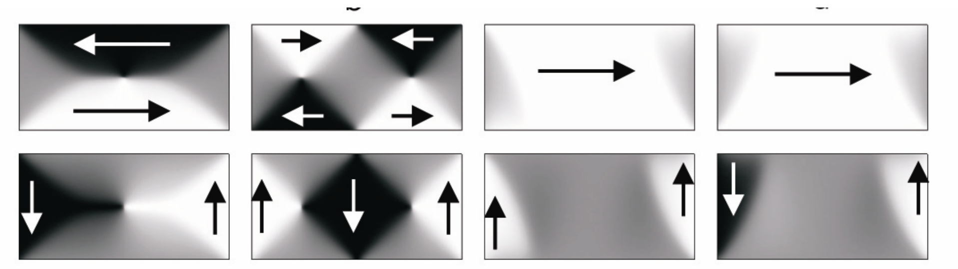

Size independence

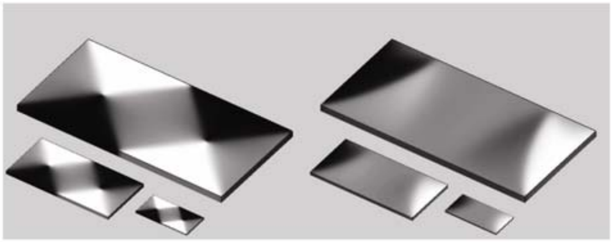

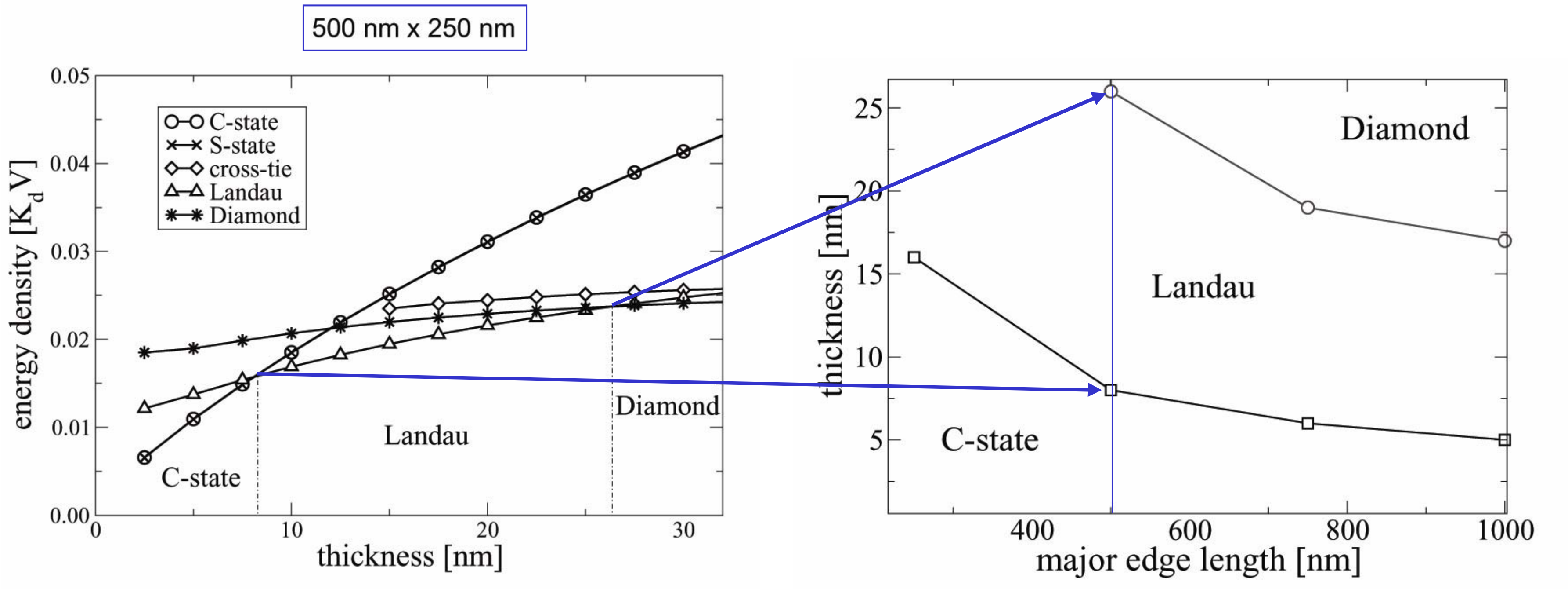

XMCDPEEM

Domain structure of 1.6 µm wide Co rings

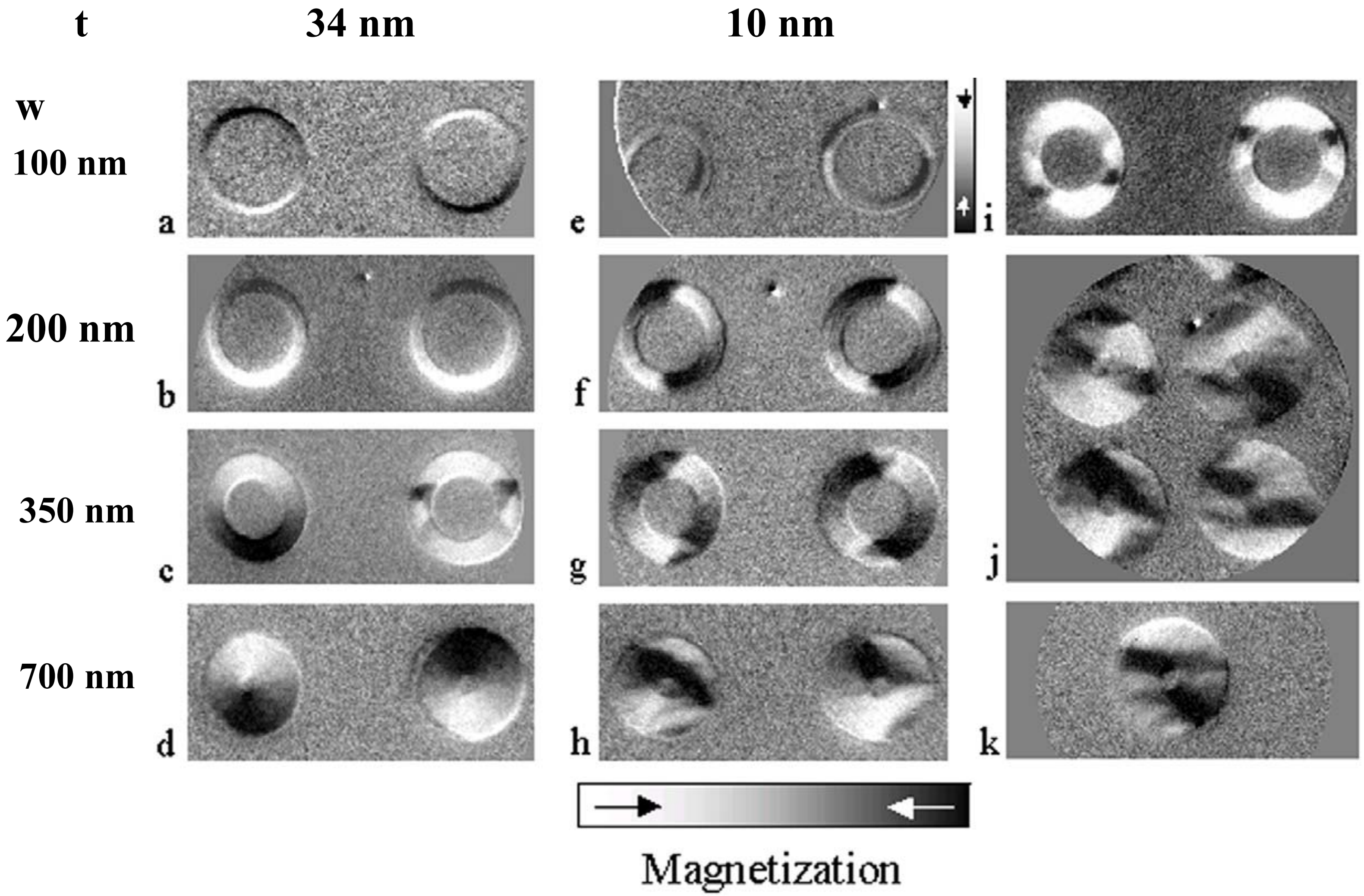

MnAs on GaAs(311)

Thickness 180 nm
cooling

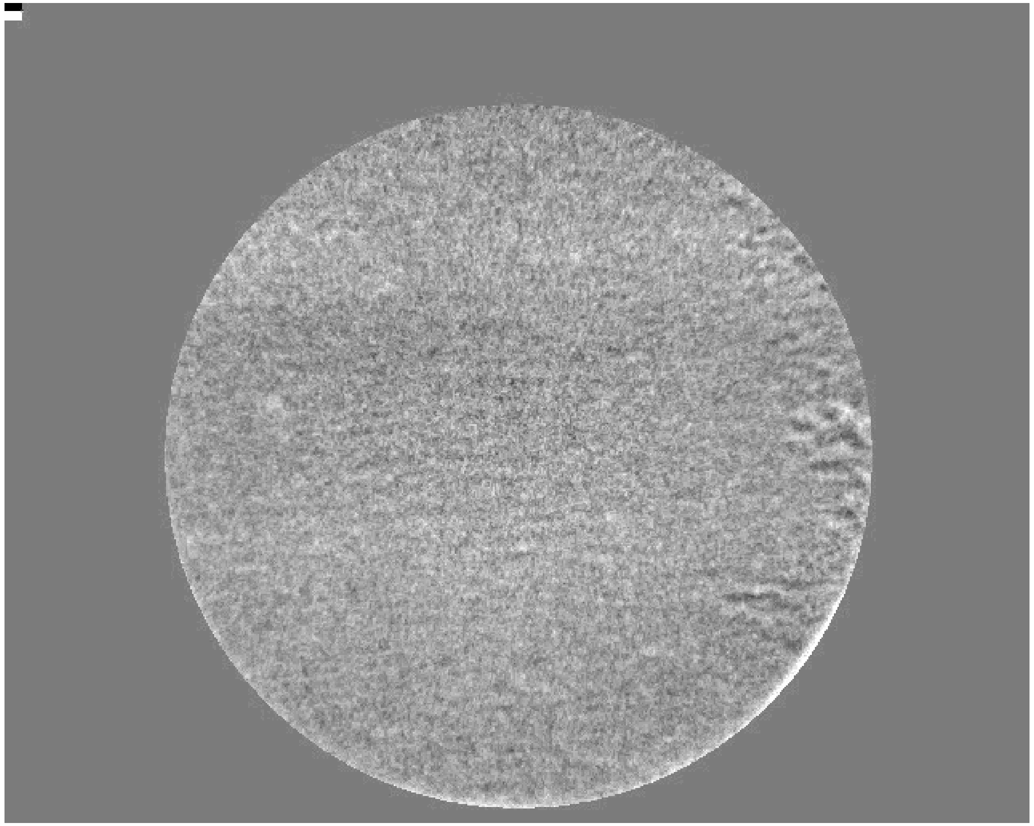

Field of view 5 μm diameter

MnAs on GaAs(100)

Thickness 300 nm
heating

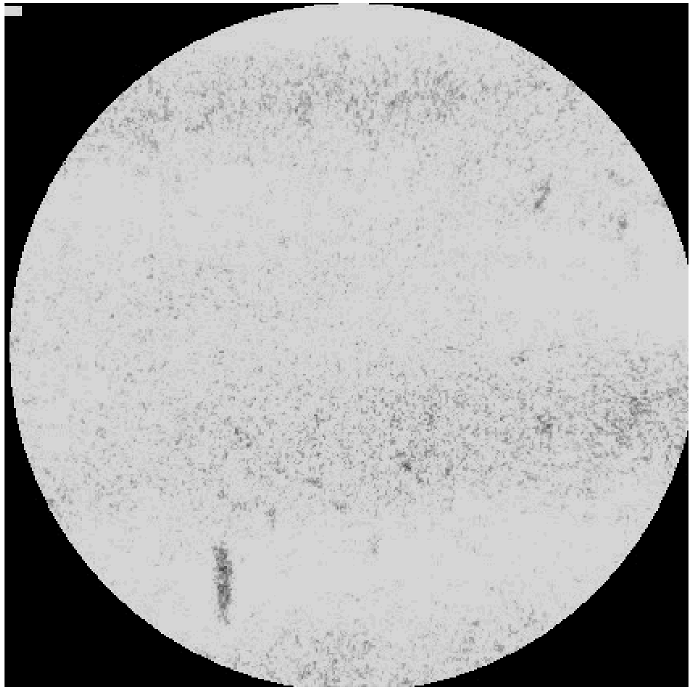

Field of view 5μm diameter

Micromagnetic simulations of ferromagnetic rings

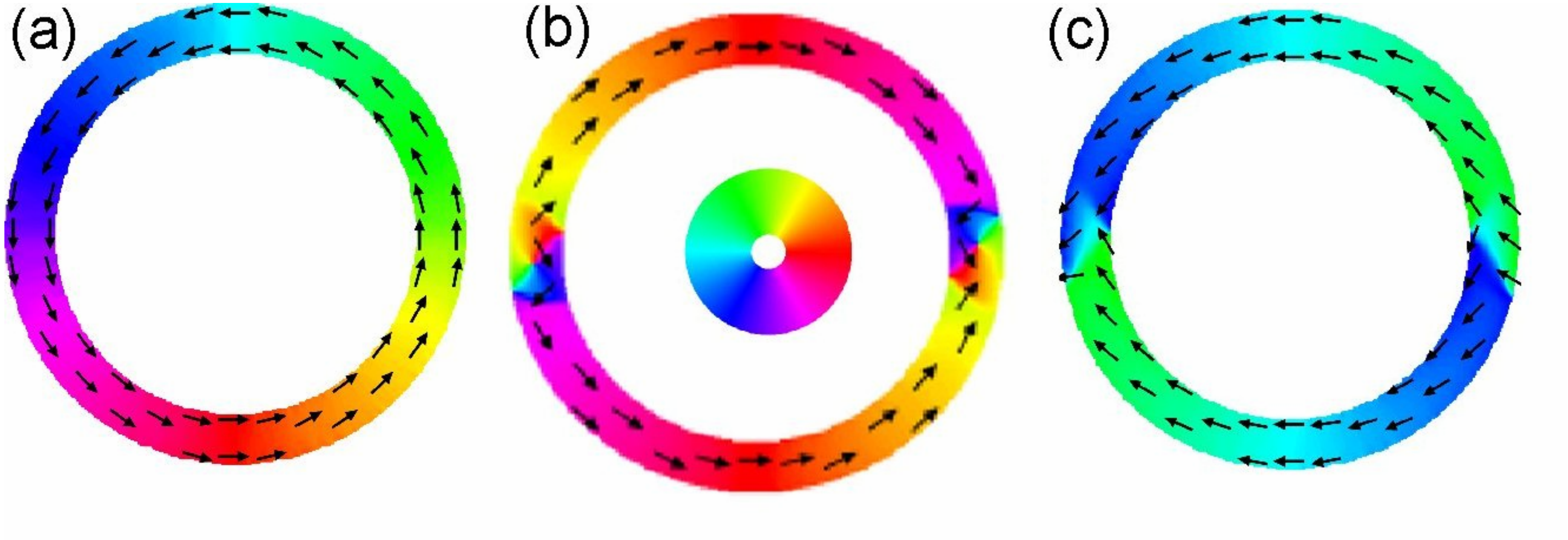

Vortex state

Onion states

Vortex walls

Transverse walls

M. Kläui, private comm.

MnAs islands on GaAs (100)
far below phase transition
surrounded by crystallized As capping

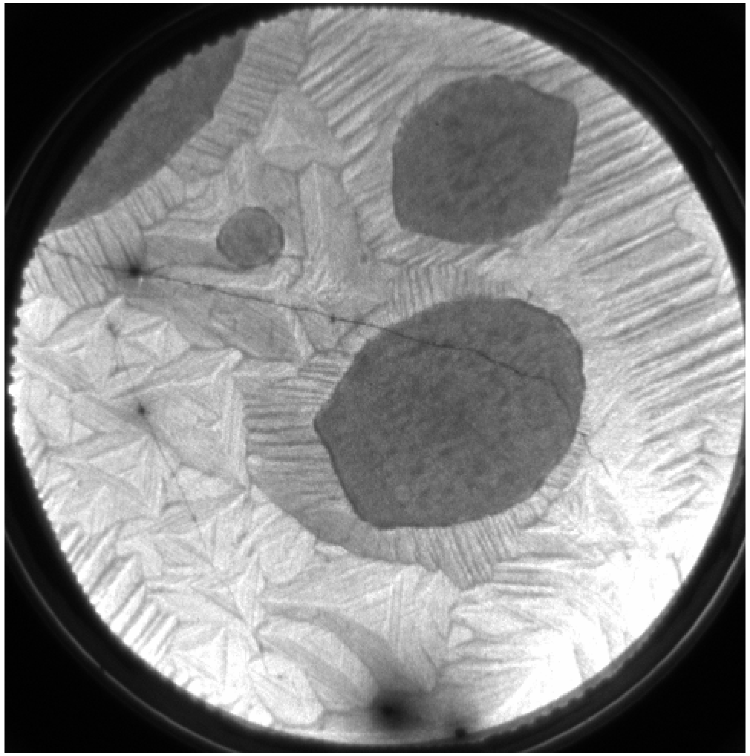

10 eV 1 μm

LEEM

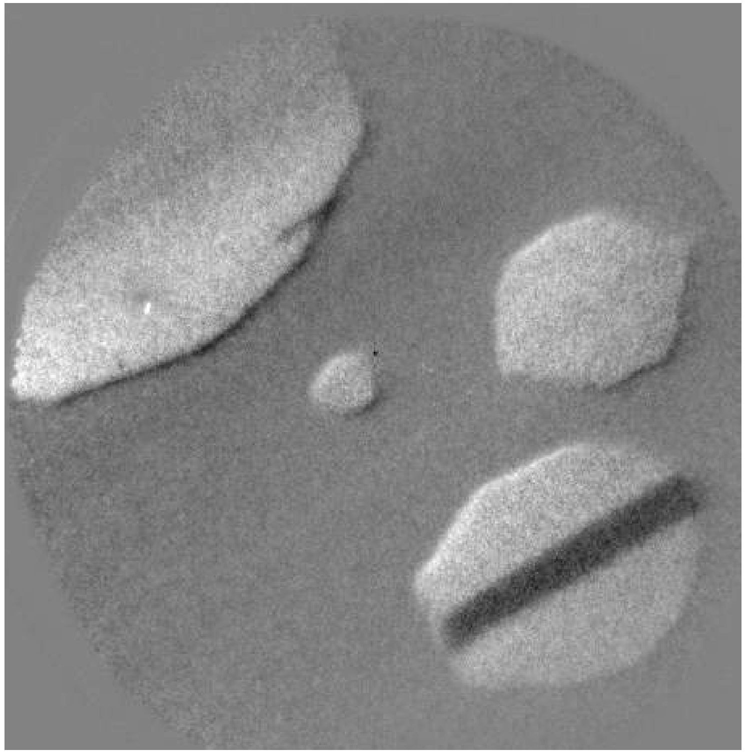

hν = 639.5 eV

XMCDPEEM

MnAs islands on GaAs(100) in the phase transition region

Phase contrast
between hexagonal and orthorhombic phase

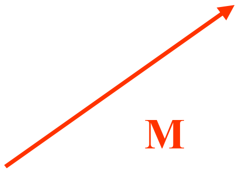

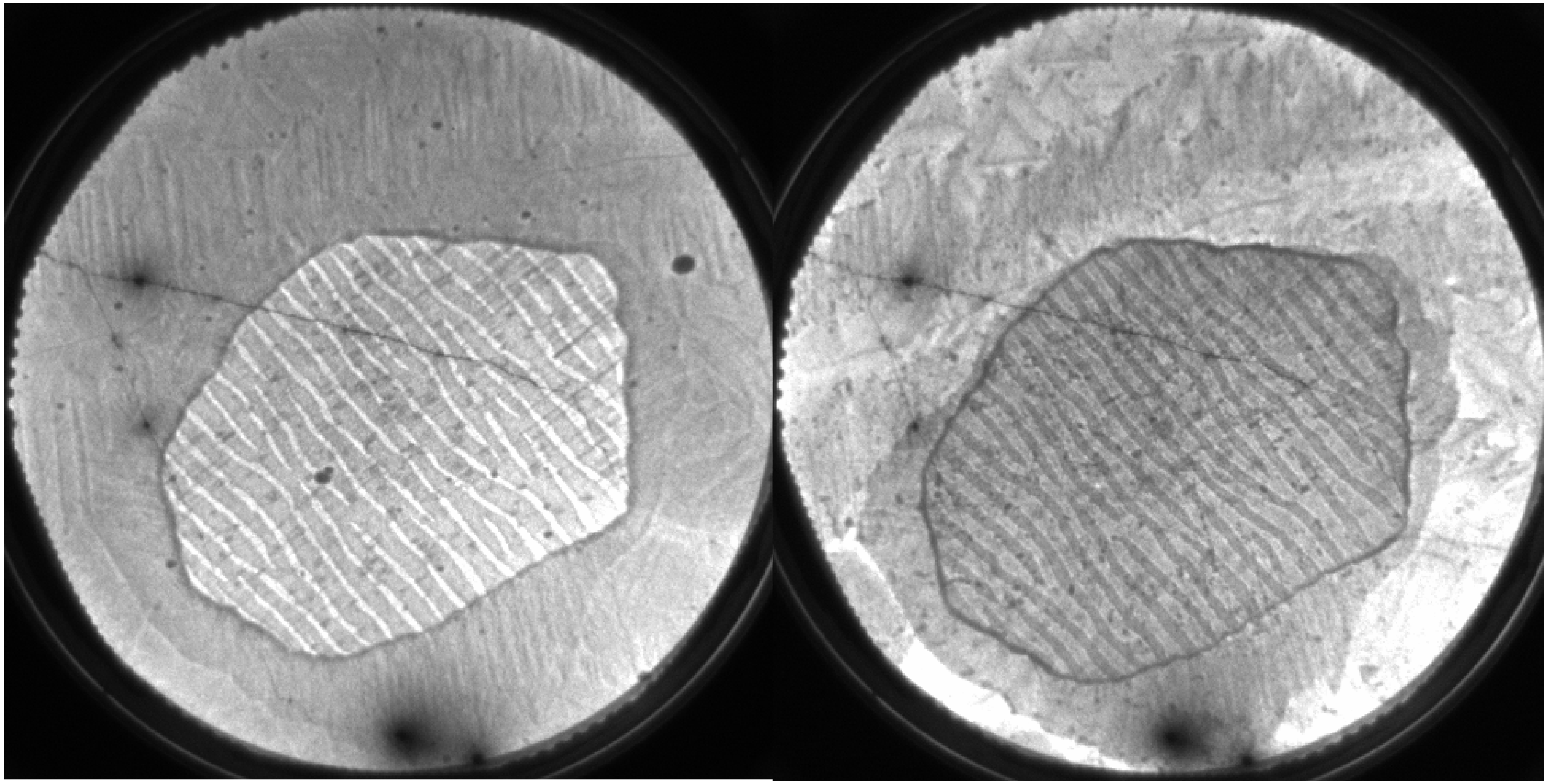

- 12 µm defocus

4.5 eV

+ 12 µm defocus

LEEM

1µm

MnAs / GaAs(100)

Thickness 40 nm

Ferromagnetic – paramagnetic phase transition

≈ 13 ^{o}C - ≈ 35 ^{o}C

black M ↙
white M ↗

gray paramagnetic

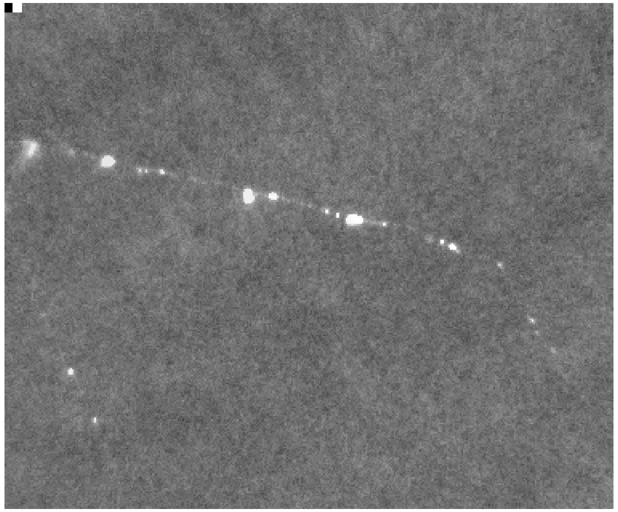

Field of view 4x4 μm^2

MnAs / GaAs (100)

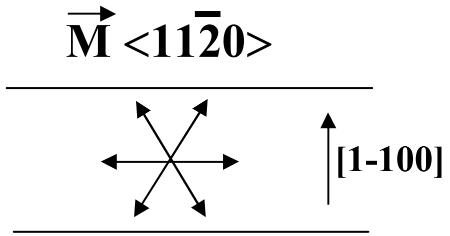

Thickness 250 nm

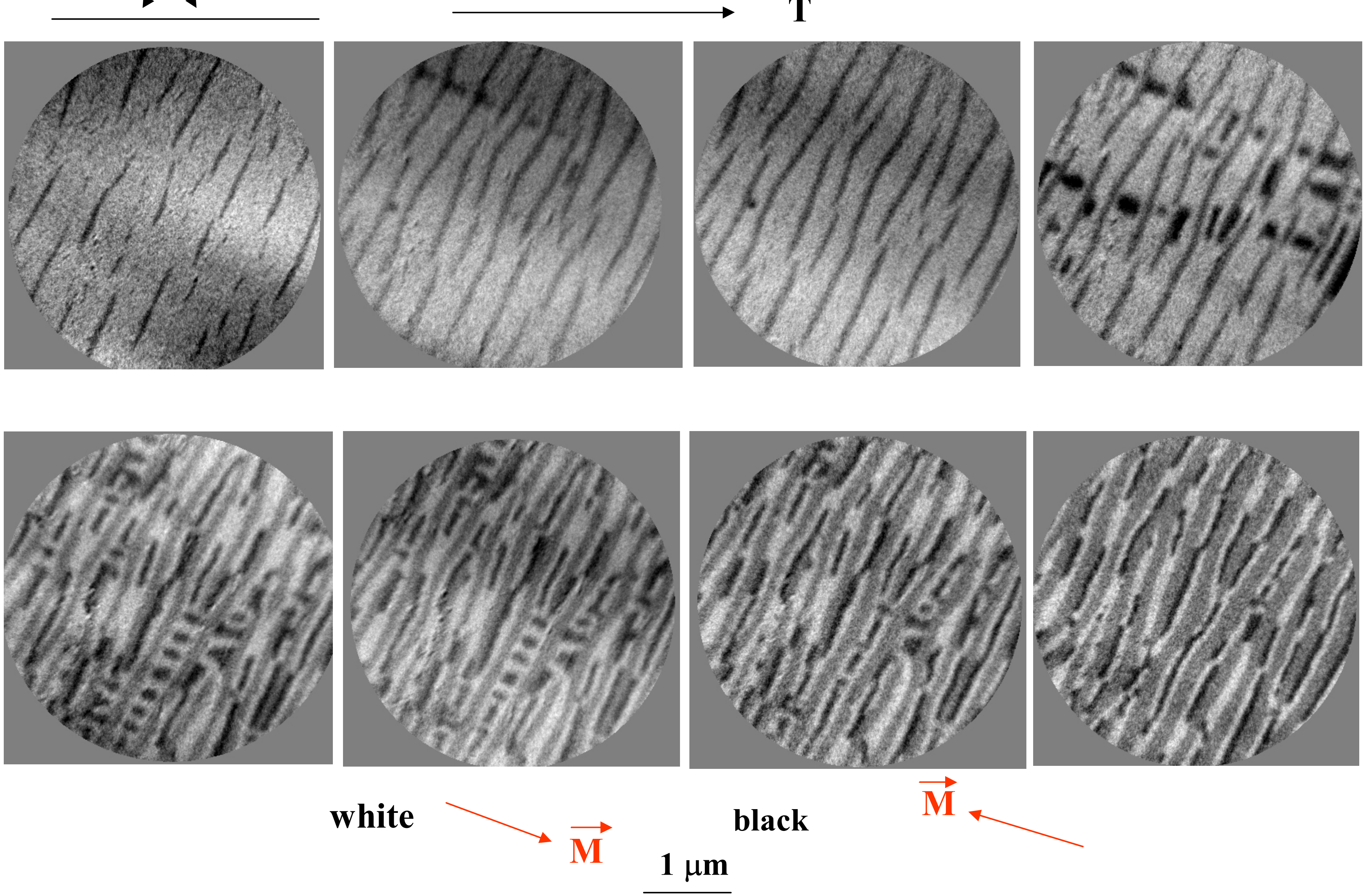

MnAs on GaAs(100)

Thickness dependence of stripe period

Structural images (LEEM)

Diameter of field of view

10 μm

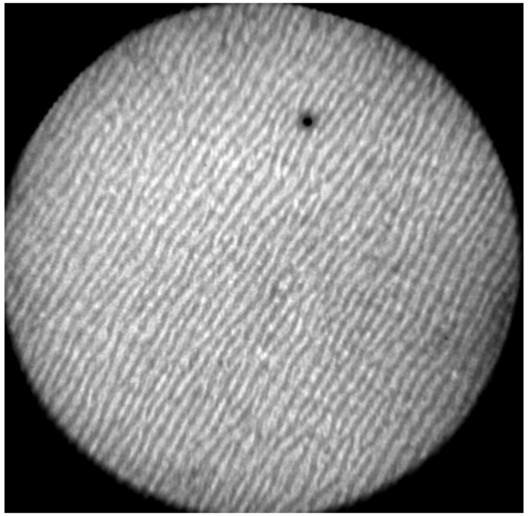

50 nm

10 μm

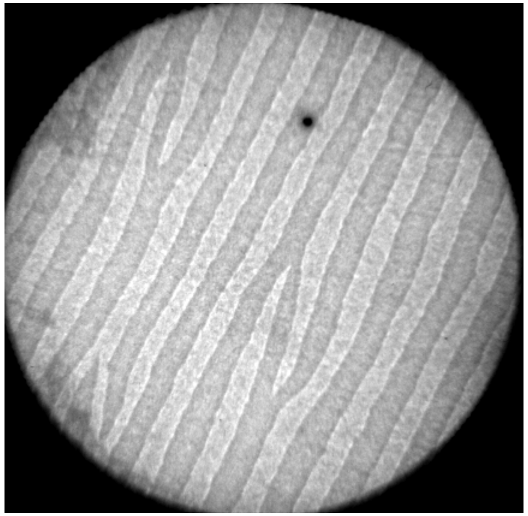

180 nm

5 μm

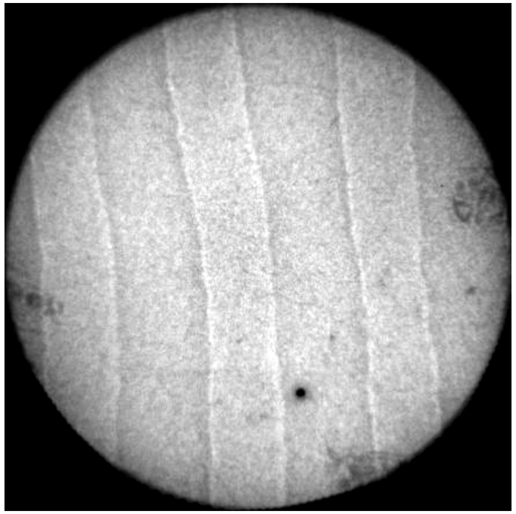

300 nm

Structural - magnetic phase transition in 40 nm thick epitaxial MnAs layer on GaAs (001)

M ↙

~ 16 °C T → ~ 39 °C

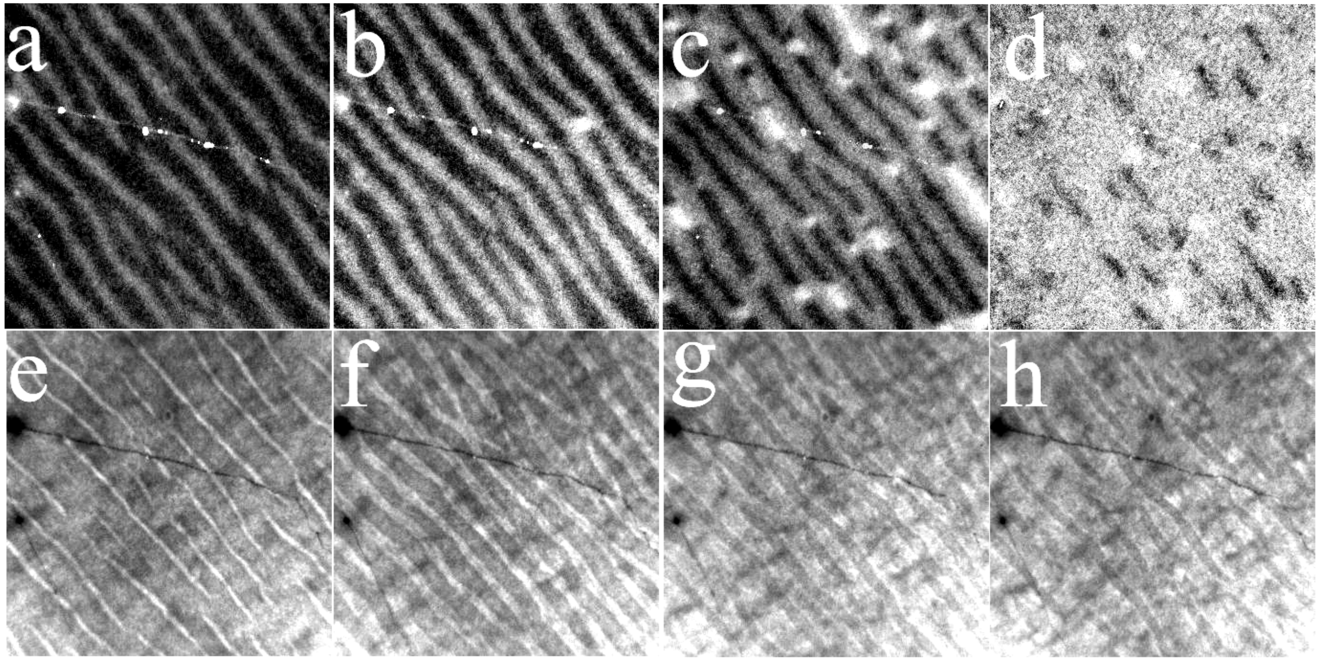

a - d XMCDPEEM
MnL_3 (639.5 eV)

1 µm

e - h LEEM
4.5eV

MnAs on GaAs(100)

Thickness 120 nm
heating

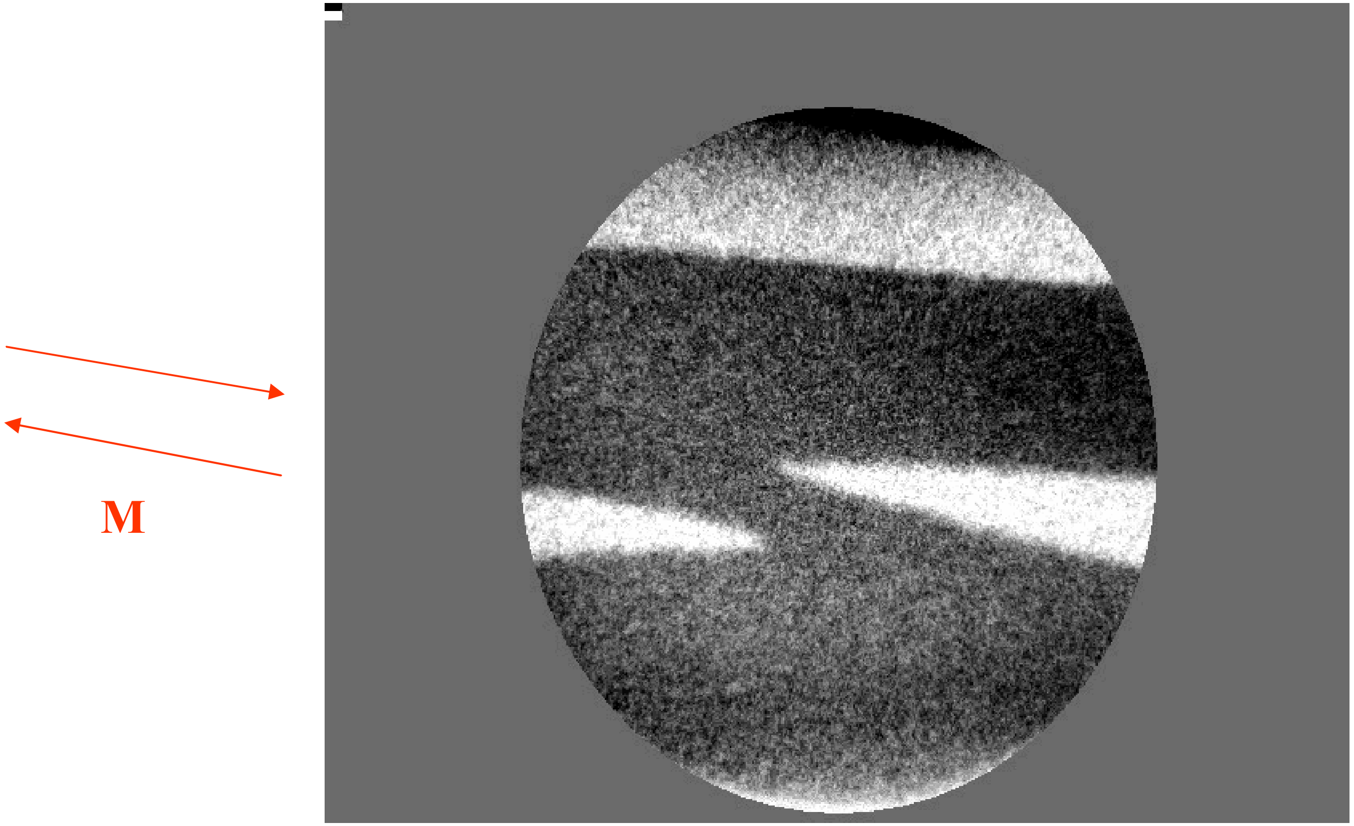

Field of view 5 µm diameter